ORGANIC CHEMISTRY FRONTIERS

RESEARCH ARTICLE

View Article Online
View Journal

Cite this: DOI: 10.1039/d3qo02000b

Novel A-*seco*-nortriterpenoids from *Ganoderma cochlear* inhibiting Tau pathology by activating AMPK-ULK1-mediated autophagy†

Rong-Can Luo, [b,c,e] Yi Luo,[a,c] Da-Shuang Fang,[a,d] Yong-Gang Yao, [b,c] Ming-Hua Qiu *[a,c] and Xing-Rong Peng *[a,c]

Received 8th December 2023,
Accepted 29th January 2024

DOI: 10.1039/d3qo02000b

rsc.li/frontiers-organic

Ten structurally diverse *Ganoderma* triterpenoids, including one unprecedented highly degraded A-*seco*-nortriterpenoid, ganolearin A (**1**) with a 6/6/5-tricyclo structure containing a unique benzene ring, three new rearranged nortriterpenoids, ganolearin B (**2**) and ganolearin C (**3**) with a rare 3/5/6/5-fused skeleton, and ganolearin D (**4**) featuring a 3 → 10 γ-lactone ring and a five-membered carbon ring, and six analogues, ganolearates E–G and J (**5–7**, **10**), and ganolearic acids H (**8**) and I (**9**), were isolated from the fruiting bodies of *Ganoderma cochlear*. Their structures were elucidated by extensive 1D and 2D NMR spectroscopy, HRESIMS, X-ray crystallography and ECD calculation analysis. A plausible biosynthetic pathway for **1–4** was proposed. Furthermore, compounds **1–4** significantly inhibited Tau pathology by inducing autophagy mediated by the AMPK-ULK1 pathway, suggesting their potential against Alzheimer's disease (AD).

Introduction

Ganoderma has attracted significant attention from pharmacologists, chemists, and phytochemists because it has long been used as a traditional medicine in many countries[1,2] and is also an important source of meroterpenoids and lanostane triterpenoids with significant bioactivities and captivating structures.[3–9] In particular, *Ganoderma* triterpenoids (GTs) have been widely studied as the main active constituents of *Ganoderma* for their anti-tumor, anti-aging, liver-protective, and neuroprotective activities. Notably, previous studies have confirmed that GTs can reverse cognitive impairment,[10] attenuate LPS-induced inflammation and apoptosis,[11] promote amyloid-β clearance and inhibit Tau pathology through activating autophagy,[6,12] suggesting that GTs exhibit huge potential in the treatment of neurodegenerative diseases.

Alzheimer's disease (AD), the most pervasive neurodegenerative disease associated with aging, seriously threatens people's lives.[13,14] The extracellular amyloid plaques (which are composed of amyloid beta (Aβ) peptides) and the intraneuronal neurofibrillary tangles (NFTs) composed of the Tau (MAPT/Tau) protein are two hallmarks of AD pathology. Autophagy is a key process wherein cellular components such as corrupted organelles or unwanted protein materials aggregate in intracellular autophagosomes and undergo degradation or/and recycling in lysosomes.[15] Various studies prove that autophagy is the main route to remove Aβ or/and MAPT/Tau aggregates.[16,17] Thus, activation of autophagy might be a vital strategy for AD treatment.[18–22]

Therefore, we continue isolating structurally diverse GTs from the fruiting bodies of *Ganoderma cochlear* in order to provide more possibilities for the development of anti-AD drugs. Interestingly, ten new A-*seco*-norlanostane triterpenoids with five different skeletons were found (Fig. 1 and Fig. S1†). Their structures were confirmed by using 1D and 2D NMR spectroscopic data, X-ray single crystollography, and electronic circular dichroism (ECD) calculation methods. The further cellular assay indicated that compounds **1–4** induced autophagy by activating the AMPK-ULK1 signaling pathway (mTOR-independent

[a]State Key Laboratory of Phytochemistry and Plant Resources in West China, Kunming Institute of Botany, Chinese Academy of Sciences, Kunming 650201, China. E-mail: mhchiu@mail.kib.ac.cn, pengxingrong@mail.kib.ac.cn
[b]State Key Laboratory of Genetic Evolution & Animal Models, Key Laboratory of Animal Models and Human Disease Mechanisms of Yunnan Province, and KIZ-CUHK Joint Laboratory of Bioresources and Molecular Research in Common Diseases, Kunming Institute of Zoology, Chinese Academy of Sciences, Kunming 650204, China
[c]Kunming College of Life Science, University of Chinese Academy of Sciences, Kunming, Yunnan 650204, China
[d]College of Chemical Engineering, Institute of Pharmaceutical Engineering Technology and Application, Key Laboratory of Green Chemistry of Sichuan Institutes of Higher Education, Sichuan University of Science & Engineering, Zigong 643000, Sichuan, China
[e]Gansu Key Laboratory of Biomonitoring and Bioremediation for Environmental Pollution, and Key Laboratory of Cell Activities and Stress Adaptations, Ministry of Education, School of Life Sciences, Lanzhou University, Lanzhou 730000, China

†Electronic supplementary information (ESI) available: 1D and 2D NMR, MS spectra, X-ray crystallographic data, and ECD calculation of **3**. CCDC 2258231, 2201713 and 2258230. For ESI and crystallographic data in CIF or other electronic format see DOI: https://doi.org/10.1039/d3qo02000b

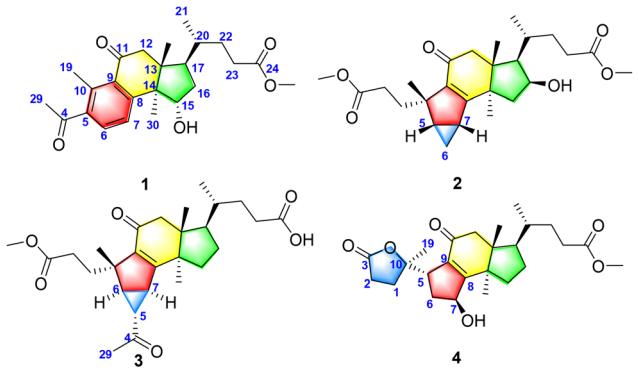

Fig. 1 Structures of compounds **1–4**.

pathway). Overall, the current data demonstrated that **1–4** could be potential compounds for AD therapy by inducing autophagy.

Results and discussion

Ganolearin A (**1**) has a molecular formula of $C_{24}H_{32}O_5$, as determined by HRESIMS at *m/z* 401.2322 $[M + H]^+$ (calcd 401.2323), indicating 9 degrees of unsaturation. The ^{1}H NMR spectroscopic data (Table S1†) of **1** showed four singlet methyls at δ_H 0.74, 1.21, 2.55, and 2.57, one doublet methyl at δ_H 0.90 (d, J = 6.4 Hz), one methoxyl at δ_H 3.68 (s), two aromatic methines at δ_H 7.47 (d, J = 7.9 Hz) and δ_H 7.54 (d, J = 7.9 Hz), and one oxygenated methine at δ_H 5.60 (dd, J = 5.1 and 9.5 Hz). In the ^{13}C-DEPT spectra of **1**, twenty-four carbon resonances were observed, comprising five methyls, one methoxyl, four methylenes, five methines, and nine quaternary carbons (two ketones, one ester carbonyl, and four aromatic quaternary carbons). The above data showed that compound **1** could be a norlanostane triterpenoid.

The HMBC correlations (Fig. 2) of H_3-18 with C-12, C-13, C-14, and C-17; of H_2-12 with C-11 (δ_C 200.4) and C-9 (δ_C 140.7); of H_3-21 with C-17, C-20, and C-22; and of H_2-22 and OMe (δ_H 3.68, s) with C-24 (δ_c 174.2), as well as a series of ^{1}H–^{1}H COSY correlations (Fig. 2) of H-15/H_2-16/H-17/H-20/H_2-22/H_2-23, indicated that compound **1** had similar C and D rings and side chains to those of fornicatin E.[23] Further analysis of the HMBC spectrum (Fig. 2) showed that H_3-30 correlated with C-13, C-14, C-15 (δ_C 74.1), and C-8 (δ_C 152.8); simultaneously, H-15 showed correlations with C-13, C-8, and C-17. The aforementioned information illustrated that the hydroxyl group was linked to C-15. These functionalities accounted for five degrees of unsaturation.

Except for a ketone carbonyl, the remaining 4 degrees of unsaturation were representative of another benzene ring, which was consistent with the observation of six aromatic signals at δ_H 7.47 (d, J = 7.9 Hz), δ_C 122.6; δ_H 7.54 (d, J = 7.9 Hz), δ_C 131.2; δ_C 131.2; δ_C 138.1; δ_C 140.7 and δ_C 152.8. The HMBC correlations (Fig. 2) of H_3-19 with C-5 (δ_C 131.2), C-9 (δ_C 140.7), and C-10 (δ_C 138.1), of H_3-29 with C-5 and C-4 (δ_C 203.9), of H-6 (δ_H 7.54, d, J = 7.9 Hz) with C-4, C-10, and C-8 (δ_C 152.8), and of H-7 (δ_H 7.47, d, J = 7.9 Hz) with C-5, C-9 (δ_C 140.7), and C-14 (δ_C 52.3) further confirmed that C-1, C-2, C-3, and C-28 were degraded and the B ring was aromatized. In the ROESY spectrum (Fig. 3) of **1**, H-15 correlated with H_3-18, indicating that 15-OH was α-oriented. Therefore, the structure of compound **1** was finally established.

The molecular formula of ganolearin B (**2**) was determined to be $C_{26}H_{38}O_6$ based on the positive HRESIMS at *m/z* 469.2564 $[M + Na]^+$ (calcd 469.2561), which indicated 8 degrees of unsaturation. The 1D NMR spectroscopic data (Table S1†) of **2** showed that the structure of **2** resembles that of ganolearic acid A,[24] except for the presence of an additional methoxyl and an oxymethine, and the absence of one methylene. The detailed comparison of the 1D NMR spectra of **2** and ganolearic acid A showed the replacement of the carboxyl at C-24 by a methyl ester carbonyl, which was confirmed by the HMBC correlations (Fig. 2) of OCH_3 (δ_H 3.71, s) with C-24 (δ_C 176.2) in **2**. Furthermore, the oxymethine proton (δ_H 4.71, dd, J = 12.9 and 5.9 Hz) showed HMBC correlations with C-13 (δ_C 48.1), C-14 (δ_C 48.2), C-15 (δ_C 40.9), and C-17 (δ_C 54.7), as well as ^{1}H–^{1}H COSY correlations (Fig. 2) of H_2-15/H-16/H-17/H-20/H_3-21, suggesting that C-15 was connected to a hydroxyl group. Thus, the planar structure of **2** was established.

The ROESY spectrum of **2** showed the correlations of H-16/H_3-30, indicating that 16-OH was β-oriented (Fig. 3). In

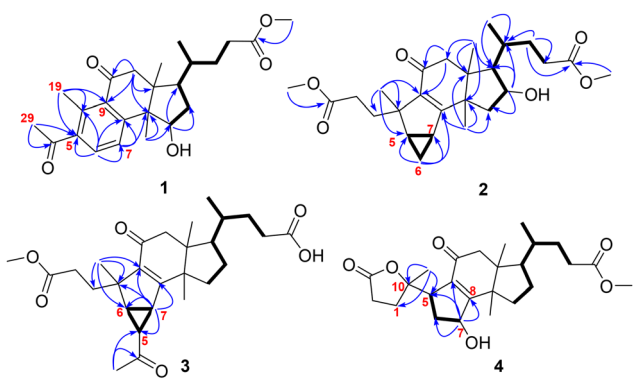

Fig. 2 Selected HMBC (H → C) and ^{1}H–^{1}H COSY (H–H) correlations of compounds **1–4**.

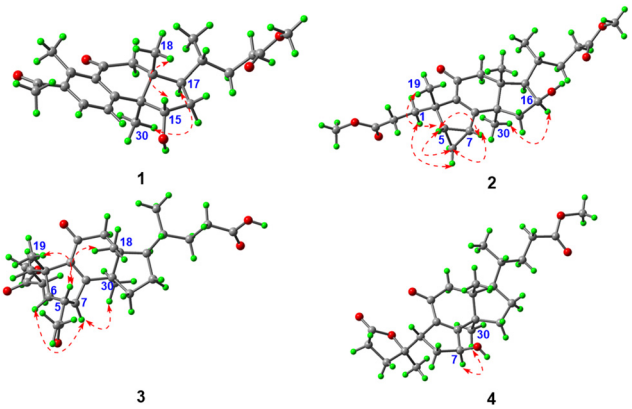

Fig. 3 Key ROESY (↷) correlations of compounds **1–4**.

addition, the ROESY correlations of H_3-19/H-5/H-7/H-6a and of H-6b/H_3-30 were observed, indicating that the relative configurations of H-5 and H-7 were β, opposite to 5α and 7α of ganolearic acid A.[24] Furthermore, the X-ray crystallographic data (Fig. 4A) proved that the absolute configuration of **2** was 5*S*,7*R*,10*S*,13*R*,14*R*,16*S*,17*R*,20*R*. Thus, the structure of compound **2** including the stereostructure was finally determined.

The HRESIMS of ganolearin C (**3**) showed an $[M - H]^-$ peak at *m*/*z* 457.2602 $[M - H]^-$ (calcd 457.2596), indicating a molecular formula of $C_{27}H_{38}O_6$ for 3 and 9 degrees of unsaturation. Its 1D NMR spectroscopic data (Table S1†) were similar to those of ganolearic acid A,[24] suggesting that compound **3** was also a norlanostane triterpenoid with a 3/4/6/4-tetracyclic skeleton. However, an additional methyl group (δ_H 2.25, s; δ_C 30.5) and a ketone group (δ_C 205.4) were present in **3**; meanwhile, one methylene in ganolearic acid A was replaced by a methine (δ_H 1.62, m; δ_C 35.7) in **3**. Furthermore, the HMBC spectrum (Fig. 2) of **3** showed the correlations of the methyl protons (δ_H 2.25, s) with the ketone carbonyl (δ_C 205.4) and methine (δ_C 35.7), of the methine proton (δ_H 1.62, m) with C-6 (δ_C 39.2), C-10 (δ_C 49.7), and C-8 (δ_C 171.8), of H-6 (δ_H 2.04, m) with C-10 (δ_C 49.7), C-9 (δ_C 135.6), and C-19 (δ_C 22.5), and of H-7 (δ_H 2.47, m) with C-9 and C-14 (δ_C 49.7). Meanwhile, the ^1H–^1H COSY correlations (Fig. 2) of H-5/H-6/H-7 illustrated that C-5 was linked with an acetyl group. The ROESY correlations (Fig. 3) of H-5/H_3-18/H_3-19 and H-6/H-7/H_3-30 indicated that H-5 was β-oriented; in contrast, H-6 and H-7 were α-oriented. Furthermore, the ECD calculation method was used to confirm its absolute configuration. As shown in Fig. 4B, the ECD curve of 5*R*,6*S*,7*R*,10*S*,13*R*,14*R*,17*R*,20*R*-3 corresponds to the experimental CD curve. Therefore, the structure of **3** was established.

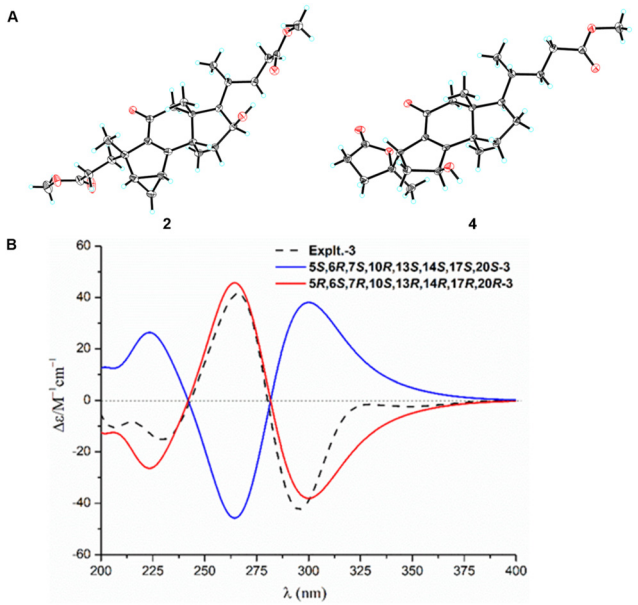

Fig. 4 (A) X-ray crystallographic structures of compounds **2** and **4**. (B) Calculated and experimental CD curves of compound **3**.

Ganolearin D (**4**) has a molecular formula of $C_{25}H_{36}O_6$, which was determined using HRESIMS at *m*/*z* 471.2143 $[M + K]^+$ (calcd 471.2143) with 8 degrees of unsaturation. It had similar 1D NMR spectroscopic data to those of ganocochlearic acid A[25] except that an oxymethine replaced the methylene in **4**. Furthermore, the oxymethine proton (δ_H 5.36, t, J = 7.3 Hz) showed the HMBC correlations of C-5 (δ_C 48.5), C-6 (δ_C 38.5), C-8 (δ_C 174.1), C-9 (δ_C 133.7), and C-14 (δ_C 49.8), which indicated that the hydroxyl group was located at C-7. The ROESY correlation of H-7/H_3-30 proved the β-configuration of 7-OH. The X-ray crystallographic data (Fig. 4A) further confirmed that the absolute configuration of **4** was 5*S*,7*S*,10*R*,13*R*,14*R*,17*R*,20*R*. Finally, the structure of **4** was determined.

Compounds **1**–**4** were highly degraded and rearranged lanostane-triterpenoids, in which major changes were present in the B ring. Biosynthetically, fornicatin A[23] was deduced to be a plausible biosynthetic precursor, which was further oxidized to a 4-oxo derivative (intermediate **I**). Subsequently, the

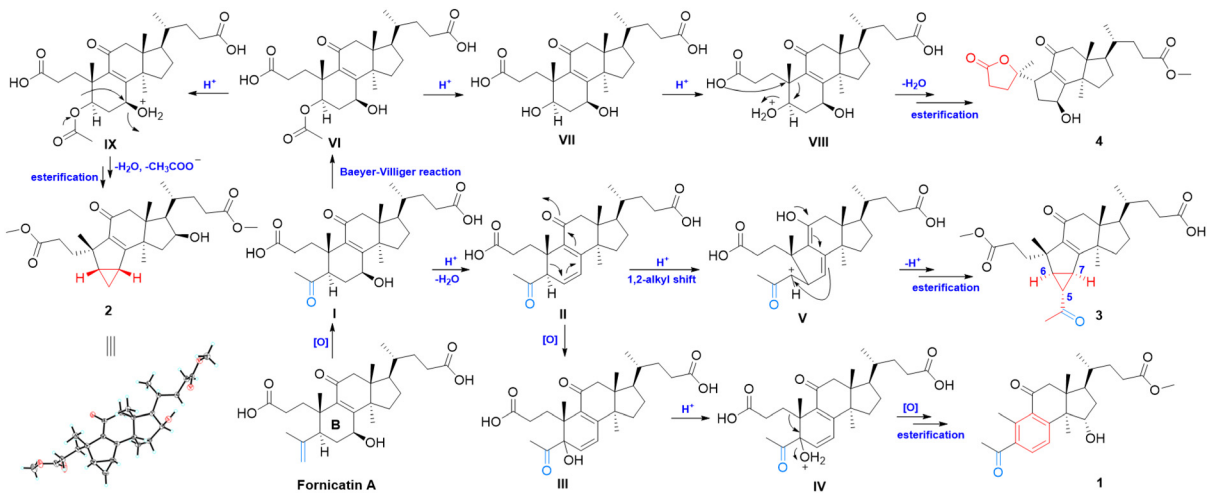

Scheme 1 A plausible biosynthetic pathway for **1**–**4**.

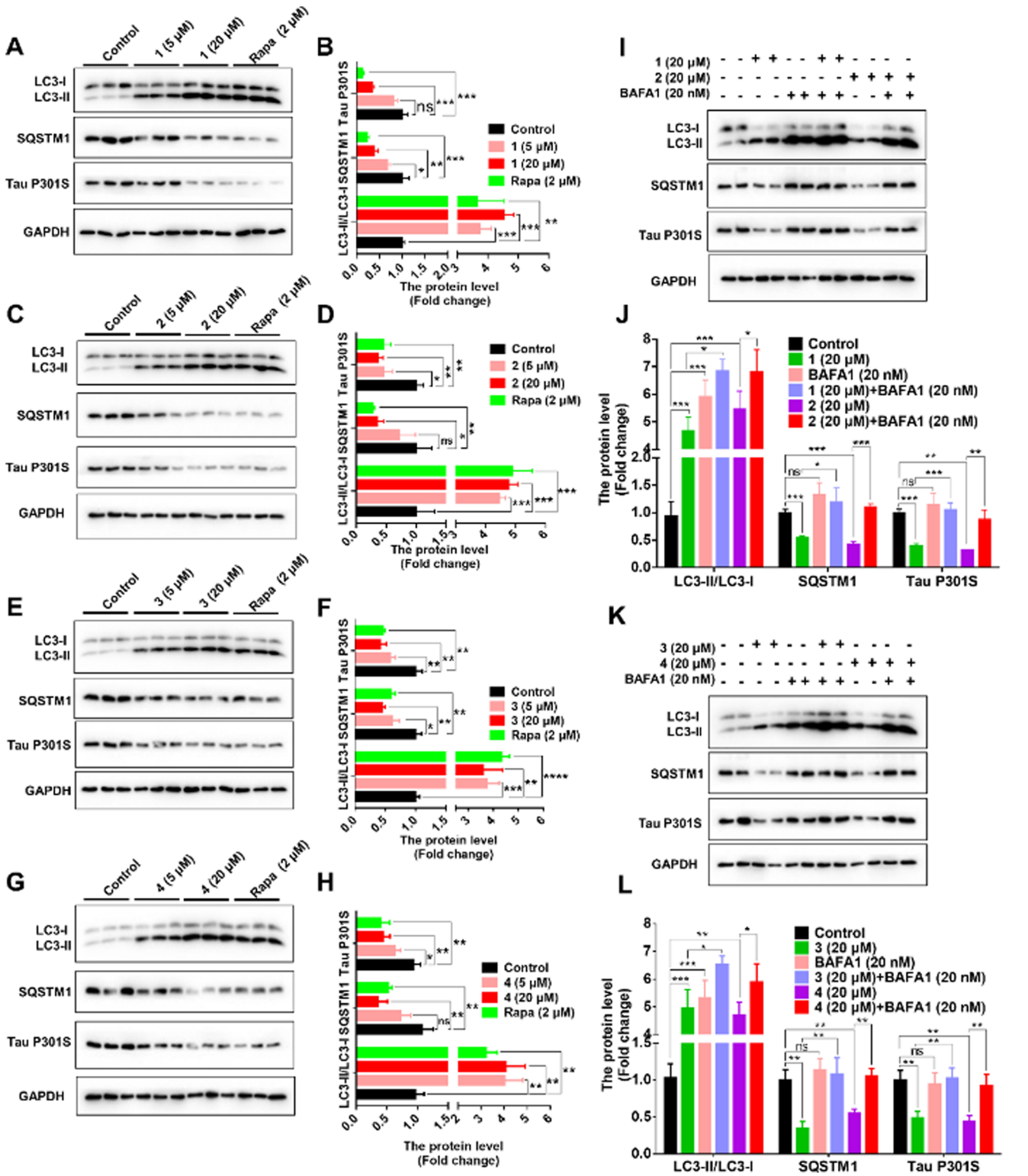

Fig. 5 Inhibition effects of compounds **1**–**4** on Tau pathology by activating autophagy in SH-SY5Y MAPT cells. (A–H) Western blotting assays showing the protein levels of autophagy markers LC3-II/LC3-I and SQSTM1, and Tau P301S in the SH-SY5Y MAPT cells treated with or without the compounds. (I, K) Western blotting analyses of autophagy markers LC3-II/LC3-I and SQSTM1, and Tau P301S in cell lysates from SH-SY5Y MAPT cells treated with BAFA1 (bafilomycin A1, 20 nM), **1**–**4** (20 μM) or both (BAFA1 and **1**, BAFA1 and **2**, BAFA1 and **3**, or BAFA1 and **4**). (A–L) A representative western blotting result (A, C, E, G, I and K) and quantification of the respective protein levels (B, D, F, H, J and L) based on 3 independent experiments. DMSO (dimethyl sulfoxide), used as a solvent for the compounds, served as the control. Rapamycin (Rapa) was used as a positive control. Relative protein abundance was normalized to GAPDH. ns, not significant; *, $P < 0.05$; **, $P < 0.01$; ***, $P < 0.001$; ****, $P < 0.0001$; one-way ANOVA with Tukey's *post-hoc* test. Bars represent mean ± SD.

dehydration of 7-OH and H-6 happened, forming **II** containing a long-range unsaturated fraction (C-6/C-7/C-8/C-9/C-11). The allylic oxidation at C-5 led to the formation of **III**, which was dehydrated to form a carbocation (**IV**). The further aromatization of ring B occurred by losing the C-1/C-2/C-3 moiety. The oxidation of C-15 and the esterification of 24-COOH finally resulted in the formation of compound **1**. In addition, **II** can also be transformed to **V** *via* a 1,2-alkyl shift under acidic conditions. The cyclization between C-7 and C-5 and esterification at C-3 resulted in the formation of **3**.

VI was obtained from **I** through a Baeyer–Villiger reaction. Then, the hydrolyzation of **VI** led to the formation of **VII** and the carbocation at C-5 was obtained as **VIII** through the dehydration of 5-OH because of the acid. Meanwhile, the cleavage of C-10/C-9 and the linkage of C-9/C-5 resulted in the formation of a carbocation at C-10. Simultaneously, 3-COOH attacked C-10 to form 3 → 10 γ-lactone (compound **4**). Additionally, the dehydration of 7-OH occurred under the acidic conditions, forming a carbocation (C-7). C-5 further attacked C-7, resulting in the formation of a unique three-membered ring accompanied by the deacetyloxy group. Both 3-COOH and 24-COOH were finally esterified to obtain compound **2** (Scheme 1).

It is well known that autophagy is a promising therapeutic strategy against tauopathy for promoting the clearance of Tau.[26] In our present study, compounds **1–4** could significantly induce autophagy and show no toxicities in SH-SY5Y mCherry-GFP-LC3 cells, at concentrations of 5 and 20 μM (Fig. S4 and S5†). Then, the human MAPT mutant MAPT-p.P301S was stably expressed in SH-SY5Y cells (named SH-SY5Y MAPT cells).[6] In the SH-SY5Y MAPT cells treated with **1–4**, an increased protein level of the lipidated (PE-conjugated) form of MAP1LC3/LC3 (microtubule-associated protein 1 light chain 3; LC3-II/LC3-I) and a decreased protein level of SQSTM1 (sequestosome 1) in a dose-dependent manner were observed (Fig. 5A–H).

Meanwhile, compounds **1–4** reduced the Tau P301S level in SH-SY5Y MAPT cells (Fig. 5A–H). Furthermore, BAFA1 (bafilo-

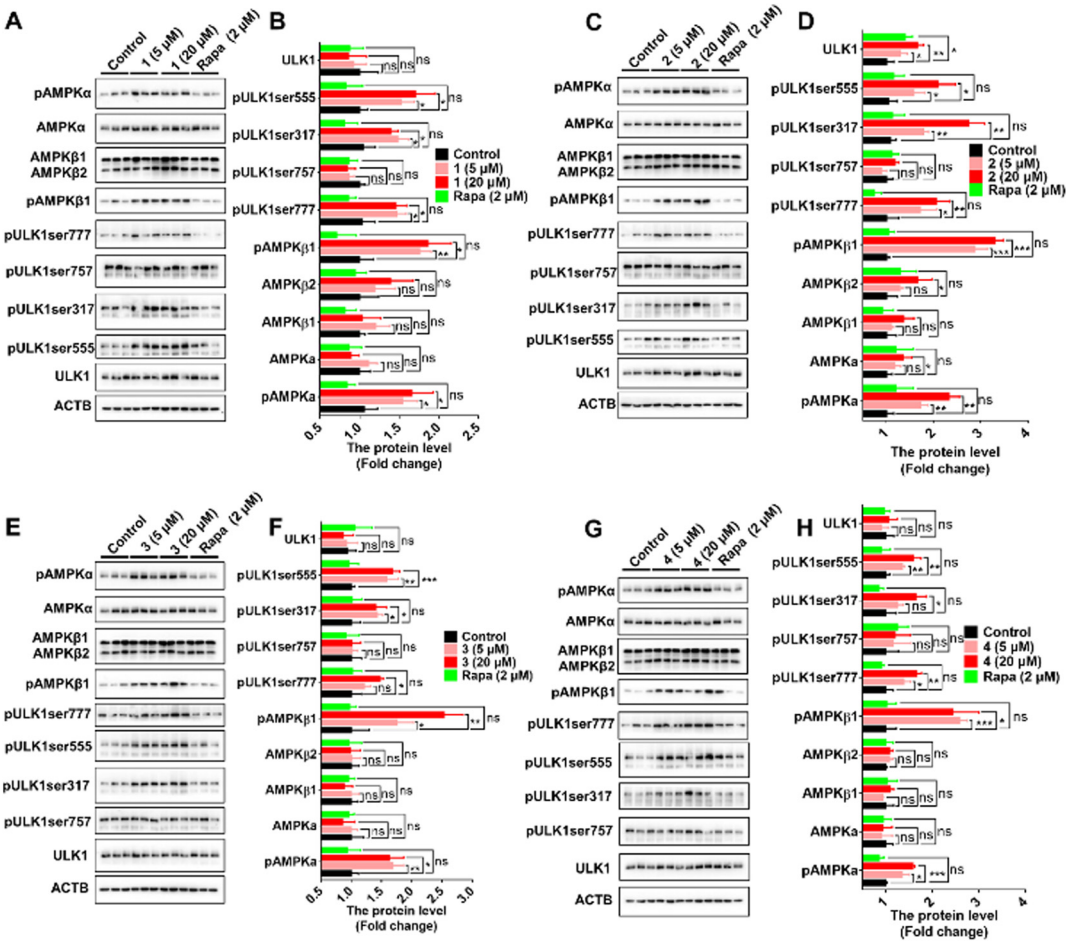

Fig. 6 Compounds **1–4** activate the AMPK-ULK1 pathway. (A–H) Western blotting assays showing the protein levels of pAMPKα, AMPKα, pAMPKβ1, AMPKβ1, AMPKβ2, pULK1ser777, pULK1ser757, pULK1ser555 and ULK1 in the SH-SY5Y MAPT cells treated with or without the compounds. (A–H) A representative western blotting result (A, C, E and G) and quantification of the respective protein levels (B, D, F and H) based on 3 independent experiments. Relative protein abundance was normalized to ACTB. ns, not significant; *, $P < 0.05$; **, $P < 0.01$; ***, $P < 0.001$; one-way ANOVA with Tukey's *post-hoc* test. Bars represent mean ± SD.

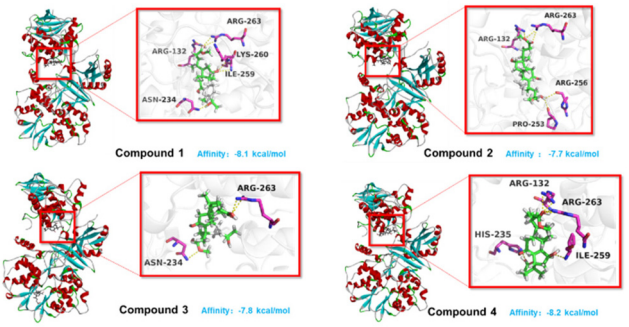

Fig. 7 The molecular docking results of compounds **1–4** with AMPK (PDB: 4CFH).

mycin A1), an inhibitor of the vacuolar(v)-type ATPase resulting in the blockage of autophagosome–lysosome fusion and accumulation of LC3-II,[27] was further used to demonstrate the role of autophagy induced by **1–4** in MAPT/Tau clearance in SH-SY5Y MAPT cells. Treatment with BAFA1 (20 nM) alone raised LC3-II/LC3-I, but with no significant effect on Tau P301S. BAFA1 could reverse the decreased levels of Tau P301S induced by compounds **1–4** (Fig. 5I–L). These results illustrated that compounds **1–4** reduce Tau P301S by activating autophagy.

Furthermore, we investigated the mechanism by which compounds **1–4** regulate autophagy. First, we checked whether these compounds would affect the mTOR activity. Rapamycin (an inhibitor of mTOR) is used as a positive control. Our results show that the activity of mTOR is not influenced by compounds **1–4** because of no significant changes in the protein levels of mTOR, pmTOR2448 and pmTOR2481 in SH-SY5Y MAPT cells (Fig. S6†).

As AMPK activation is one of the critical pathways involved in autophagy induction,[28] recent studies have reported that the inactivation of mTOR is not always necessary for autophagy.[29] AMPK can also directly phosphorylate and activate ULK1 at Ser317, Ser555, and Ser777 to initiate autophagy.[30] In the present study, compounds **1–4** significantly increased the protein levels of pAMPKα, pAMPKβ1, pULKser777, pULKser317, and pULKser555, whereas the protein levels of AMPKα, AMPKβ1, AMPKβ2, ULK1 and pULKser757 did not significantly change after treatment with compounds **1–4** in SH-SH5Y MAPT cells (Fig. 6). The further molecular docking revealed the interaction mode of compounds **1–4** with AMPK, and their binding energy ranged from −7.7 to −8.2 kcal mol^{-1}. Compounds **1–4** bound the key domain of AMPK containing ARG263 (Fig. 7), which affects AMPK phosphorylation. These results suggest that compounds **1–4** induce autophagy by activating the AMPK-ULK1 pathway rather than the mTOR-dependent signaling pathway.

Conclusions

In summary, we isolated ten A-*seco*-nortriterpenoids with six different types of skeletons from *G. cochlear*, of which compound **1** is the first example of a 6/6/5-tricyclic-hexanortriterpenoid containing a unique aromatic ring. Although **2** and **3** have similar skeletons, combined analysis of their detailed structures and stereochemistry suggests that they could be derived *via* different biosynthetic pathways. The autophagy process is mainly regulated through mTOR-dependent and mTOR-independent signaling pathways.[28] Previous research studies showed that GTs reverse cognitive impairment by suppressing PI3K/AKT/mTOR expression.[10] However, in our study, compounds **1–4** could significantly reduce Tau pathology by activating autophagy mediated by the AMPK-ULK1 pathway rather than the mTOR-dependent pathway, indicating that GTs with different skeletons can exhibit anti-neurodegeneration *via* multiple targets and signaling pathways. Meanwhile, these results also provide scientific evidence for the application of *Ganoderma* in anti-neurodegenerative diseases.

Experimental section

General experimental procedures

Silica gel (200–300 mesh, Qingdao Marine Chemical, Inc.), Lichroprep RP-18 (40–63 μm, Fuji) and Sephadex LH-20 (20–150 μm, Pharmacia) were used for column chromatography. Methanol, chloroform, ethyl acetate, acetone, petroleum ether, *n*-hexane and 2-propanol were purchased from Tianjin Chemical Reagents Co. (Tianjin, China). A Shimadzu UV-2401PC spectrometer was used for recording ultraviolet (UV) spectra. A Horiba SEPA-300 polarimeter was used for optical rotations. A Chirascan instrument was used for recording CD spectra. A Bruker AV-600 MHz spectrometer (Bruker, Zurich, Switzerland) was used for recording nuclear magnetic resonance (NMR) spectra and tetramethyl chlorosilane (TMS) was used as an internal standard for chemical shifts. Electrospray ionization mass spectrometry (ESIMS) and HRTOF-ESIMS spectra were recorded using an API QSTAR Pulsar spectrometer. A Bruker Tensor-27 instrument with KBr pellets was used for recording IR spectra. An Agilent 1100 series instrument equipped with an Agilent ZORBAX SB-C18 column (5 μm, 9.6 mm × 250 mm) was used for high-performance liquid chromatography (HPLC) separation.

Fungal materials

Ganoderma cochlear samples (44 kg) were purchased in December 2020 from the Traditional Chinese Medicine Market in Kunming, Yunnan, China, which was identified by Prof. Yang Zhuliang, Kunming Institute of Botany, Chinese Academy of Sciences (voucher no. 20202501).

Extraction and isolation

G. cochlear samples (44 kg) were extracted three times with 95% ethanol (EtOH) (80 L × 3) under reflux (3 h per extraction). The combined ethanol extracts were evaporated under reduced pressure. The residue (4 kg) was suspended in H_2O and extracted with ethyl acetate (EtOAc). The volume of the combined EtOAc extracts (1.5 kg) was reduced to one-third under

reduced pressure. The residue was fractionated by using a silica gel column (CH_2Cl_2–MeOH, 100 : 0, 80 : 1, 50 : 1, 20 : 1, 10 : 1, and 5 : 1, v/v): fractions I–VI.

Fraction III (523 g) was further fractioned by using a silica gel column with CH_2Cl_2–acetone as the mobile phase (100 : 0 → 10 : 1), yielding five subfractions (Fr. III-1 → Fr. III-5). Fr. III-3 (37 g) was further subjected to an Rp-18 column (MeOH-H_2O = 35% → 100%, v/v) to afford eight subfractions. Furthermore, Fr. III-3-1 (304 mg) was separated by using a silica gel column (petroleum ether–ethyl acetate) to obtain five parts (1a–1e). Then, Fr. III-3-1a (42 mg) was purified by semi-preparative HPLC (CH_3CN–H_2O = 41%, v/v, flow rate: 3 mL min^{-1}) to yield compound **9** (11.8 mg, t_R = 36.5 min). Fr. III-3-1b (54 mg) was subjected to semi-preparative HPLC (CH_3CN–H_2O = 36%, v/v, flow rate: 3 mL min^{-1}) to obtain compound **7** (7.2 mg, t_R = 32.6 min). Similarly, compounds **6** (5.7 mg, t_R = 23.9 min) and **4** (7.8 mg, t_R = 33.3 min) were respectively obtained from Fr. III-3-1c (93 mg) and Fr. III-3-1d (35 mg) by semi-preparative HPLC (CH_3CN–H_2O = 55% and 53%, v/v, flow rate: 3 mL min^{-1}). Fr. III-3-2 (502 mg) was further subjected to LH-20 (MeOH) to afford six subfractions (2a–2f), of which Fr. III-3-2c was purified to yield compound **10** (8.2 mg, t_R = 43.8 min, t_R = 43.8 min) by semi-preparative HPLC (CH_3CN–H_2O = 40%, v/v, flow rate: 3 mL min^{-1}). Additionally, Fr. III-3-2d was subjected to semi-preparative HPLC (CH_3CN–H_2O = 40%, v/v, flow rate: 3 mL min^{-1}) to obtain compound **1** (5.8 mg, t_R = 34.5 min). Compound **5** (6.1 mg, t_R = 43.8 min) was isolated from Fr. III-3-2e by semi-preparative HPLC (CH_3CN–H_2O = 40%, v/v, flow rate: 3 mL min^{-1}).

Fr. III-4 (35 g) was subjected to a silica gel column (CH_2Cl_2-MeOH = 80 : 1, 50 : 1, 20 : 1, 10 : 1, 5 : 1, v/v) to obtain five fractions: Fr. III-4a–Fr. III-4e. Fr. III-4b was subjected to LH-20 (MeOH) to obtain five subfractions (4b-1–4b-5). Fr. III-4b-3 was purified by semi-preparative HPLC (CH_3CN–H_2O = 55%, v/v, flow rate: 3 mL min^{-1}) to obtain compound **2** (5.4 mg, t_R = 33.8 min). Similarly, 4b-4 and 4b-5 were respectively subjected to semi-preparative HPLC (CH_3CN–H_2O = 42%, v/v, flow rate: 3 mL min^{-1}) to yield compounds **8** (31.7 mg, t_R = 36.5 min) and **3** (13.2 mg, t_R = 49.3 min).

Ganolearin A (1). White powder (MeOH); $[\alpha]_D^{24}$ 22.75 (*c* 0.16, MeOH); UV (MeOH); λ_{max} (log ε): 201 (3.72), 234 (3.88), and 297 (2.87); ^{1}H NMR and ^{13}C NMR data: see Table S1;† HRMS (ESI-TOF) *m*/*z*: 401.2322 $[M + H]^+$ (calcd for $C_{24}H_{33}O_5$, 401.2323).

Ganolearin B (2). White powder (MeOH); $[\alpha]_D^{20}$ + 51.13 (*c* 0.13, MeOH); UV (MeOH) λ_{max} (log ε): 277 (2.09), 195 (2.03); ^{1}H NMR and ^{13}C NMR data: see Table S1;† HRMS (ESI-TOF) *m*/*z*: 469.2564 $[M + Na]^+$ (calcd for $C_{26}H_{38}O_6Na$, 469.2561).

Ganolearin C (3). White powder (MeOH); $[\alpha]_D^{24}$−53.39 (*c* 0.23, MeOH); UV (MeOH); λ_{max} (log ε): 202 (3.68), and 273 (3.80); ^{1}H NMR and ^{13}C NMR data: see Table S1;† HRMS (ESI-TOF) *m*/*z*: 457.2602 $[M - H]^-$ (calcd for $C_{27}H_{37}O_6$, 457.2596).

Ganolearin D (4). White powder (MeOH); $[\alpha]_D^{24}$12.67 (*c* 0.18, MeOH); UV (MeOH); λ_{max} (log ε): 202 (3.25), and 256 (3.33); ^{1}H NMR and ^{13}C NMR data: see Table S1;† HRMS (ESI-TOF) *m*/*z*: 471.2143 $[M + K]^+$ (calcd for $C_{25}H_{36}O_6K$, 471.2143).

Ganolearate E (5). White powder (MeOH); $[\alpha]_D^{24}$97.07 (*c* 0.13, MeOH); UV (MeOH); λ_{max} (log ε): 202 (3.72), and 257 (3.77); ^{1}H NMR and ^{13}C NMR data: see Table S1;† HRMS (ESI-TOF) *m*/*z*: 490.3162 $[M + NH_4]^+$ (calcd for $C_{28}H_{40}O_6NH_4$, 490.3163).

Ganolearate F (6). White powder (MeOH); $[\alpha]_D^{23}$7.61 (*c* 0.16, MeOH); UV (MeOH); λ_{max} (log ε): 201 (3.72), 234 (3.88), and 297 (2.87); ^{1}H NMR and ^{13}C NMR data: see Table S1;† HRMS (ESI-TOF) *m*/*z*: 497.2511 $[M + Na]^+$ (calcd for $C_{27}H_{38}O_7Na$, 497.2510).

Ganolearate G (7). White powder (MeOH); $[\alpha]_D^{23}$ + 17.74 (*c* 0.10, MeOH); UV (MeOH); λ_{max} (log ε): 258 (2.98), 201 (2.77); ^{1}H NMR and ^{13}C NMR data: see Table S1;† HRMS (ESI-TOF) *m*/*z*: 513.2821 $[M + Na]^+$ (calcd for $C_{28}H_{42}O_7Na$, 513.2823).

Ganolearic aicd H (8). White powder (MeOH); $[\alpha]_D^{23.9}$20.56 (*c* 0.25, MeOH); UV (MeOH); λ_{max} (log ε): 203 (3.58), 254 (3.58), and 270 (3.57); ^{1}H NMR and ^{13}C NMR data: see Table S2;† HRMS (ESI-TOF) *m*/*z*: 473.2550 $[M - H]^-$ (calcd for $C_{27}H_{37}O_7$, 473.2545).

Ganolearic acid I (9). White powder (MeOH); $[\alpha]_D^{23}$8.95 (*c* 0.05, MeOH); UV (MeOH); λ_{max} (log ε): 260 (2.57), 202 (2.78); ^{1}H NMR and ^{13}C NMR data: see Table S2;† HRMS (ESI-TOF) *m*/*z*: 445.2586 $[M + H]^+$ (calcd for $C_{26}H_{37}O_6$, 445.2585).

Ganolearate J (10). White powder (MeOH); $[\alpha]_D^{24}$ 14.59 (*c* 0.17, MeOH); UV (MeOH); λ_{max} (log ε): 202 (3.29), and 260 (3.54); ^{1}H NMR and ^{13}C NMR data: see Table S2;† HRMS (ESI-TOF) *m*/*z*: 511.2673 $[M + Na]^+$ (calcd for $C_{28}H_{40}O_7Na$, 511.2666).

The crystallographic data (excluding structure factor tables) for the reported structures have been deposited at the Cambridge Crystallographic Data Center (CCDC) as supplementary publication no. CCDC 2258231 for **2** and CCDC 2201713 for **4**, and CCDC 2258230 for **5**. Copies of the data can be obtained free of charge from the CCDC, 12 Union Road, Cambridge CB2 1EZ, UK [fax: + 44(0)1223 336 033; e-mail: deposit@ccdc.cam.ac.uk).‡

‡**Crystal data for 2**: $C_{26}H_{38}O_6$, M = 446.56, a = 10.8614(3) Å, b = 36.7053(9) Å, c = 6.0922(2) Å, α = 90°, β = 90°, γ = 90°, V = 2428.78(12) Å^3, T = 150.(2) K, space group $P21212$, Z = 4, μ(Cu Kα) = 0.689 mm^{-1}, 15579 reflections measured, 4402 independent reflections (R_{int} = 0.0887). The final R_1 value was 0.0335 ($I > 2\sigma(I)$). The final w$R(F^2)$ value was 0.0856 ($I > 2\sigma(I)$). The final R_1 value was 0.0597 (all data). The final w$R(F^2)$ value was 0.0960 (all data). The goodness of fit on F^2 was 1.099. Flack parameter = −0.05(6).

Crystal data for 4: $C_{25}H_{36}O_6$, M = 432.54, a = 7.7089(3) Å, b = 8.1588(3) Å, c = 36.7130(13) Å, α = 90°, β = 90°, γ = 90°, V = 2309.08(15) Å^3, T = 150.(2) K, space group $P212121$, Z = 4, μ(Cu Kα) = 0.709 mm^{-1}, 16444 reflections measured, 4355 independent reflections (R_{int} = 0.0890). The final R_1 value was 0.0449 ($I > 2\sigma(I)$). The final w$R(F^2)$ value was 0.1142 ($I > 2\sigma(I)$). The final R_1 value was 0.0600 (all data). The final w$R(F^2)$ value was 0.1190 (all data). The goodness of fit on F^2 was 1.146. Flack parameter = 0.07(8).

Crystal data for 5: $C_{28}H_{40}O_6$, M = 472.60, a = 8.1802(3) Å, b = 13.5202(4) Å, c = 11.2870(4) Å, α = 90°, β = 92.6960(10)°, γ = 90°, V = 1246.94(7) Å^3, T = 150.(2) K, space group $P1211$, Z = 2, μ(Cu Kα) = 0.701 mm^{-1}, 22359 reflections measured, 4854 independent reflections (R_{int} = 0.0348). The final R_1 value was 0.0311 ($I > 2\sigma(I)$). The final w$R(F^2)$ value was 0.1015 ($I > 2\sigma(I)$). The final R_1 value was 0.0312 (all data). The final w$R(F^2)$ value was 0.1017 (all data). The goodness of fit on F^2 was 0.978. Flack parameter = −0.09(3).

ECD calculation method for 3

The theoretical calculations of compound **3** were performed using Gaussian 16.[31] Conformational analysis was carried out. The optimized conformation geometries and thermodynamic parameters of all conformations are provided. The conformers were optimized at the B3LYP/6-311G (d,p) level. The theoretical calculation of ECD was performed using time-dependent density functional theory (TDDFT) at the B3LYP/6-311G(d,p) level in MeOH with the PCM model. The ECD spectra of compound **3** were obtained by weighing the Boltzmann distribution rate of each geometric conformation.

Cell culture and treatment

The SH-SY5Y mCherry-GFP-LC3 and SH-SY5Y MAPT cells generated in our previous study were used.[6] These cells were maintained in Dulbecco's modified Eagle's medium (DMEM) supplemented with 10% fetal bovine serum (FBS), 1 × MEM nonessential amino acid solution (Gibco, 11140050), 100 U ml^{-1} penicillin and 100 mg ml^{-1} streptomycin at 37 °C in a humidified atmosphere incubator with 5% CO_2 and 95% humidity, as described in our previous studies.[6,32] Cells were seeded in prewarmed growth medium in 6-well plates or 12-well plates. Rapamycin (InvivoGen, trl-rap) or bafilomycin A1 (tlrl-baf) was used as a positive control. Drugs were applied directly to the culture medium for treatment, and cells were harvested at 24 h after treatment for further analysis.

Cell counting kit-8 (CCK-8) cell viability assay

For cell viability assays, the CCK-8 kit was used as described by the manufacturer (Beyotime, C0038). Briefly, the SH-SY5Y mCherry-GFP-LC3 cells were plated at 4×10^3 cells per well in 96-well culture plates. Twenty-four hours after treatment with compounds **1–10**, the CCK-8 reagent was added into each well. Cell viability was evaluated by gauging the optical density at 450 nm.

Flow cytometry analysis

SH-SY5Y mCherry-GFP-LC3 cells, that is, the SH-SY5Y cells stably expressing a triple fusion protein (red fluorescent protein (mCherry), green fluorescent protein (GFP) and the autophagosome marker LC3),[33,34] which can directly reflect the strength of autophagic flux, were used in detecting the bioactivities of compounds **1–10**. These cells show yellow fluorescence due to the co-expression of red mCherry and green GFP in the absence of autophagy. When the autophagy process goes well, autophagosomes and lysosomes fuse to form autolysosomes, and the acidic lysosomal environment quenches the fluorescence of acid-sensitive GFP, while mCherry is not affected, and then the autolysosomes show red fluorescence. Therefore, red fluorescence in the cells can indicate the formation of autolysosomes.[34–36] A higher red fluorescence and a lower green fluorescence indicate a smoother flux from autophagosomes to autolysosomes. SH-SY5Y mCherry-GFP-LC3 cells were cultured in DMEM supplemented with 10% fetal bovine serum (Gibco-BRL, 10099–141) at 37 °C in an incubator with 5% CO_2 and 95% humidity. These cells were cultured in 12-well plates for 24 h, and the compound was added directly to the culture medium (5 μM and 20 μM). Twenty-four hours after the treatment, the cells were harvested and fixed using 4% paraformaldehyde. The fixed cells were then subjected to a flow cytometry test to check the autophagic flux. Data were analyzed using FlowJo software (FLOWJO, LLC).

Western blot analysis

For western blotting, the method described in our previous studies was used.[22,32,37] In brief, the SH-SY5Y and SH-SY5Y MAPT cells were lysed with RIPA lysis buffer (Beyotime, P0013). The protein concentration was determined using the BCA protein assay kit (Beyotime, P0012). A total of 20 μg of protein was separated by 12% or 8% (vol/vol) SDS-polyacrylamide gel and electrophoretically transferred onto a polyvinylidene difluoride membrane (Bio-Rad, L1620177 Rev D). The membrane was soaked with 5% (wt/vol.) skim milk for 2 h at room temperature. The membrane was incubated with primary antibodies (ACTB [Beijing Zhong Shan-Golden Bridge Biological Technology Co., Ltd, TA-09], GAPDH, glyceraldehyde-3-phosphate dehydrogenase [Proteintech, 60004-1-Ig], LC3 [Proteintech, 14600-1-AP], phospho-AMPKβ1 (ser108) (E8N3N) [Cell Signaling Technology, 23021], AMPKα (D63G4) [Cell Signaling Technology, 5832], phospho-AMPKα (thr172) (D4D6D) [Cell Signaling Technology, 50081], AMPKβ1/2 (57C12) [Cell Signaling Technology, 4150], mTOR (7C10) [Cell Signaling Technology, 2983], phospho-mTOR (ser2448) (D9C2) [Cell Signaling Technology, 5536], phospho-mTOR (ser2481) [Cell Signaling Technology, 2974], phospho-ULK1 (ser757) (D7O6U) [Cell Signaling Technology, 14202], phospho-ULK1 (ser317) [Cell Signaling Technology, 37762], ULK1 (D8H5) [Cell Signaling Technology, 8054], phospho-ULK1 (ser555) [Cell Signaling Technology, 5869], phospho-ULK1 (ser777) [Sigma-Aldrich, ABC213], SQSTM1, sequestosome 1 [Elabscience, EAP3350] and Tau (D1M9X) [Cell Signaling Technology, 46687S]) overnight at 4 °C. After three washes with TBST (Tris-buffered saline [Cell Signaling Technology, 9997] with Tween 20 [0.1%; Sigma, P1379]), each lasting 5 min, the membranes were incubated for 1 h with the peroxidase-conjugated anti-mouse (474–1806) or antirabbit (474–1516) IgG (1 : 5000; KPL) at room temperature. The epitope was visualized using an ECL western blot detection kit (Millipore, WBKLS0500). ImageJ software (National Institutes of Health, Bethesda, Maryland, USA) was used for densitometric analysis. GAPDH or ACTB was used as a loading control for the densitometric analysis of the target protein.

Confocal laser scanning assay

The SH-SY5Y mCherry-GFP-LC3 cells were cultured overnight in DMEM supplemented with 10% FBS, 1 × MEM nonessential amino acid solution (Gibco, 11140050), 100 U ml^{-1} penicillin and 100 mg ml^{-1} streptomycin in a glass-bottom cell culture dish (NEST, 801001). For evaluating tandem fluorescent LC3 puncta, 24 h after treatment with rapamycin and compounds **1**, **2**, **3** or **4**, the cells were washed three times with PBS and

fixed with 4% paraformaldehyde. The fixed intact cells were observed using a FluoView 1000 confocal microscope (Olympus, America).

Statistics

Statistical analysis was performed using GraphPad Prism 8 software. The one-way ANOVA (analysis of variance) was performed using Tukey's *post hoc* test for comparison between the treated group and the control group, and the values were expressed as mean ± standard deviation (SD). A *P*-value <0.05 was considered statistically significant throughout the study.

Molecular docking

The crystal structure of the AMPK complex (PDB code: 4CFH) was used for preparing new docking templates through the Swiss-model server. The best configuration of small molecules was refined through energy minimization and molecular docking was performed using Autodock Vina with a center box: $x = -14.105$, $y = 38.735$, $z = -12.962$ and the dimensions: 72 × 82 × 64 Å. The docking results were analyzed and shown using Discovery Studio® Visualizer (BIOVIA, San Diego, USA) and PyMOL software (Schrödinger, LLC: NY, USA).[5]

Author contributions

M. H. Q. and X. R. P. designed this study. X. R. P. supervised the project. Y. L. and D. S. F. performed the isolation and structural analysis. X. R. P. performed the ECD calculation. X. R. P. and R. C. L. wrote the paper. R. C. L. performed cell assays and statistical analysis. Y. G. Y. and M. H. Q. revised the whole manuscript. All authors contributed to the discussion and interpretation of the results.

Conflicts of interest

There are no conflicts to declare.

Acknowledgements

This research work was supported by the National Natural Science Foundation of China (32170988 to R. C. L.), the Basic Research Program of Yunnan Province (202301AT070332 to X. R. P., 202201AW070010 and 202001AT070107 to R. C. L., 202003AD150009, and 202305AH340006), Yunnan Province Science and Technology Department (202305AH340005), the Original Innovation Project "from 0 to 1" of the Basic Frontier Scientific Research Program, CAS (ZDBS-LY-SM031 to R. C. L.), the Youth Innovation Promotion Association of CAS (2019383 to X. R. P. and 2021000011 to R. C. L.), the Young Scientific and Technological Talents Promotion Project of Yunnan Association for Science and Technology (2022000043 to R. C. L.), and the Yunnan Revitalization Talent Support Program "Young Talent" Project (XDYC-QNRC-2022-0480).

References

1 M. S. Swallah, P. Bondzie-Quaye, Y. Wu, A. Acheampong, F. L. Sossah, S. M. Elsherbiny and Q. Huang, Therapeutic potential and nutritional significance of *Ganoderma lucidum*-a comprehensive review from 2010 to 2022, *Food Funct.*, 2023, **14**, 1812–1838.

2 F. Kou, Y. Ge, W. Wang, Y. Mei, L. Cao, X. Wei, H. Xiao and X. Wu, A review of *Ganoderma lucidum* polysaccharides: Health benefit, structure-activity relationship, modification, and nanoparticle encapsulation, *Int. J. Biol. Macromol.*, 2023, **243**, 125199–125211.

3 X. R. Peng, S. B. Unsicker, J. Gershenzon and M. H. Qiu, Structural diversity, hypothetical biosynthesis, chemical synthesis, and biological activity of *Ganoderma* meroterpenoids, *Nat. Prod. Rep.*, 2023, **40**, 1354–1392.

4 X. R. Peng, R. C. Luo, H. G. Su, L. Zhou, X. Q. Ran, Y. R. Guo, Y. G. Yao and M. H. Qiu, (+/-)-Spiroganoapplanin A, a complex polycyclic meroterpenoid dimer from *Ganoderma applanatum* displaying potential against Alzheimer's disease, *Org. Chem. Front.*, 2022, **9**, 3093–3101.

5 X. R. Peng, H. G. Su, H. R. Wang, G. L. Hu, K. Hu, L. Zhou and M. H. Qiu, Applanmerotic acids A and B, two meroterpenoid dimers with an unprecedented polycyclic skeleton from *Ganoderma applanatum* that inhibit formyl peptide receptor 2, *Org. Chem. Front.*, 2021, **8**, 3381–3389.

6 X. R. Peng, R. C. Luo, X. Q. Ran, Y. R. Guo, Y. G. Yao and M. H. Qiu, Ganoapplins A and B with an unprecedented 6/6/6/5/6-fused pentacyclic skeleton from *Ganoderma* inhibit Tau pathology through activating autophagy, *Bioorg. Chem.*, 2023, **132**, 106375.

7 H. G. Su, H. F. Liang, G. L. Hu, L. Zhou, X. R. Peng, H. C. Bi and M. H. Qiu, Applanoids A-E as the first examples of C-15/C-20 Michael adducts in *Ganoderm*a, triterpenoids and their PXR agonistic activity, *Chin. J. Chem.*, 2022, **40**, 2633–2641.

8 Z. Wang, Y. Tang, R. Li, S. Tian, Y. Tang and D. Li, Bioinspired synthesis of cochlearol B and ganocin A, *Chin. Chem. Lett.*, 2023, DOI: **10.1016/j.cclet.2023.109247**.

9 A. D. Richardson, T. R. Vogel, E. F. Traficante, K. J. Glover and C. S. Schindler, Total synthesis of (+)-cochlearol B by an approach based on a catellani reaction and visible-light-enabled [2 + 2] cycloaddition, *Angew. Chem., Int. Ed.*, 2022, **61**, e202201213–e202201218.

10 A. Wang, C. Xiao, J. Zheng, C. Ye, Z. Dai, Q. Wu, J. Liu, P. Strappe and Z. Zhou, Terpenoids of *Ganoderma lucidum* reverse cognitive impairment through attenuating neurodegeneration via suppression of PI3K/AKT/mTOR expression in vivo model, *J. Funct. Foods*, 2020, **73**, 104142–104150.

11 R. W. Kou, Y. Q. Gao, B. Xia, J. Y. Wang, X. N. Liu, J. J. Tang, X. Yin and J. M. Gao, Ganoderterpene A, a new triterpenoid from *Ganoderma lucidum*, attenuates LPS-induced inflammation and apoptosis via suppressing MAPK and TLR-4/NF-kappaB pathways in BV-2 Cells, *J. Agric. Food Chem.*, 2021, **69**, 12730–12740.

12 L. F. Qi, S. Liu, Y. C. Liu, P. Li and X. Xu, Ganoderic acid A promotes amyloid-beta clearance (in vitro) and ameliorates cognitive deficiency in Alzheimer's disease (mouse model) through autophagy induced by activating Axl, *Int. J. Mol. Sci.*, 2021, **22**, 5559–5577.
13 J. Gaugler, B. James, T. Johnson, J. Reimer, M. Solis, J. Weuve, R. F. Buckley and T. J. Hohman, 2022 Alzheimer's disease facts and figures, *Alzheimers Dement.*, 2022, **18**, 700–789.
14 D. M. Wilson 3rd, M. R. Cookson, L. Van Den Bosch, H. Zetterberg, D. M. Holtzman and I. Dewachter, Hallmarks of neurodegenerative diseases, *Cell*, 2023, **186**, 693–714.
15 N. Mizushima and B. Levine, Autophagy in human diseases, *N. Engl. J. Med.*, 2020, **383**, 1564–1576.
16 B. L. Heckmann, B. J. W. Teubner, B. Tummers, E. Boada-Romero, L. Harris, M. Yang, C. S. Guy, S. S. Zakharenko and D. R. Green, LC3-associated endocytosis facilitates β-amyloid clearance and mitigates neurodegeneration in murine Alzheimer's disease, *Cell*, 2019, **178**, 536–551.
17 A. Wani, S. B. Al Rihani, A. Sharma, B. Weadick, R. Govindarajan, S. U. Khan, P. R. Sharma, A. Dogra, U. Nandi, C. N. Reddy, S. S. Bharate, G. Singh, S. B. Bharate, R. A. Vishwakarma, A. Kaddoumi and A. Kumar, Crocetin promotes clearance of amyloid-beta by inducing autophagy via the STK11/LKB1-mediated AMPK pathway, *Autophagy*, 2021, **17**, 3813–3832.
18 M. Eshraghi, M. Ahmadi, S. Afshar, S. Lorzadeh, A. Adlimoghaddam, N. R. Jalal, R. West, S. Dastghaib, S. Igder, S. R. N. Torshizi, A. Mahmoodzadeh, P. Mokarram, T. Madrakian, B. C. Albensi, M. J. Los, S. Ghavami and S. Pecic, Enhancing autophagy in Alzheimer's disease through drug repositioning, *Pharmacol. Ther.*, 2022, **237**, 108171–108208.
19 A. Di Meco, M. E. Curtis, E. Lauretti and D. Pratico, Autophagy dysfunction in Alzheimer's disease: mechanistic insights and new therapeutic opportunities, *Biol. Psychiatry*, 2020, **87**, 797–807.
20 I. Choi, M. Wang, S. Yoo, P. Xu, S. P. Seegobin, X. Li, X. Han, Q. Wang, J. Peng, B. Zhang and Z. Yue, Autophagy enables microglia to engage amyloid plaques and prevents microglial senescence, *Nat. Cell Biol.*, 2023, **25**, 963–974.
21 X. W. Zhang, X. X. Zhu, D. S. Tang and J. H. Lu, Targeting autophagy in Alzheimer's disease: Animal models and mechanism, *Zool. Res.*, 2023, **44**, 1132–1145.
22 R. C. Luo, L. Y. Su, G. Li, J. Yang, Q. Liu, L. X. Yang, D. F. Zhang, H. Zhou, M. Xu, Y. Fan, J. Li and Y. G. Yao, Activation of PPARA-mediated autophagy reduces Alzheimer disease-like pathology and cognitive decline in a murine model, *Autophagy*, 2020, **16**, 52–69.
23 X. R. Peng, J. Q. Liu, C. F. Wang, X. Y. Li, Y. Shu, L. Zhou and M. H. Qiu, Hepatoprotective effects of triterpenoids from *Ganoderma cochlear*, *J. Nat. Prod.*, 2014, **77**, 737–743.
24 X. R. Peng, Y. J. Huang, S. Y. Lu, J. Yang and M. H. Qiu, Ganolearic acid A, a hexanorlanostane triterpenoid with a 3/5/6/5-fused tetracyclic skeleton from *Ganoderma cochlear*, *J. Org. Chem.*, 2018, **83**, 13178–13183.
25 X. R. Peng, X. Wang, L. Zhou, B. Hou, Z.-L. Zuo and M. H. Qiu, Ganocochlearic acid A, a rearranged hexanorlanostane triterpenoid, and cytotoxic triterpenoids from the fruiting bodies of *Ganoderma cochlear*, *RSC Adv.*, 2015, **5**, 95212–95222.
26 M. Subramanian, S. J. Hyeon, T. Das, Y. S. Suh, Y. K. Kim, J. S. Lee, E. J. Song, H. Ryu and K. Yu, UBE4B, a microRNA-9 target gene, promotes autophagy-mediated Tau degradation, *Nat. Commun.*, 2021, **12**, 3291–3306.
27 D. C. Rubinsztein, A. M. Cuervo, B. Ravikumar, S. Sarkar, V. Korolchuk, S. Kaushik and D. J. Klionsky, In search of an "autophagomometer", *Autophagy*, 2009, **5**, 585–589.
28 J. Kim, M. Kundu, B. Viollet and K. L. Guan, AMPK and mTOR regulate autophagy through direct phosphorylation of Ulk1, *Nat. Cell Biol.*, 2011, **13**, 132–141.
29 C. M. Xie, X. Y. Liu, K. W. Y. Sham, J. M. Y. Lai and C. H. K. Cheng, Silencing of EEF2K (eukaryotic elongation factor-2 kinase) reveals AMPK-ULK1-dependent autophagy in colon cancer cells, *Autophagy*, 2014, **10**, 1495–1508.
30 P. J. Roach, AMPK → ULK1 → Autophagy, *Mol. Cell. Biol.*, 2011, **31**, 3082–3084.
31 M. Srebro-Hooper and J. Autschbach, Calculating natural optical activity of molecules from first principles, *Annu. Rev. Phys. Chem.*, 2017, **68**, 399–420.
32 R. C. Luo, Y. Fan, J. Yang, M. Ye, D. F. Zhang, K. Guo, X. Li, R. Bi, M. Xu, L. X. Yang, Y. Li, X. Ran, H. Y. Jiang, C. Zhang, L. Tan, N. Sheng and Y. G. Yao, A novel missense variant in ACAA1 contributes to early-onset Alzheimer's disease, impairs lysosomal function, and facilitates amyloid-beta pathology and cognitive decline, *Signal Transduction Targeted Ther.*, 2021, **6**, 325–341.
33 L. Y. Su, R. Luo, Q. Liu, J. R. Su, L. X. Yang, Y. Q. Ding, L. Xu and Y. G. Yao, Atg5- and Atg7-dependent autophagy in dopaminergic neurons regulates cellular and behavioral responses to morphine, *Autophagy*, 2017, **13**, 1496–1511.
34 X. Q. Ran, Q. Y. Lu, Y. Li, X. X. Pu, Y. Guo, M. R. Yuan, S. P. Guan, M. Sun, L. Jiao, Y. G. Yao, Y. T. Di, X. J. Hao and R. C. Luo, Euphejolkinolide A, a newabietane lactone from *Euphorbia peplus* L. with promising biological activity in activating the autophagy-lysosomal pathway, *Heliyon*, 2023, **9**, e13691–e13704.
35 T. E. Hansen and T. Johansen, Following autophagy step by step, *BMC Biol.*, 2011, **9**, 39–43.
36 S. Kimura, T. Noda and T. Yoshimori, Dissection of the autophagosome maturation process by a novel reporter protein, tandem fluorescent-tagged LC3, *Autophagy*, 2007, **3**, 452–460.
37 X. H. Tang, R. C. Luo, M. S. Ye, H. Y. Tang, Y. L. Ma, Y. N. Chen, X. M. Wang, Q. Y. Lu, S. Liu, X. N. Li, Y. Yan, J. Yang, X. Q. Ran, X. Fang, Y. Zhou, Y. G. Yao, Y. T. Di and X. J. Hao, Harpertrioate A, an A,B,D-*seco*-Limonoid with promising biological activity against Alzheimer's disease from twigs of *Harrisonia perforata* (Blanco) Merr, *Org. Lett.*, 2021, **23**, 262–267.

Electronic Supplementary Material (ESI) for Organic Chemistry Frontiers.

Novel A-*seco*-nortriterpenoids from *Ganoderma cochlear* inhibiting Tau pathology by activating AMPK-ULK1-mediated autophagy

Rong-Can Luo,[b,c,e] Yi Luo,[a,c] Da-Shuang Fang,[a,d] Yong-Gang Yao,[b,c] Ming-Hua Qiu[a,c*], Xing-Rong Peng[a,c*]

[a]*State Key Laboratory of Phytochemistry and Plant Resources in West China, Kunming Institute of Botany, Chinese Academy of Science, Kunming 650201, China*

[b]*Key Laboratory of Animal Models and Human Disease Mechanisms of the Chinese Academy of Sciences & Yunnan Province, and KIZ-CUHK Joint Laboratory of Bioresources and Molecular Research in Common Diseases, Kunming Institute of Zoology, Chinese Academy of Sciences, Kunming 650204, China*

[c]*Kunming College of Life Science, University of Chinese Academy of Sciences, Kunming 650204, China*

[d] *College of Chemical Engineering, Institute of Pharmaceutical Engineering Technology and Application, Key Laboratory of Green Chemistry of Sichuan Institutes of Higher Education, Sichuan University of Science & Engineering, Zigong 643000, Sichuan, China*

[e] *Gansu Key Laboratory of Biomonitoring and Bioremediation for Environmental Pollution, and Key Laboratory of Cell Activities and Stress Adaptations, Ministry of Education, School of Life Sciences, Lanzhou University, Lanzhou 730000, China*

Table of Content

1. Structural elucidation of compounds 5–10

The molecular formula of ganolearate E (**5**) (**Figure S1**) was determined to be $C_{28}H_{40}O_6$ on the basis of HRESIMS ion peak *m/z*: 490.3162 $[M + NH_4]^+$ (calcd. 490.3163). Its 1D NMR spectroscopic data (**Table S1**) showed similarity with those of cochlearic acid A with the only difference in the presence of an additional methoxyl at C-3, which was confirmed by the HMBC correlations (**Figure S2**) of OMe (δ_H 3.63, s) with C-3 (δ_C 174.1), of H_2-1 and H_2-2 with C-3, and of H_3-19 with C-1, C-5, and C-10. The further X-ray crystallographic analysis (**Figure S3**) proved that the absolute configuration of **5** was 5*S*,7*S*,10*S*,13*R*,14*R*,17*S*,20*S*. Thus, the structure of compound **5** was determined.

Comparison of molecular weight and 1D NMR spectroscopic data (**Table S1**) between **6** and **5** showed that compound **6** had a similar structure with **5**, except for the absence of the terminal double bond at C-4 and C-28 and the presence of an additional ketone carbonyl (δ_C 214.0). The HMBC correlations of H_3-29 with the ketone carbonyl and C-5 (δ_C 52.5), and of H_3-19 with C-1, C-5, and C-9 (δ_C 137.3) confirmed that C-4 was the ketone carbonyl. Subsequently, the ROESY correlation of H-7/H_3-30 proved that 7-OH was β-oriented. Finally, the structure of **6** (ganolearate F) was established.

Ganolearate G (**7**) had a molecular formula of $C_{28}H_{42}O_7$ determined by the HRESIMS *m/z*: 513.2821 $[M + Na]^+$ (calcd. 513.2823). Meanwhile, compound **7** showed similar 1D NMR spectra with those of compound **6**. However, an additional methoxyl group (δ_H 3.67, s; δ_C 51.4) was observed in 1D NMR spectra of **7**, rather than an oxygenated quaternary carbon in **6**. Furthermore, the methoxyl group showed HMBC correlation (**Figure S2**) with C-24 (δ_C 174.4), simultaneously, H_3-21 exhibited a doublet methyl signals at δ_H 0.89 (d, J = 6.4 Hz) in the ^{1}H NMR spectrum of **7**. Thus, we speculated that the methoxyl was connected to C-24 and the oxygenated quaternary carbon at C-20 was transformed into a methine. Therefore, the structure of **7** was confirmed.

According to the 1D NMR spectra (**Table S2**) of **8**, the structure of **8** resembled that of **7** except for the absence of a methoxyl at C-24 and a ketone carbonyl instead of the hydroxyl at C-7. The HMBC correlations of H_3-19 (δ_H 1.31, s) with C-5 (δ_C 52.5) and C-9 (δ_C 145.6), of H-5 (δ_H 3.05, t, J = 4.5 Hz) with C-10 (δ_C 39.2) and C-7 (δ_C 196.7), of H_3-21 (δ_H 0.88, d, J = 6.4 Hz) with C-20 (δ_C 35.6), C-17 (δ_C 49.0), and C-22 (δ_C 30.6), and of H_2-22 (δ_H 2.20, m; 2.46, m) with C-24 (δ_C 178.8) confirmed above deduction. Thus, the structure of **8** was determined and name as ganoclearic acid

H.

The molecular formula of compound **9** was determined to be $C_{26}H_{36}O_6$ based on the HRESIMS *m/z*: 445.2586 $[M + H]^+$ (calcd. 445.2585) with **9** degrees of unsaturation. Its ^1H NMR spectrum (**Table S2**) showed that three singlet methyl proton signals at δ_H 0.91 (s), δ_H 1.25 (s), δ_H 1.77 (s), one doublet methyl proton signal at δ_H 0.88 (d, J = 6.4 Hz), one methoxyl proton signal at δ_H 3.63 (s), one oxymethine proton signal at δ_H 4.59 (d, J = 5.2 Hz), and two terminal double bond proton signals at δ_H 4.84 (s) and δ_H 4.94 (s). except for the methoxyl, ^{13}C-DEPT NMR spectra of **9** showed 25 carbon resonances, which were assigned as four methyls, eight methylenes (one terminal double bond), four methines (one oxymethine), and nine quaternary carbons (one ester carbonyl, one carboxyl, one ketone, three olefiniccarbons, and one oxygenated carbon). These data suggested that compound **9** was a highly degraded lanostane triterpenoid and had a similar 7/6/5-tricyclo skeleton with that of cochlate B, which was confirmed by the HMBC correlations (**Figure S2**) of H_3-29 with C-4 (δ_C 145.8), C-28 (δ_C 114.7), and C-5 (δ_C 54.8), of H-5 (δ_H 2.75, m) with C-1 (δ_C 31.8), C-10 (δ_C 83.5), C-7 (δ_C 75.0), and C-19 (δ_C 36.0), of H-7 (δ_H 4.50, d, J = 5.2 Hz) with C-5, C-9, and C-10, C-14 (δ_C 50.8), and of H_2-19 with C-1, C-8 (δ_C 167.9), and C-11 (δ_C 201.2). However, combination the absence of two methylenes and the HMBC correlations (**Figure S2**) of H_3-21 (δ_H 1.16, d, J = 6.5 Hz) with C-17 (δ_C 47.7), C-20 (δ_C 45.1), and C-22 (δ_C 181.7), indicating that C-23 and C-24 were degraded. The ROESY correlations (**Figure S2**) of H-5/H_3-30/H-7, which demonstrated that H-7 was α-oriented. Therefore, the structure of **9** was established and named as ganoclearic acid I.

Ganolearate J (**10**) had a molecular formula of $C_{28}H_{40}O_7$ based on the HRESIMS *m/z*: 511.2673 $[M + Na]^+$ (calcd. 511.2666). Its 1D NMR spectroscopic data (**Table S2**) were similar with those of cochlate A with the difference in the absence of double bond at C-4 and C-28 and the presence of one oxygenated methylene (δ_H 3.77, d, J = 12.0 Hz, 4.21, d, J = 12.0 Hz; δ_C 64.9) and one quaternary carbon containing oxygen (δ_C 86.0). The detailed analysis of HMBC spectrum (**Figure S2**) of **10** showed the correlations of H_3-29 (δ_H 1.39, s) and H-5 (δ_H 2.36, d, J = 7.6 Hz) with the oxygenated methylene and quaternary carbons, suggesting that C-4 and C-28 were linked to hydroxyl group, respectively. Considering the molecular weight of **10** and the chemical shift of C-3 (δ_C 175.8), an ester bond between C-4 and C-3 was deduced. Finally, the structure of **10** was determined.

Table S1.[1]H and [13]C-DEPT NMR spectroscopic data of **1**–**7** (600/150 MHz,δ in *ppm*, *J* in Hz).

position	**1**[a]		**2**[a]		**3**[a]		**4**[a]		**5**[a]		**6**[b]		**7**[b]	
	δ_H	δ_C	δ_H	δ_C	δ_H	δ_C	δ_H	δ_C	δ_H	δ_C	δ_H	δ_C	δ_H	δ_C
1			1.58, m	31.7 CH_2	1.86, m; 2.19, m	34.8 CH_2	2.60, m; 1.84, m	31.7 CH_2	1.94, m; 2.16, m	33.1 CH_2	1.89, m; 2.13, m	35.1 CH_2	1.70, m; 2.31, m	33.6 CH_2
2			2.49, m	31.2 CH_2	2.26, m; 2.46, m	29.3 CH_2	2.10, m; 1.46, m	29.0 CH_2	1.97, m; 2.21, m	29.4 CH_2	2.20, m; 2.33, m	30.2 CH_2	2.54, m; 1.36, m	29.4 CH_2
3				174.8 C		174.0 C		176.7 C		174.1 C		175.9 C		173.8 C
4		203.9 C				205.4 C				147.0 C		214.0 C		217.1 C
5		131.2 C	1.44, m	27.2 CH	1.62, m	35.7 CH	3.15, d (8.8)	48.5 CH	2.13, m	44.7 CH	2.83, m	52.5 CH	2.92, m	50.9 CH
6	7.54, d (7.9)	131.2 CH	1.09, dd, (7.8, 4.3); 0.29, dd, (7.2, 4.3)	17.3 CH_2	2.04, m	39.2 CH	1.78, m 2.52, m	38.5 CH_2	2.06, m; 2.14, m	32.4 CH_2	2.49, m; 2.67, m	32.1 CH_2	2.10, m	28.8 CH_2
7	7.47, d (7.9)	122.6 CH	1.85, m	22.5 CH	2.47, m	34.0 CH	5.36, t (7.3)	77.2 CH	4.29, t (6.0)	66.8 CH	4.23, t (6.0)	64.3 CH	4.03, dd (10.4, 4.0)	62.5 CH
8		152.8 C		174.5 C		171.8 C		174.1 C		160.7 C		160.5 C		158.6 C
9		140.7 C		137.7 C		135.6 C		133.7 C		137.2 C		137.3 C		135.1 C
10		138.1 C		48.8 CH		49.7 C		89.3 C		39.1 C		38.6 C		37.4 C
11		200.4 C		197.5 C		196.3 C		198.9 C		199.1 C		202.0 C		200.1 C
12	2.58, d (18.8); 2.91, d (18.8)	52.3 CH_2	2.43, d, (7.4)	50.1 CH_2	2.38, d (17.6); 2.54, d (17.6)	49.2 CH_2	2.58, d (16.6) 2.69, d (16.6)	49.6 CH_2	2.62, d (17.4); 2.74, d (17.4)	51.1 CH_2	2.51, d (18.0); 2.77, d (18.0)	52.3 CH_2	2.43, d (18.8) 2.59, d (18.8)	51.4 CH_2
13		45.2 C		48.1 C		48.0 C		49.7 C		45.6 C		46.5 C		44.1 C
14		52.3 C		48.2 C		49.7 C		49.8 C		51.9 C		52.8 C		51.2 C
15	5.60, dd (9.5, 5.1)	74.1 CH	2.27, dd, (12.8, 7.9); 1.88, dd, (12.8, 4.8)	40.9 CH_2	1.52, m; 1.72, m	29.5 CH_2	1.25, m; 2.15, m	29.3 CH_2	1.47, m; 2.56, m	30.2 CH_2	1.43, m; 2.20, m	30.7 CH_2	1.25, m; 2.15, m	29.5 CH_2
16	2.20, m; 1.94, m	39.0 CH_2	4.71, dd, (12.9, 5.9)	72.0 CH	2.12, m; 1.51, m	27.4 CH_2	1.45, m; 2.05, m	27.8 CH_2	1.71, m; 1.89, m	21.7 CH_2	1.95, m; 1.65, m	22.8 CH_2	1.45, m; 2.03, m	27.3 CH_2
17	1.90 m	49.0 CH	1.73, m	54.7 CH	1.76, m	49.2 CH	1.72, m	48.9 CH	2.19 m	52.9 CH	2.34, m	54.3 CH	1.63, m	50.5 CH
18	0.74, s	18.5 CH_3	1.05, s	17.7 CH_3	0.77, s	17.4 CH_3	0.87, s	17.2 CH_3	1.11, s	19.2 CH_3	1.15, s	19.7 CH_3	1.10, s	17.7 CH_3
19	2.57, s	18.3	1.21, s	24.5	1.30, s	22.5	1.50, s	27.7	1.25 s	22.4	1.23, s	22.4	1.17, s	21.2

		CH_3		CH_3		CH_3		CH_3		CH_3		CH_3	CH_3
20	1.40, m	35.4 CH	1.75, m	29.5 CH	1.46, m	35.7 CH	1.45, m	35.5 CH		87.7 C		90.1 C	1.43, m	35.6 CH
21	0.90, d (6.4)	17.7 CH_3	0.94, d (5.6)	18.0 CH_3	0.89, d (6.3)	17.8 CH_3	0.91, d (6.4)	18.1 CH_3	1.45, s	26.0 CH_3	1.46, s	26.3 CH_3	0.89, d (6.4)	17.7 CH_3
22	1.31, m; 1.82, m	30.7 CH_2	2.46, m	30.3 CH_2	1.33, m; 1.83, m	30.7 CH_2	1.84, m; 1.34, m	31.0 CH_2	2.03, m; 2.17, m	32.4 CH_2	1.98, m; 2.23, m	34.5 CH_2	1.84, m; 1.34, m	30.8 CH_2
23	2.27, m;		1.97, m	30.7 CH_2	2.27, m; 2.40, m	31.0 CH_2	2.24, m; 2.48, m	31.1 CH_2	2.49, m	27.9 CH_2	2.45, m; 2.69, m	28.6 CH_2	2.24, m; 2.48, m	31.1 CH_2
24	2.39, m	31.0 CH_2		176.2 C		178.7 C		174.4 C		177.1 C		180.1 C		174.4 C
28		174.2 C							4.82, s; 5.05, s	114.9 CH				
29					2.25, s	30.5 CH_3			1.83, s	24.0 CH_3	2.21, s	31.3 CH_3	2.28, s	33.5 CH_3
30	2.55, s	30.9 CH_3	1.11, s	26.3 CH_3	1.16, s	24.7 CH_3	1.13, s	24.4 CH_3	1.17, s	25.7 CH_3	1.13, s	26.6 CH_3	0.99, s	26.1 CH_3
3-OCH_3	1.21, s	19.3 CH_3	3.66, s	51.8 CH_3	3.63, s	51.6 CH_3	3.67, s	51.5 CH_3	3.63, s	51.5 CH_3	3.63, s	52.1 CH_3	3.67, s	51.7 CH_3
24-OCH_3	3.68, s	51.6 CH_3	3.71, s	52.3 CH_3									3.67, s	51.4 CH_3

[a]: $CDCl_3$; [b]: CD_3OD

Table S2.[1]H and [13]C-DEPT NMR spectroscopic data of **8–10** (600/150 MHz, δ in ppm, J in Hz).

position	**8**[b]		**9**[b]		**10**[a]	
	δ_H	δ_C	δ_H	δ_C	δ_H	δ_C
1	2.07, m; 2.38, m	33.4 CH_2	1.83, m	31.8 CH_2	1.86, m	32.6 CH_2
2	2.29, m; 2.38, m	29.4 CH_2	2.40, m; 2.45, m	29.5 CH_2	2.47, m; 2.84, m	27.7 CH_2
3		173.7 C		175.9 C		175.8 C
4		20.9 C		145.8 C		86.0 C
5	3.05, t (4.5)	52.5 CH	2.75, m	54.8 CH	2.36, d (7.6)	54.6 CH
6	2.52, m; 2.66, m	36.8 CH_2	2.28, m	42.1 CH_2	1.67, m 2.72, m	36.2 CH_2
7		196.7 C	4.59, d (5.2)	75.0 CH	4.64, t (8.9)	74.4 CH
8		152.3 C		167.9 C		168.8 C
9		145.6 C		126.5 C		127.3 C
10		39.2 C		83.5 C		86.3 C
11		202.3 C		201.2 C		199.1 C
12	2.50, d (18.0); 2.63, d (18.0)	51.1 CH_2	2.44, d (17.6); 2.78, d (17.6)	49.9 CH_2	2.56, d (18.8)	48.4 CH_2
13		45.2 C		48.8 C		45.8 C
14		48.4 C		50.8 C		51.0 C
15	2.18, m; 2.07, m	31.7 CH_2	1.27, m; 1.90, m	30.8 CH_2	1.51, m; 1.91, m	31.0 CH_2
16	1.43, m; 2.05, m	27.6 CH_2	1.53, m; 2.07, m	27.7 CH_2	1.51, m; 2.07, m	26.6 CH_2
17	1.62 m	49.0 CH	2.32, m	47.7 CH	1.73, m	49.6 CH
18	0.95, s	17.7 CH_3	0.91, s	17.8 CH_3	0.87, s	17.2 CH_3
19	1.31 s	22.0 CH_3	2.06, m; 2.32, m	36.0 CH_2	3.09, d (14.8); 3.24, d (14.8)	29.6 CH_3
20	1.45, m	35.6 CH	2.42, m	45.1 CH	1.45, m	35.7 CH
21	0.88, d (6.4)	17.6 CH_3	1.16, d (6.5)	17.8 CH_3	0.89, d (6.5)	17.5 CH_3
22	2.20, m; 2.46, m	30.6 CH_2		181.7 C	2.24, m; 2.48, m	30.7 CH_2
23	1.89, m;2.08, m	31.1 CH_2			1.84, m; 1.34, m	31.1 CH_2
24		178.8 C				174.4 C
28			4.84, s; 4.94, s	114.7 CH_2	3.77, d (12.0); 4.21, d (12.0)	64.9 CH_2
29	2.23, s	32.6 CH_3	1.77, s	22.4 CH_3	1.39, s	24.9 CH_3
30	1.08, s	24.4 CH_3	1.25, s	26.5 CH_3	1.11, s	25.7 CH_3
OCH_3	3.67, s	51.8 CH_3	3.63, s	52.1 CH_3	3.67, s	51.5 CH_3

[a]: $CDCl_3$; [b]: CD_3OD

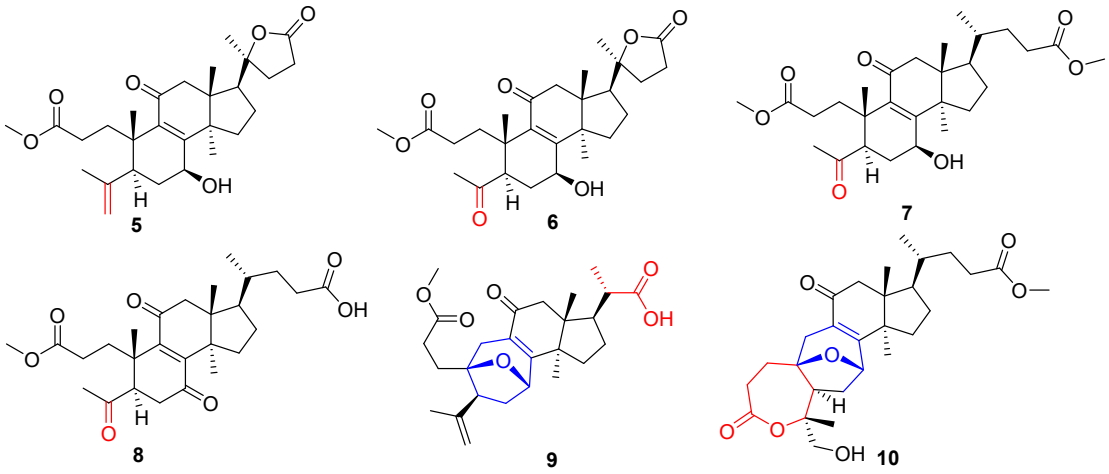

Figure S1. Structures of compounds **5**–**10**.

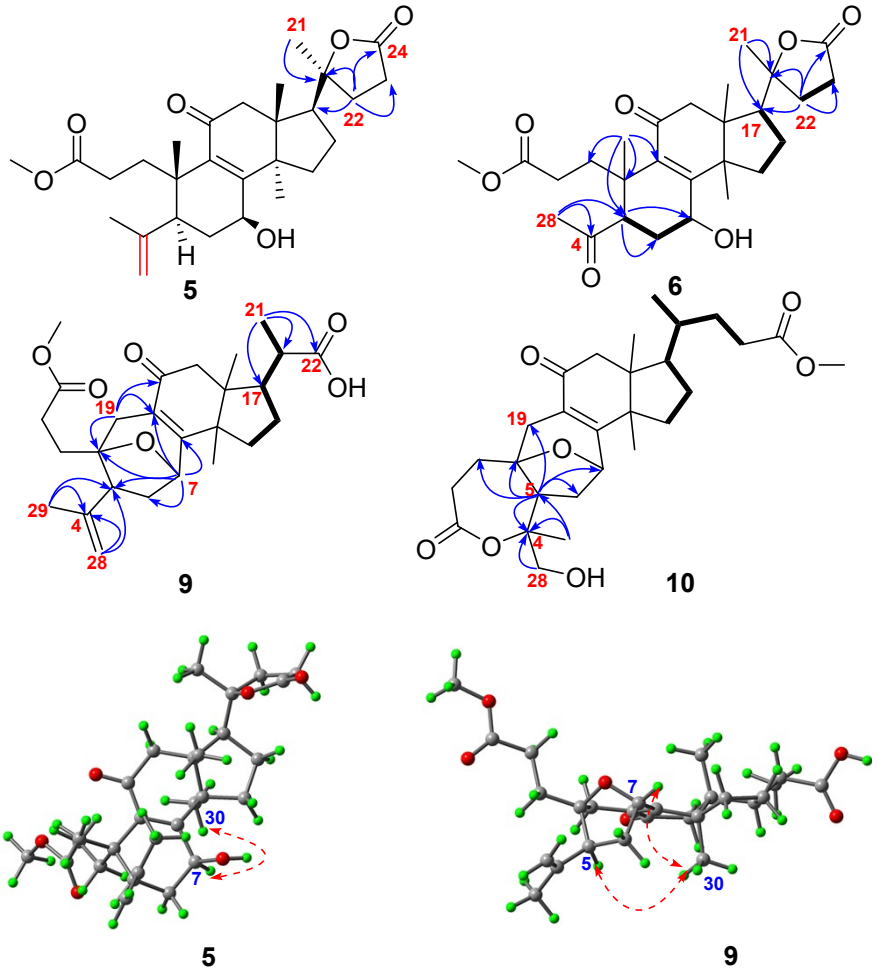

Figure S2. Selected HMBC (H→C), ^{1}H-^{1}H COSY (H-H) correlations of compounds **5, 6, 9, 10**, and ROESY (⇢⇠) correlations of compounds **5** and **9**.

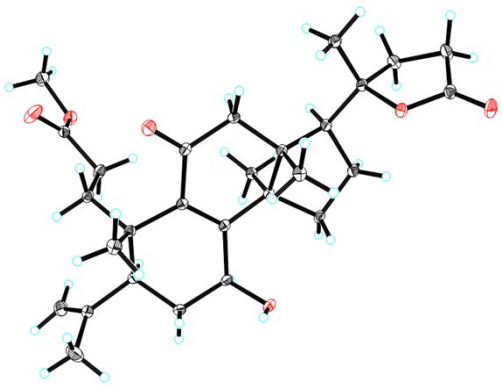

5

Figure S3. X-ray crystallographic structure of compound **5**.

2. Autophagy activation of compounds 1–10

In order to test whether compounds**1**–**10** would affect autophagy, we used the SH-SY5Y mCherry-GFP-LC3 cell line, which contains thetandem monomeric mCherry-GFP-tagged LC3 (mCherry-GFP-LC3) reporter and was reported in our previous study.[1] The mCherry-GFP-LC3 in autolysosomes displayed more stable red mCherry fluorescence in the acidic lysosome while the GFP signal was sensitive to the acidic condition.[2] DMSO (dimethyl sulfoxide) and rapamycin were respectively as blank and positive controls.[3] The flow cytometry analysis results showed that compounds **1**–**10** significantly increased the autophagic flux (**FigureS4A–B**). Moreover, all of them displayed no toxicities in SH-SY5Y mCherry-GFP-LC3 cells by using the CCK-8 assay (**FigureS5A**). Compounds **1**–**4** with diverse rearranged skeleton were further investigated for their effect on autophagy and anti-ADs. Treatment with compounds **1**–**4** can increase autophagic flux in the SH-SY5Y mCherry-GFP-LC3 cells, similar as rapamycin (**Figure S5B–C**). Collectively, these results demonstrated that compounds **1**–**4** can activate autophagy.

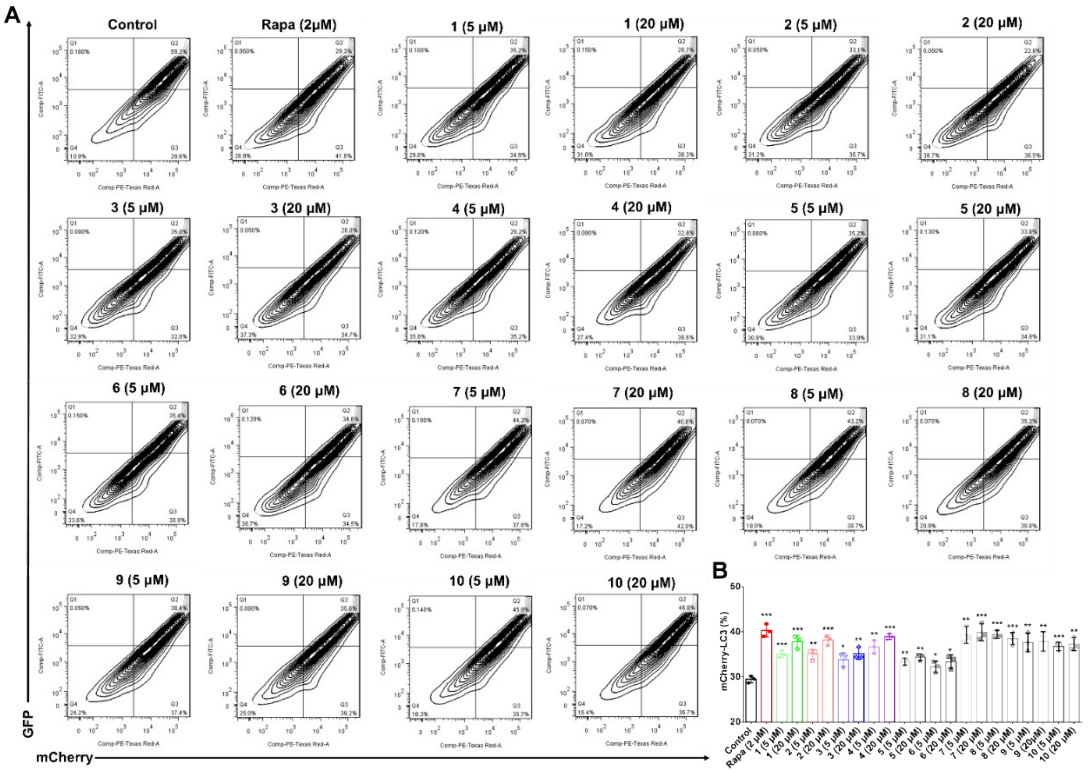

Figure S4. Compounds **1**–**10** induced autophagy in SH-SY5Y mCherry-GFP-LC3 cells by flow cytometry analysis. (A) Flow cytometry of SH-SY5Y mCherry-GFP-LC3 cells with or without drug treatment. The percentage of 10,000 cells expressing GFP or/and mCherry were counted. The Q1 area represents the proportion of cells with green fluorescence; the Q2 area represents the proportion of cells with yellow fluorescence; the Q3 area represents the proportion of cells with only red fluorescence; the Q4 area represents the proportion of cells showing no red and green fluorescence. (B) Quantification of the Q3 area in (A) based on 3 independent experiments. Record the proportion of cells that only emit red fluorescence in Q3 area under each treatment.

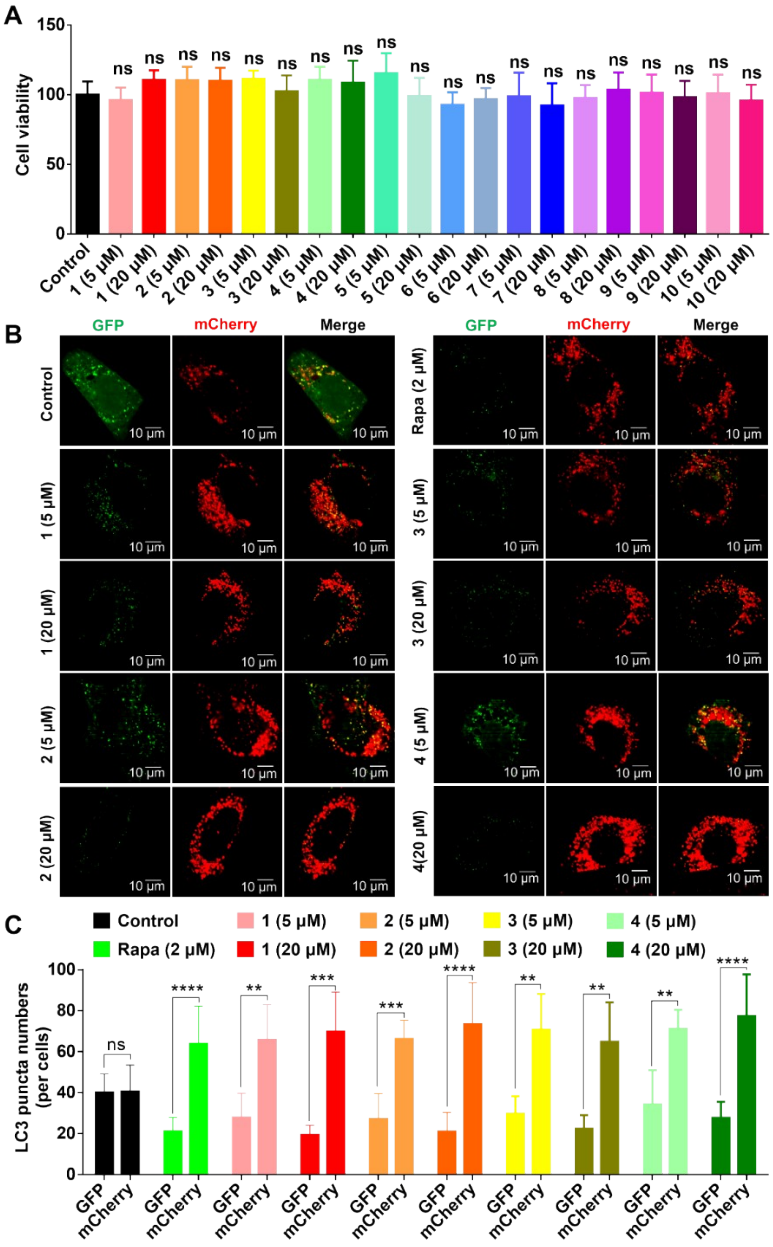

Figure S5. Increase of autophagic flux by compound **1**–**10** in SH-SY5Y mCherry-GFP-LC3 cells. (A) The CCK-8 assay showing the effects of compound **1**–**10** on cell viability. (B-C) Increased autophagic flux in response to **1**–**4** or Rapamycin (Rapa) treatment in SH-SY5Y mCherry-GFP-LC3 cells. (B) **1**–**4** treatment increased the maturation of autolysosomes as shown by the increased red puncta of mRFP-GFP-LC3 in cells, and this effect was similar to that of Rapamycin. (C) Quantification of LC3 puncta in (B) based on 3 independent experiments. ns, not significant; *, $P< 0.05$; **, $P< 0.01$; ***, $P< 0.001$; ****, $P< 0.0001$; one-way ANOVA with the Tukey's post-hoc test. Bars represent mean ± SD.

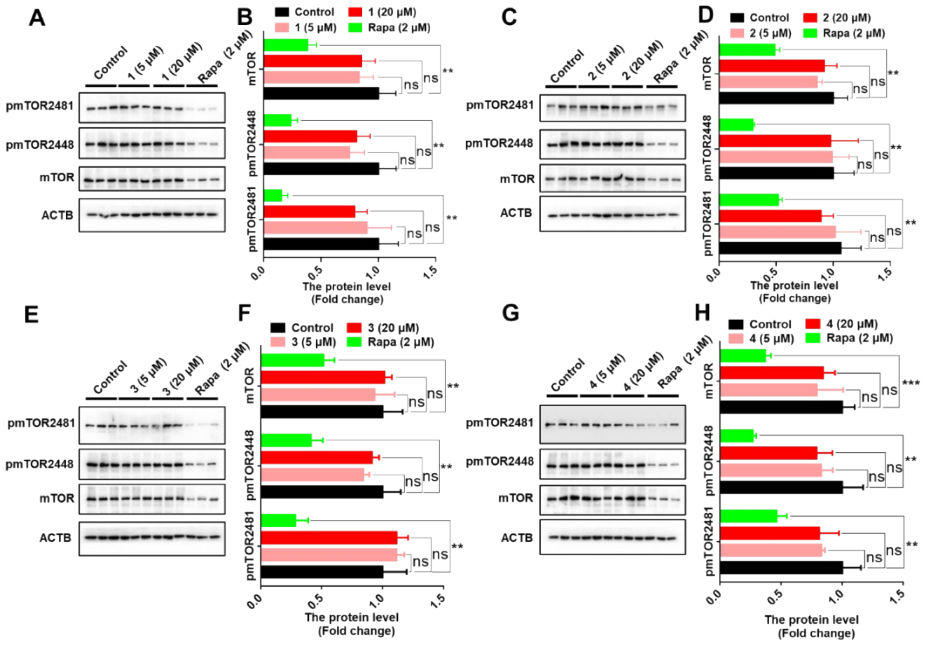

Figure S6. No inhibition effect of compounds **1**–**4** on mTOR. (A-H) Western blotting assays showing the protein levels of mTOR, pmTOR2448 and pmTOR2481 in the SH-SY5Y MAPT cells treated with or without compounds. Rapamycin (Rapa) as a positive control. (A-H) A representative Western blotting result (A, C, E, G) and quantification of respective protein levels (B, D, F, H) based on 3 independent experiments were presented. Relative protein abundance was normalized to ACTB. ns, not significant; **, $P< 0.01$; ***, $P< 0.001$; one-way ANOVA with the Tukey's post-hoc test. Bars represent mean ± SD.

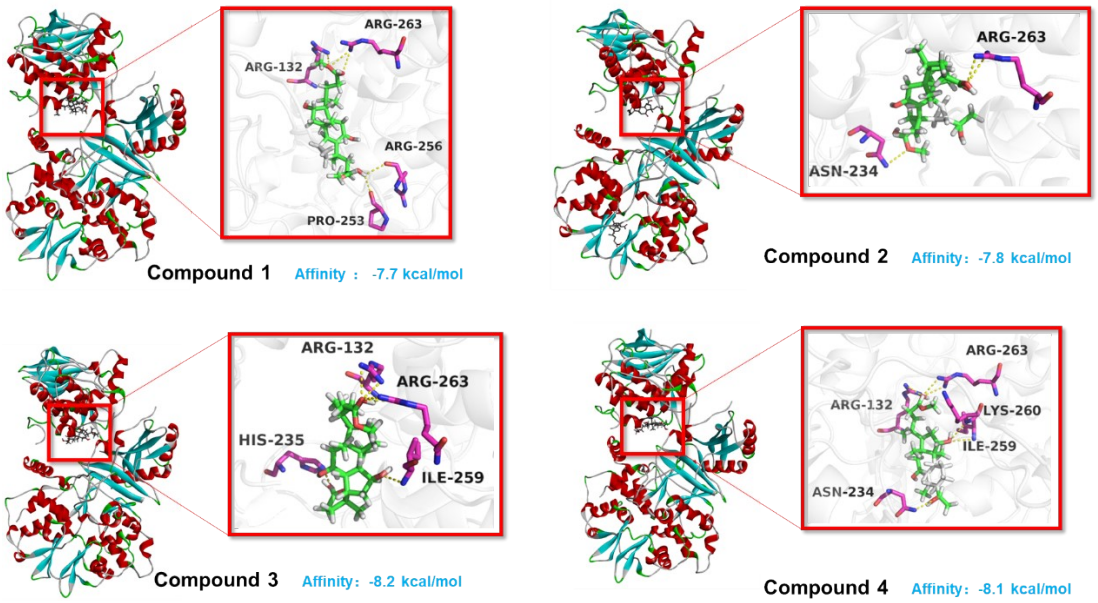

Figure S7. The molecular docking results of compounds **1**–**4** with AMPK (PDB: 4CFH).

NMR spectra of new compounds 1–10

Figure S8. ^{1}H NMR spectrum (600 MH, $CDCl_3$) of compound 1.

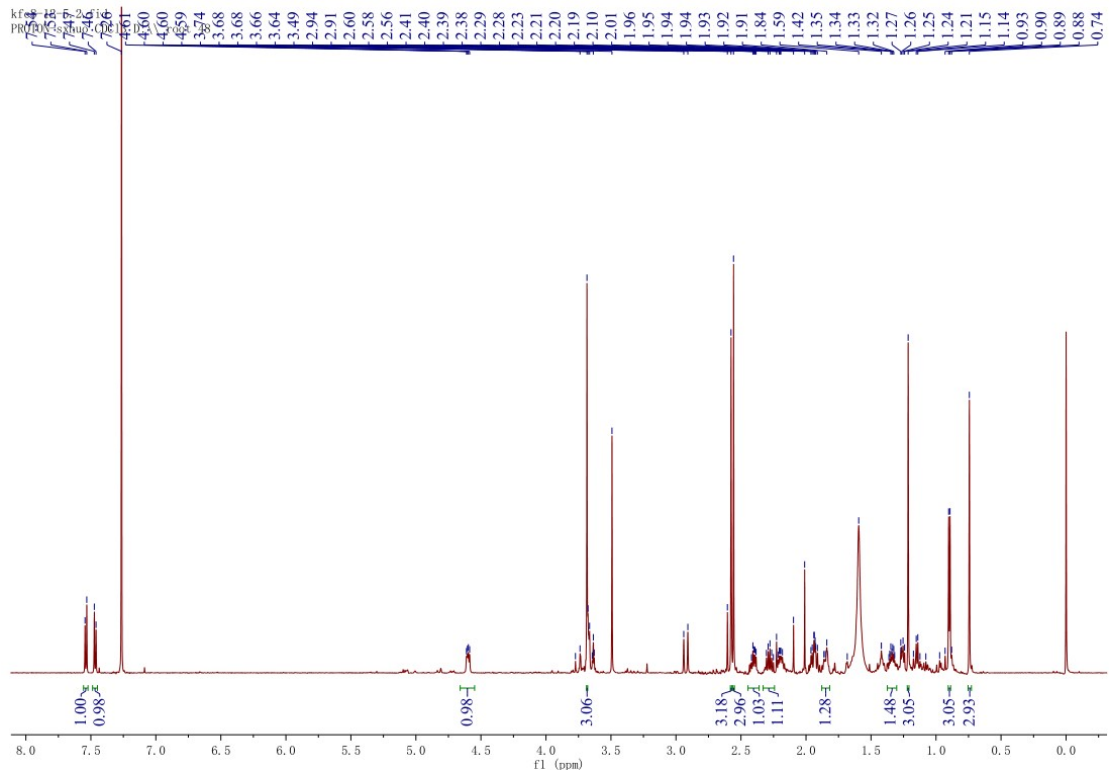

Figure S9. ^{13}C NMR spectrum (150 MH, $CDCl_3$) of compound 1.

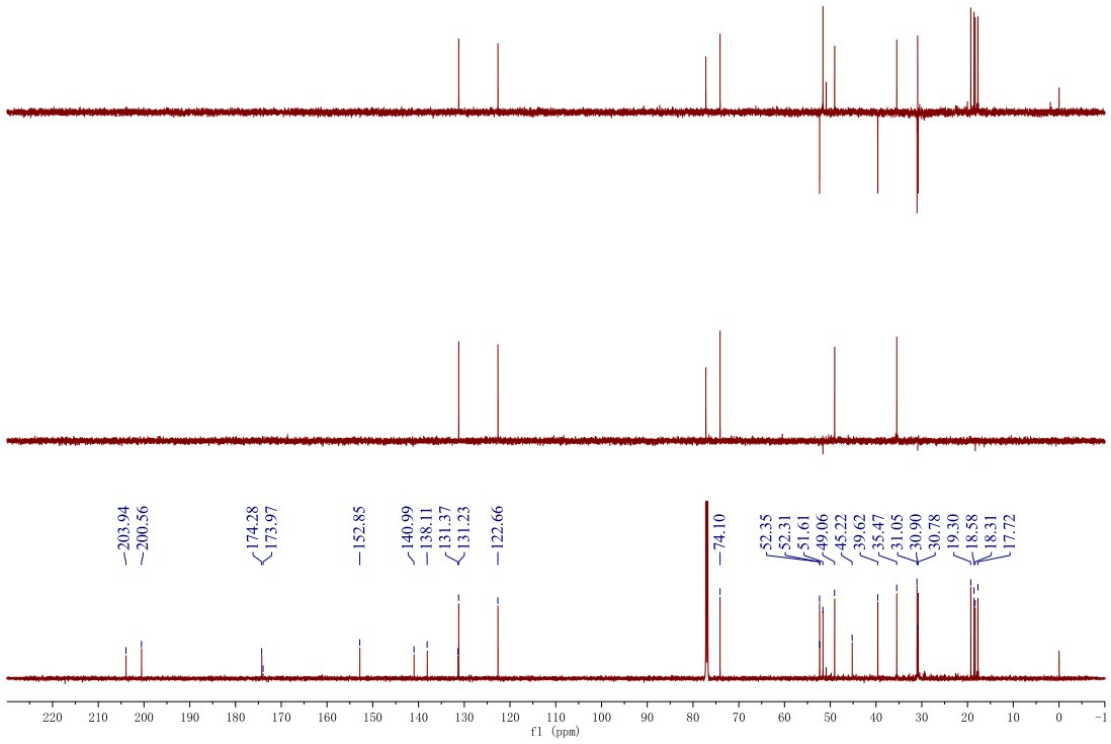

Figure S10. HSQC spectrum (600/150 MH, $CDCl_3$) of compound 1.

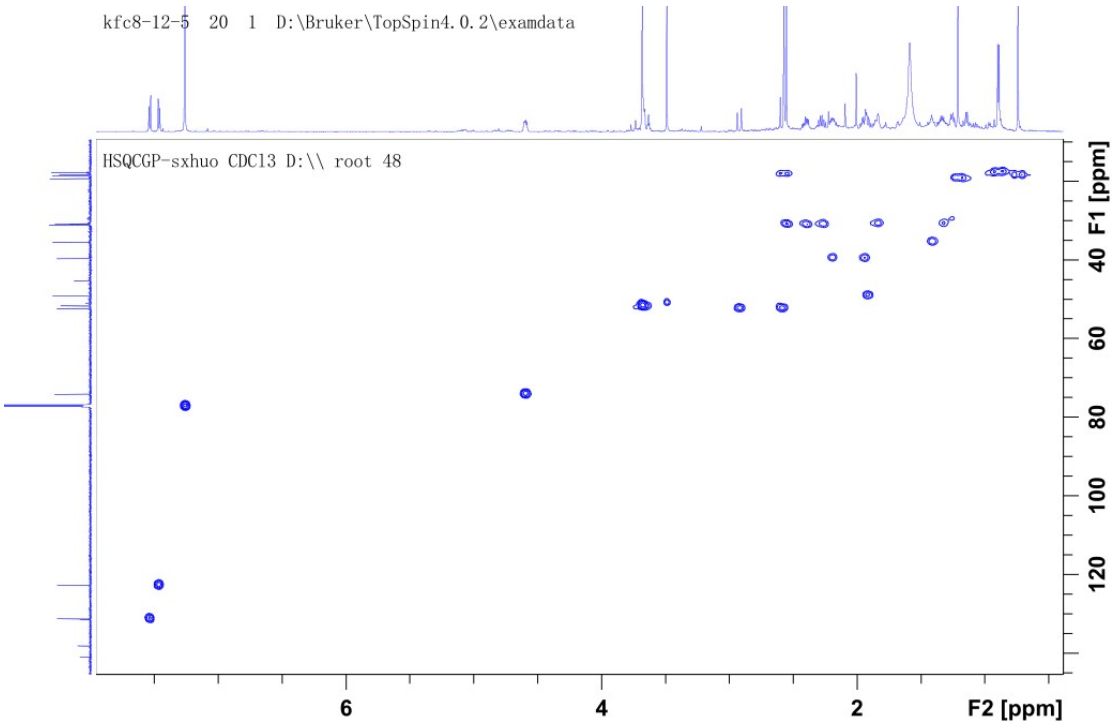

Figure S11. HMBC spectrum (600/150 MH, $CDCl_3$) of compound 1.

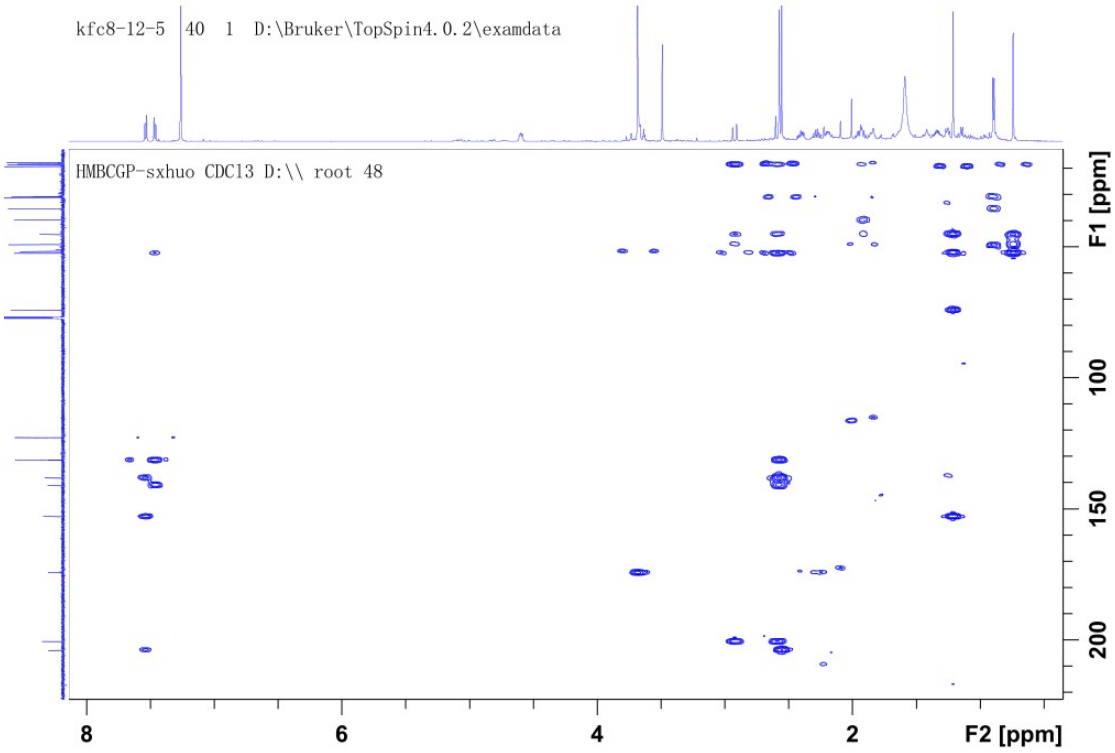

Figure S12. ^{1}H-^{1}H COSY spectrum (600 MH, $CDCl_3$) of compound 1.

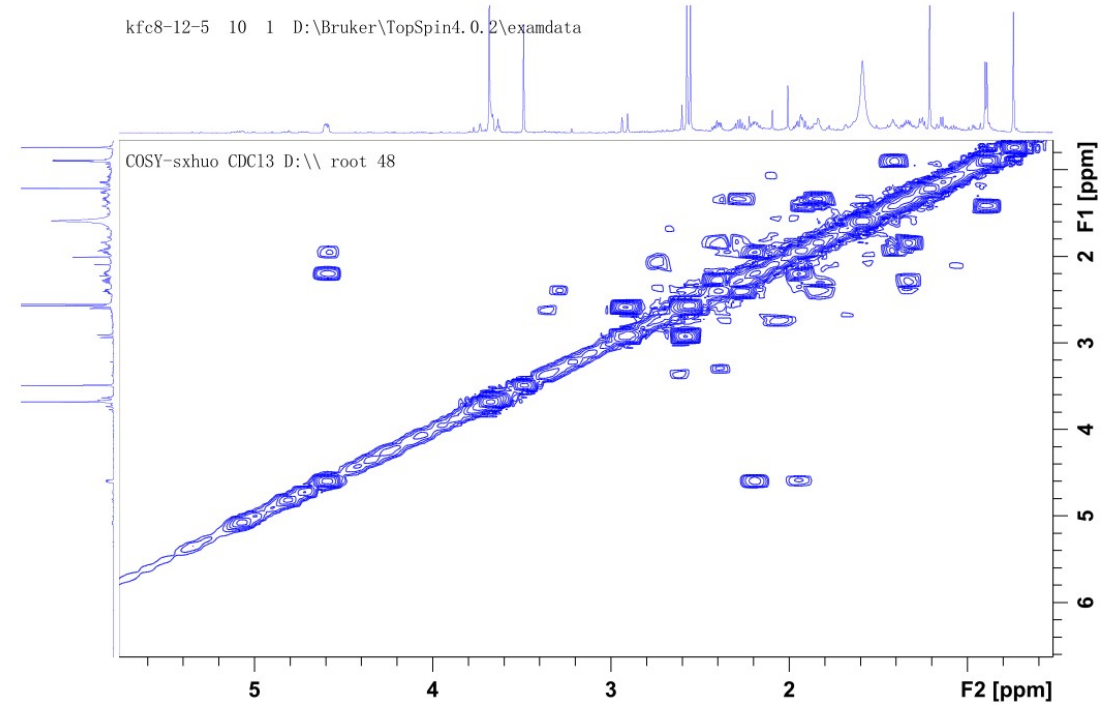

Figure S13. ROESY spectrum (600 MH, $CDCl_3$) of compound 1.

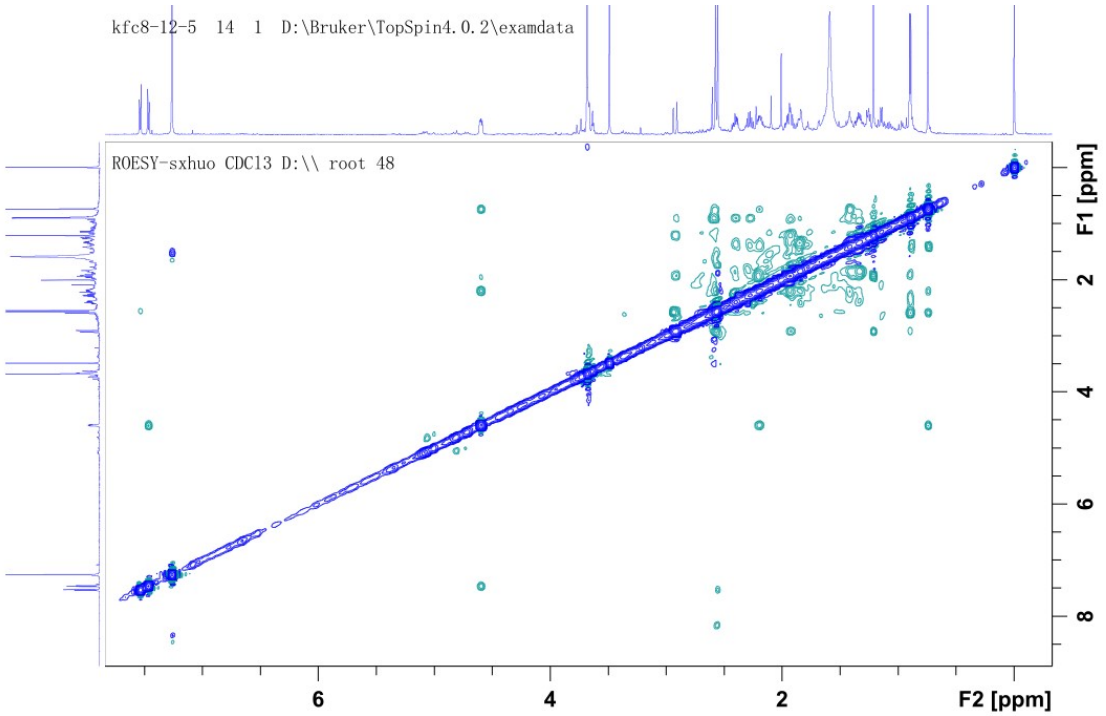

Figure S14. ^{1}H NMR spectrum (600 MH, $CDCl_3$) of compound 2.

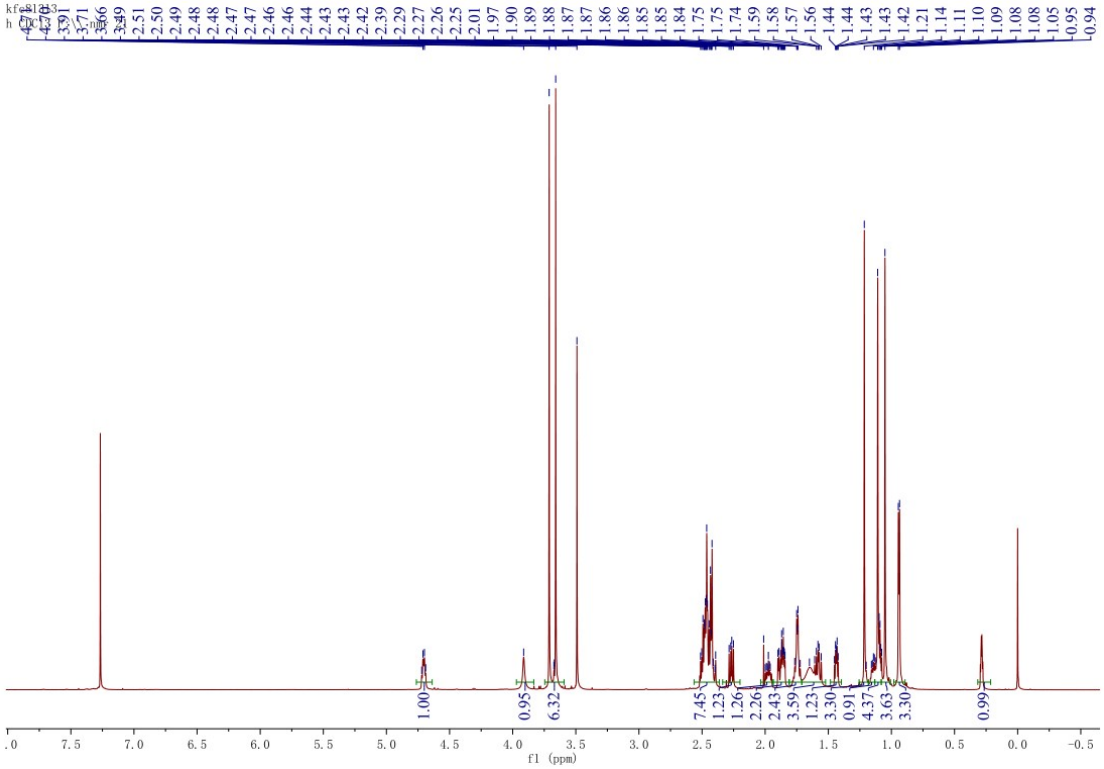

Figure S15. ^{13}C NMR spectrum (150 MH, $CDCl_3$) of compound 2.

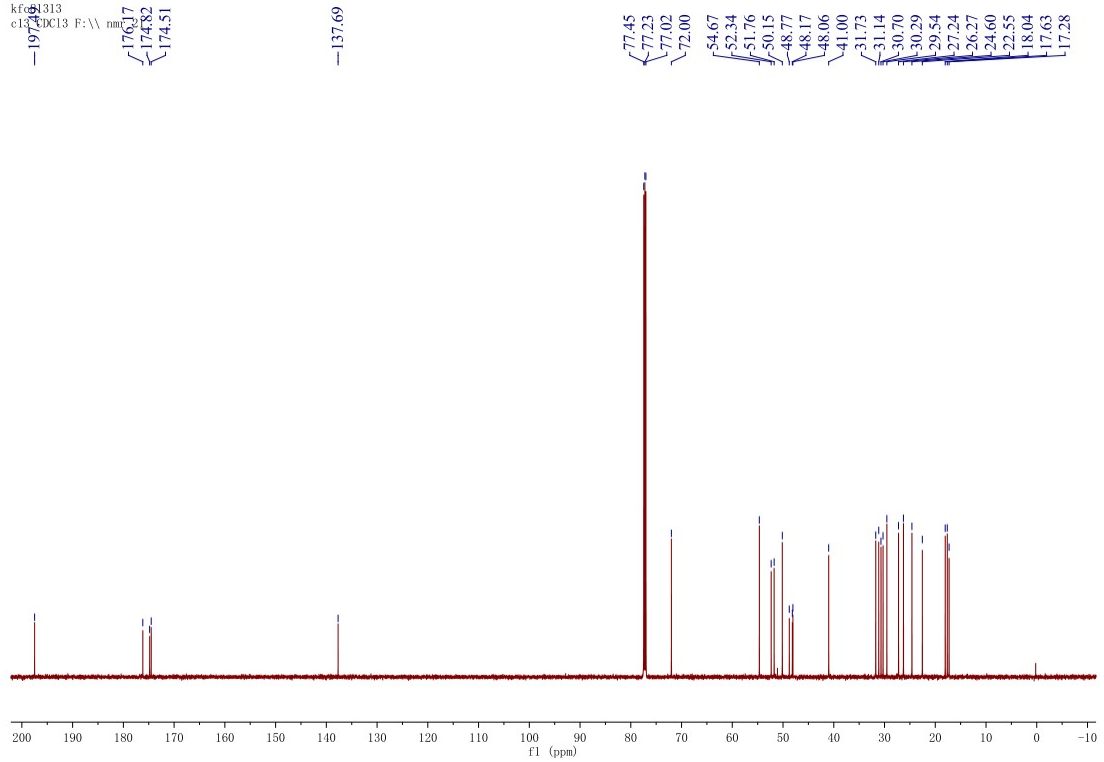

Figure S16. HSQC spectrum (600/150 MH, $CDCl_3$) of compound 2.

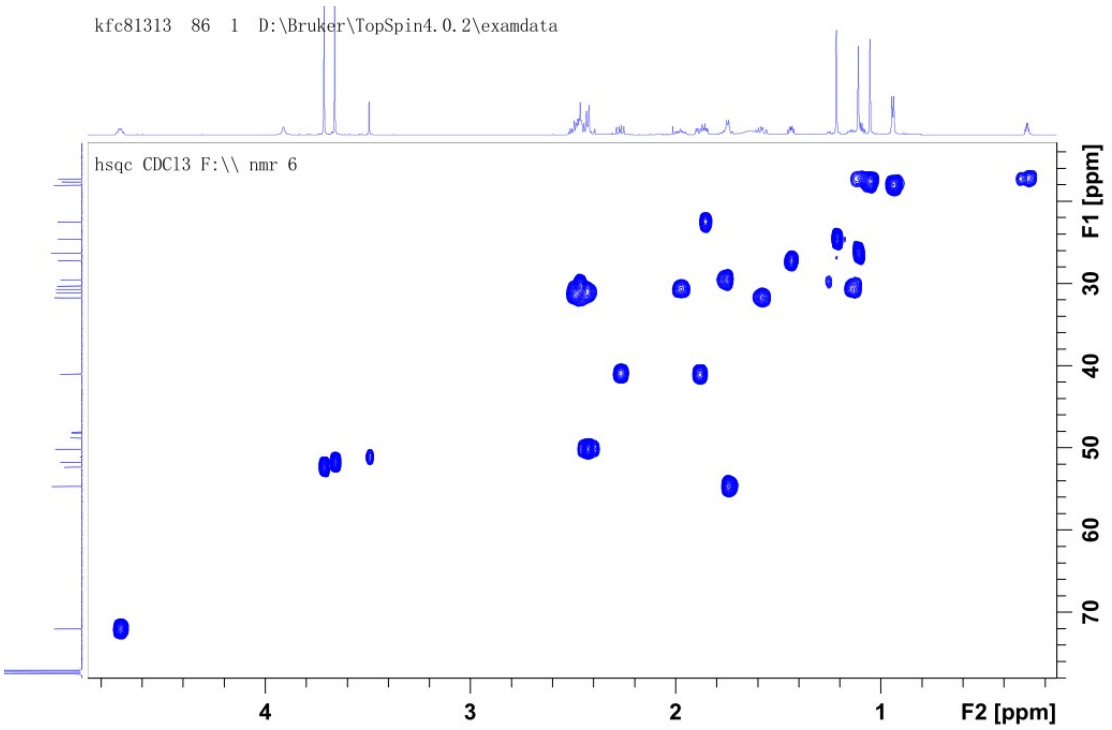

Figure S17. HMBC spectrum (600/150 MH, $CDCl_3$) of compound 2.

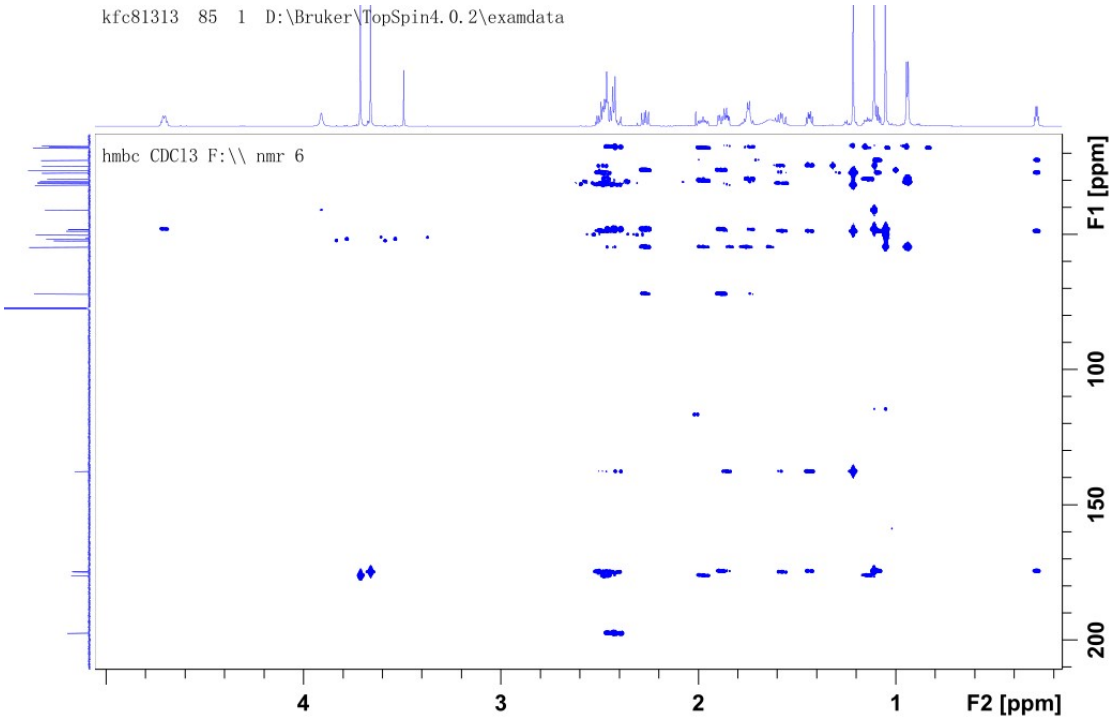

Figure S18. ^{1}H-^{1}H COSY spectrum (150 MH, $CDCl_3$) of compound 2.

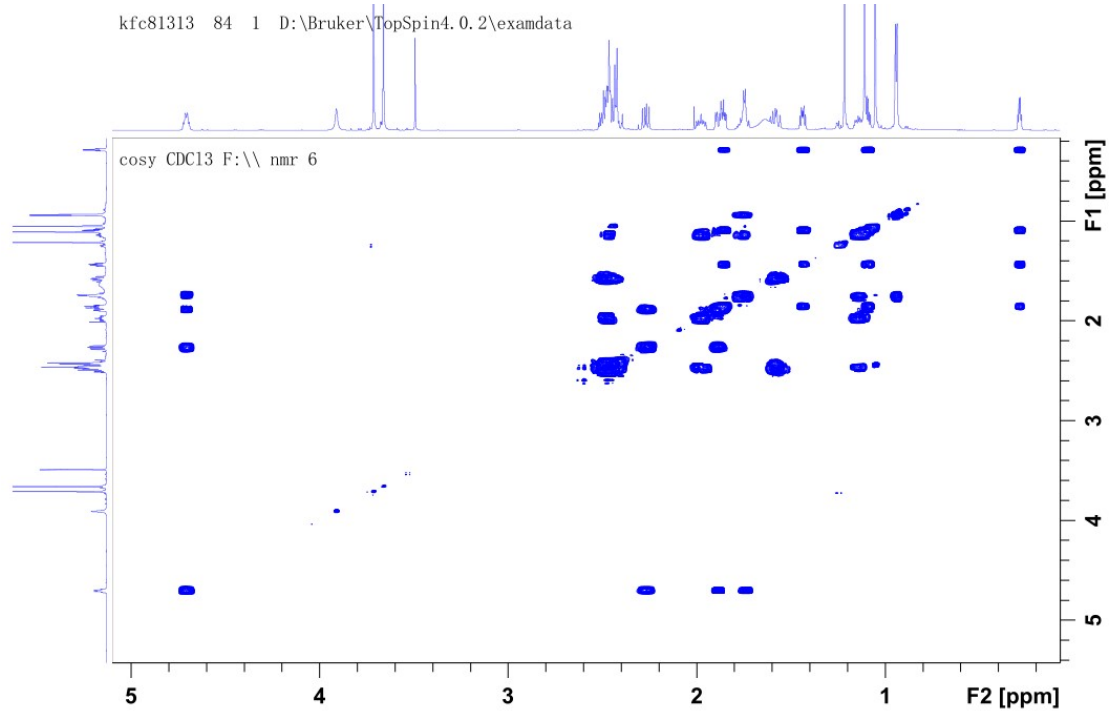

Figure S19. ROESY spectrum (150 MH, $CDCl_3$) of compound 2.

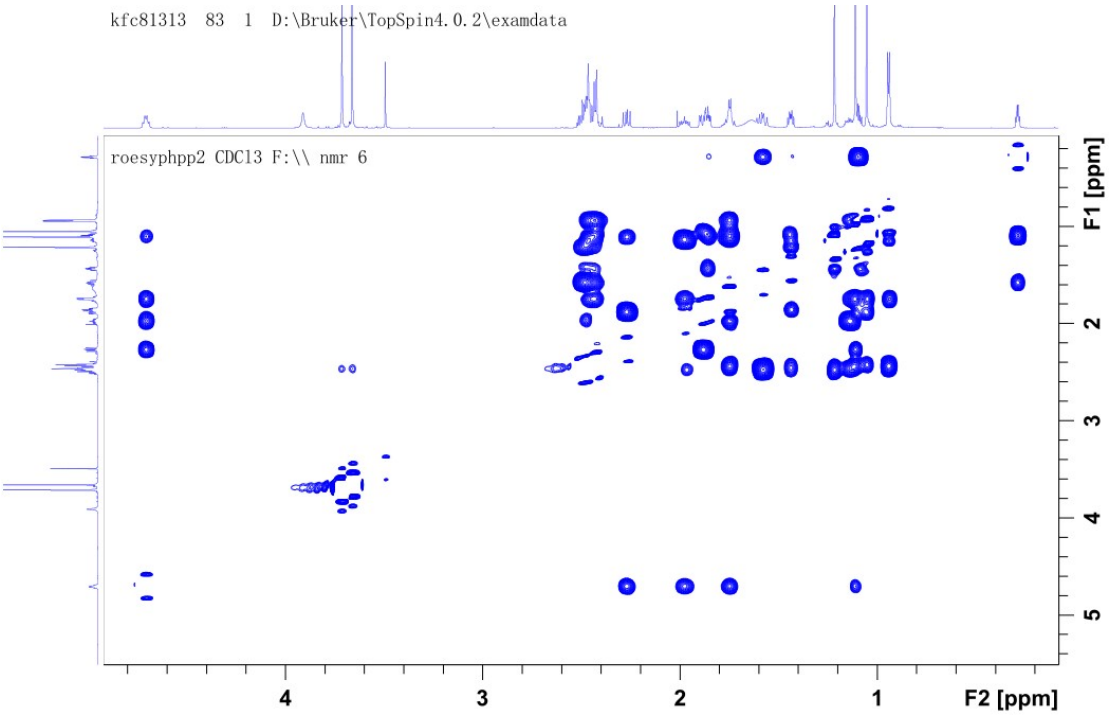

Figure S20. ^{1}H NMR spectrum (600 MH, $CDCl_3$) of compound 3.

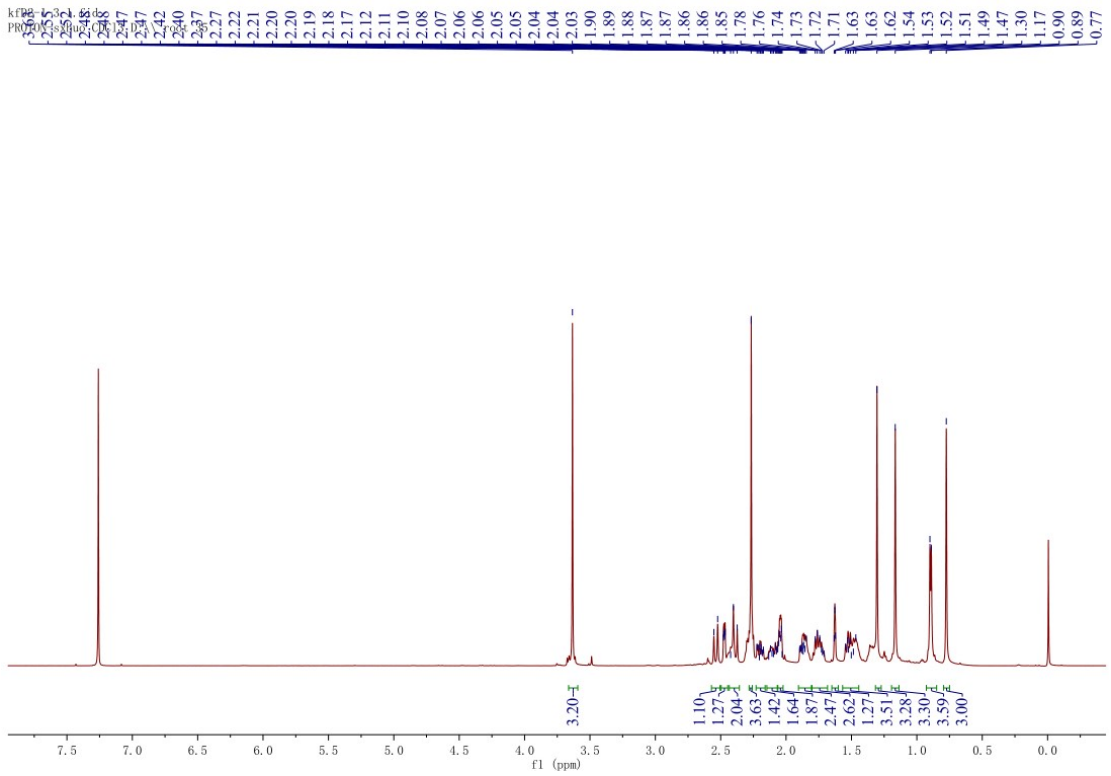

Figure S21. ^{13}C NMR spectrum (150 MH, $CDCl_3$) of compound 3.

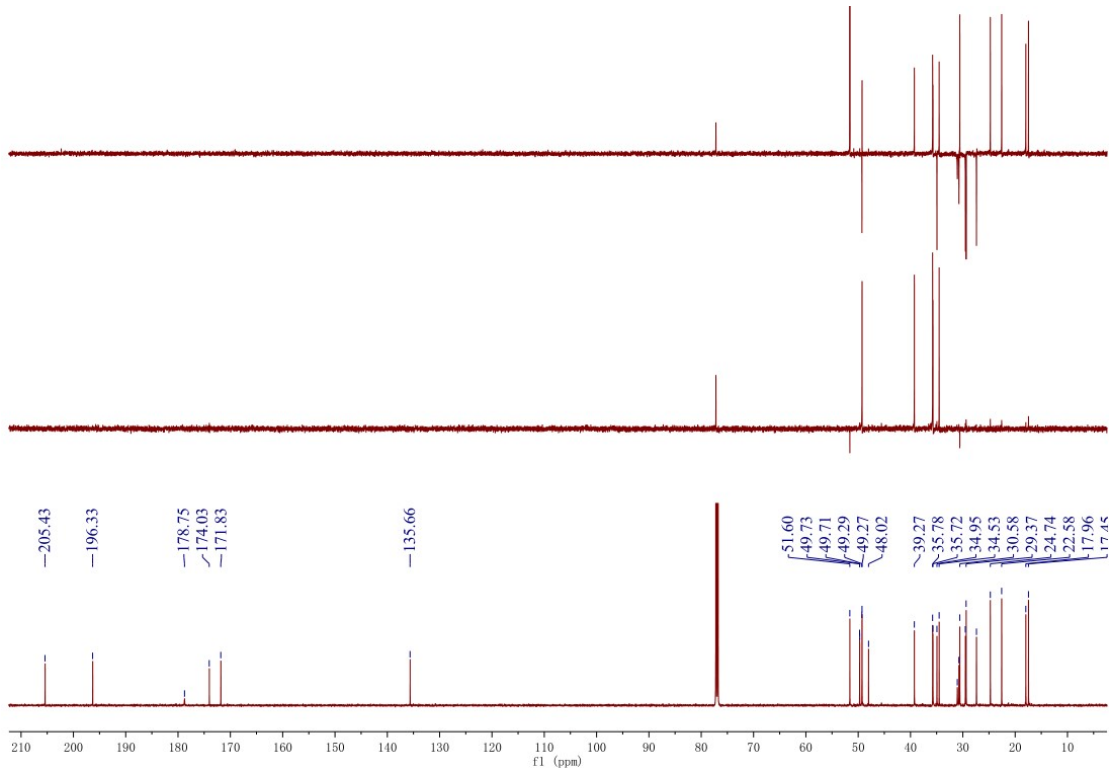

Figure S22. HSQC spectrum (600/150 MH, $CDCl_3$) of compound 3.

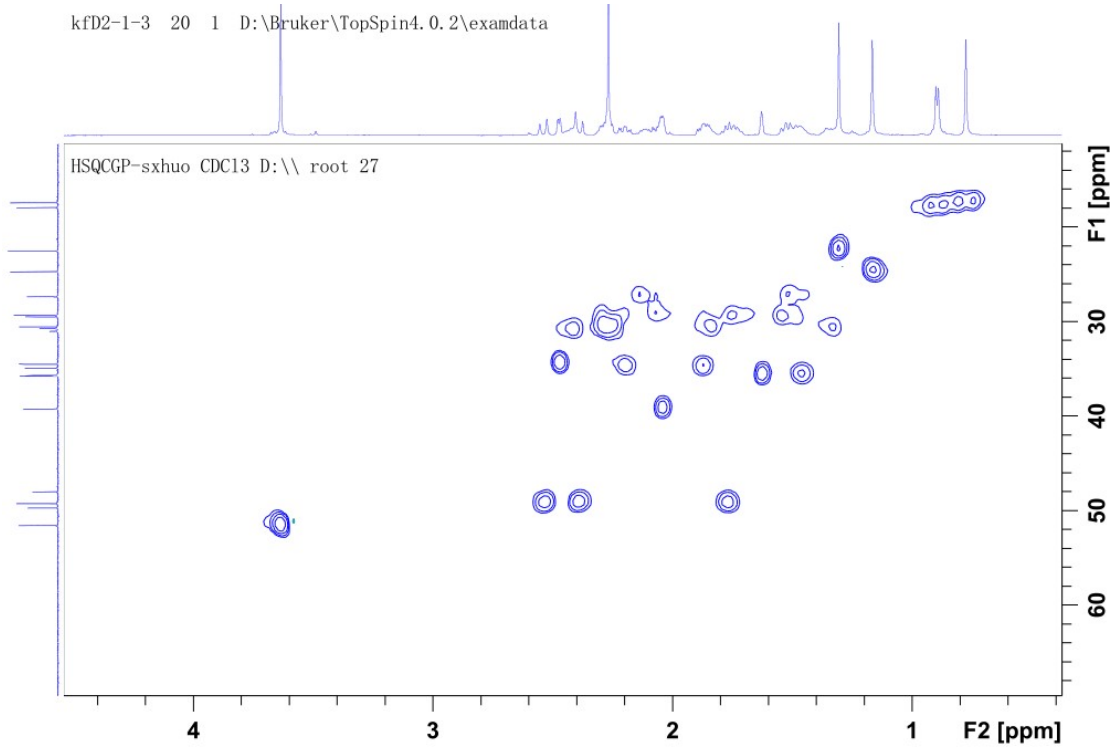

Figure S23. HMBC spectrum (600/150 MH, $CDCl_3$) of compound 3.

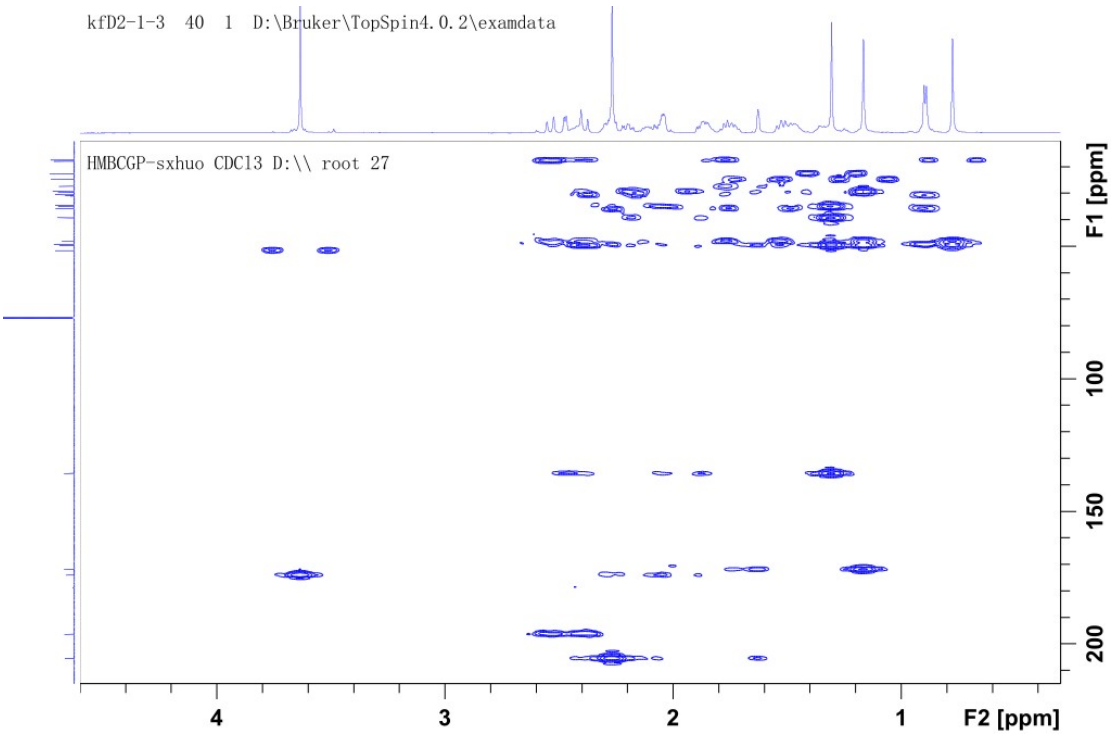

Figure S24. ^{1}H-^{1}H COSY spectrum (600 MH, $CDCl_3$) of compound 3.

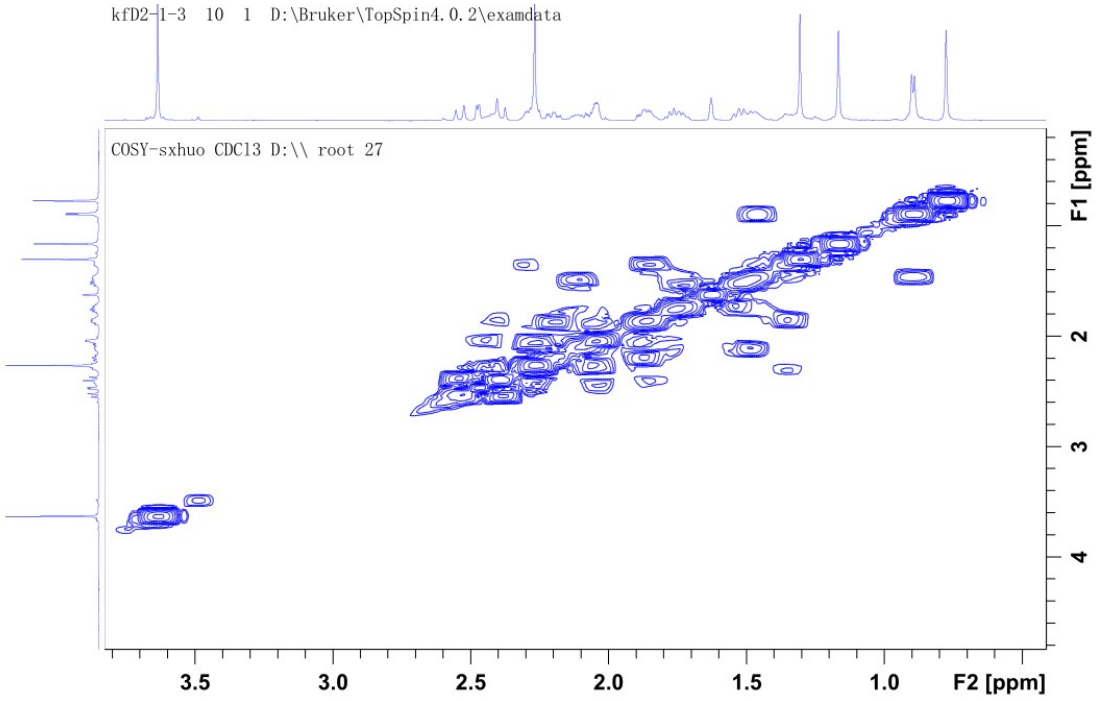

Figure S25. ROESY spectrum (600 MH, $CDCl_3$) of compound 3.

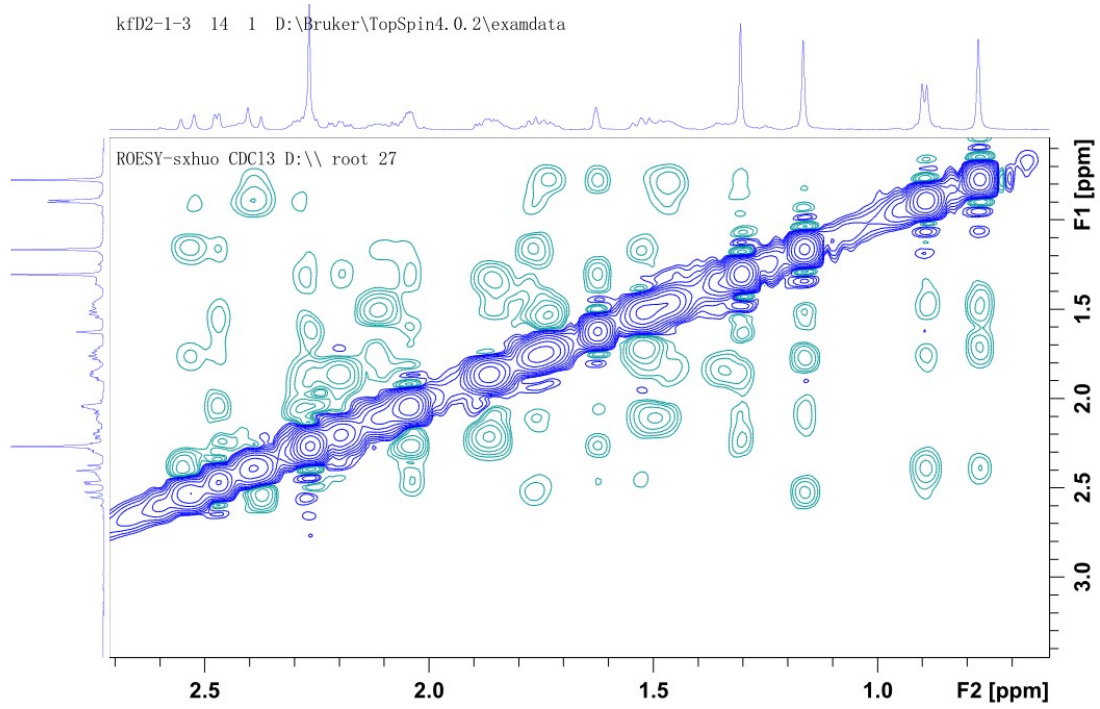

Figure S26. ^{1}H NMR spectrum (600 MH, $CDCl_3$) of compound 4.

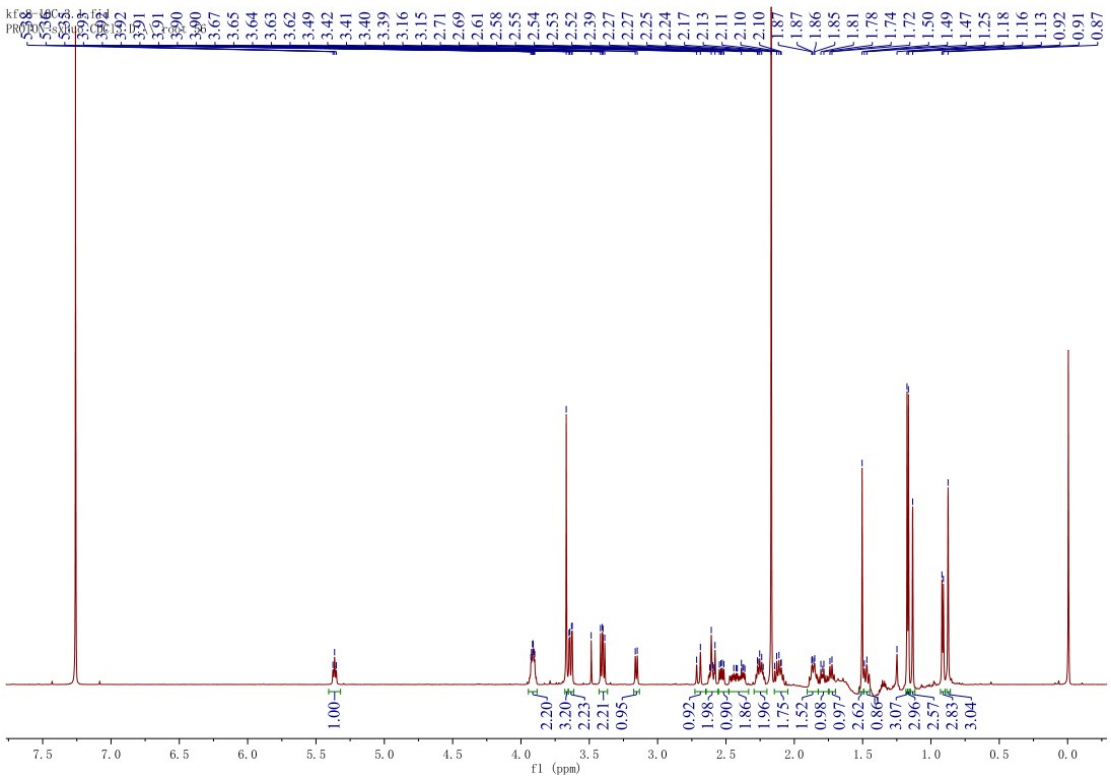

Figure S27. ^{13}C NMR spectrum (150 MH, $CDCl_3$) of compound 4.

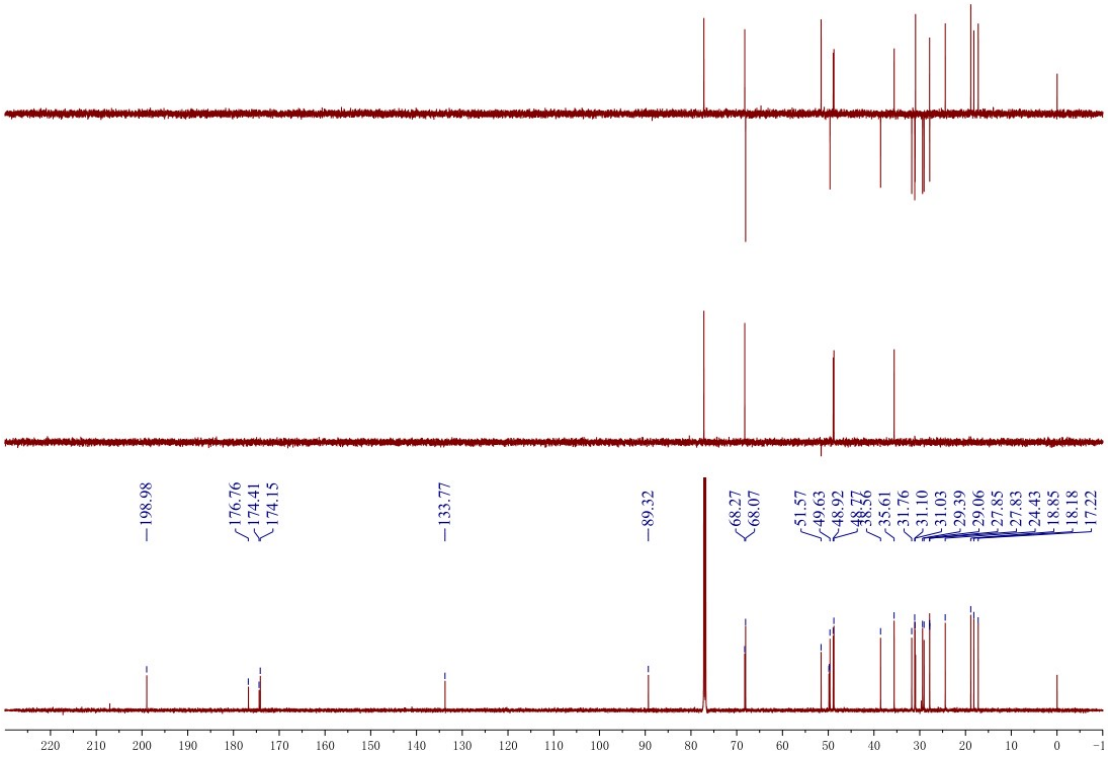

Figure S28. HSQC spectrum (600/150 MH, $CDCl_3$) of compound 4.

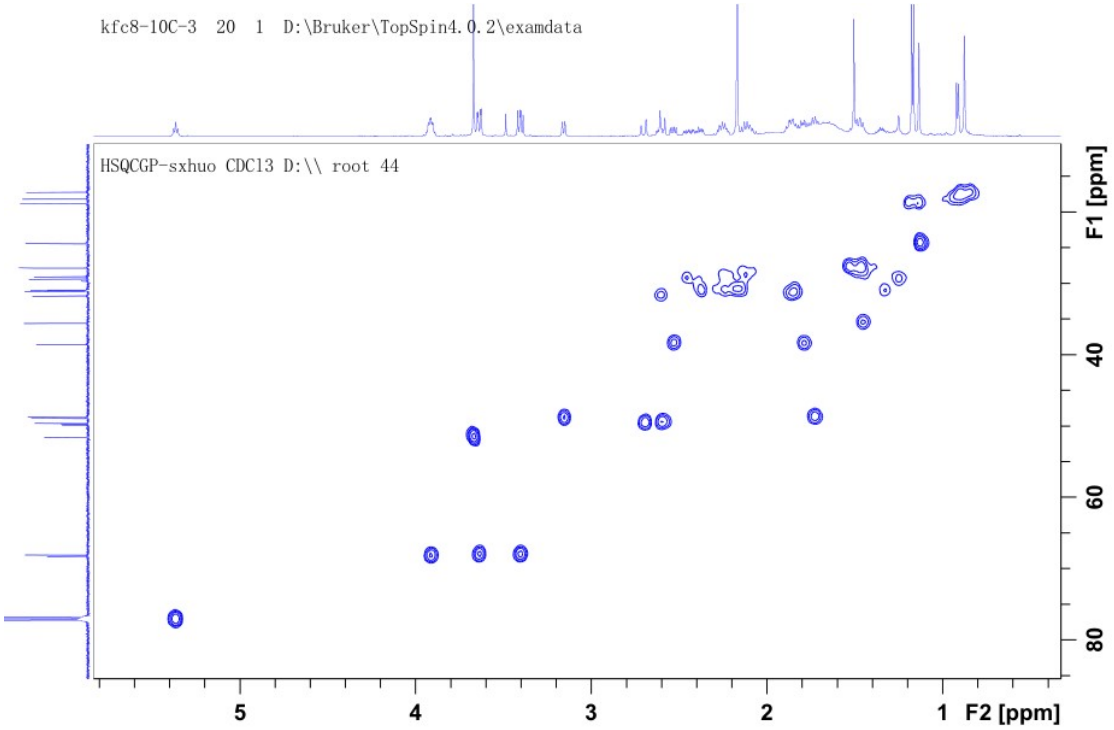

Figure S29. HMBC spectrum (600/150 MH, $CDCl_3$) of compound 4.

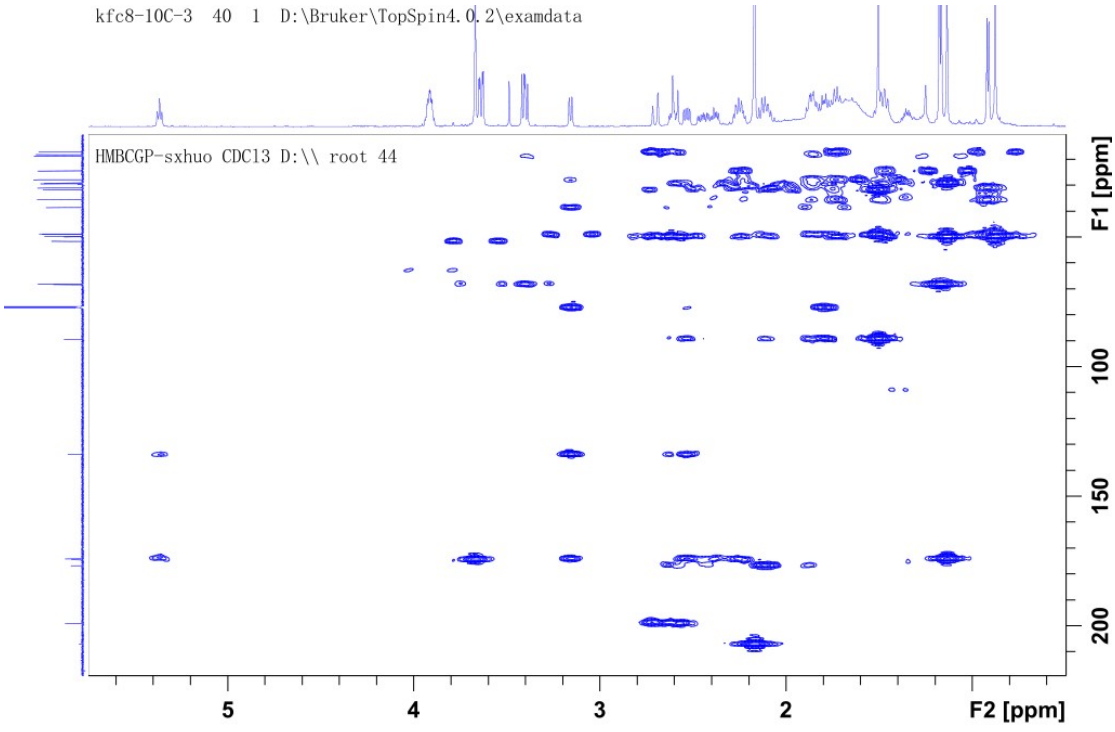

Figure S30. ^{1}H-^{1}H COSY spectrum (600 MH, $CDCl_3$) of compound 4.

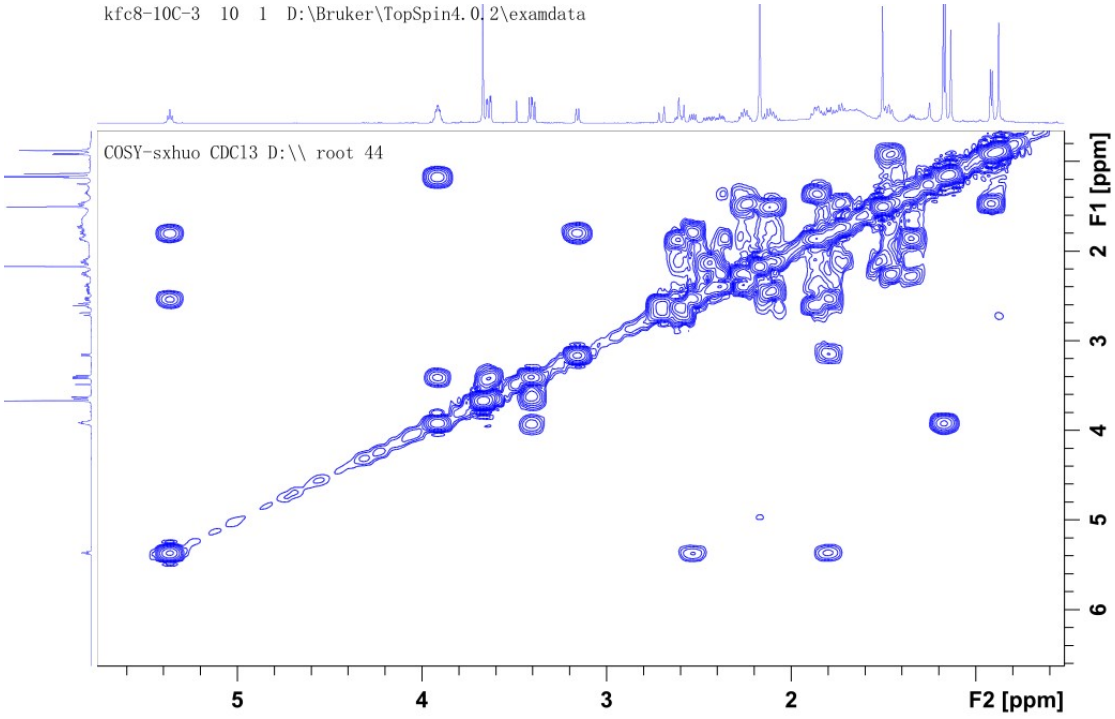

Figure S31. ROESY spectrum (600 MH, $CDCl_3$) of compound 4.

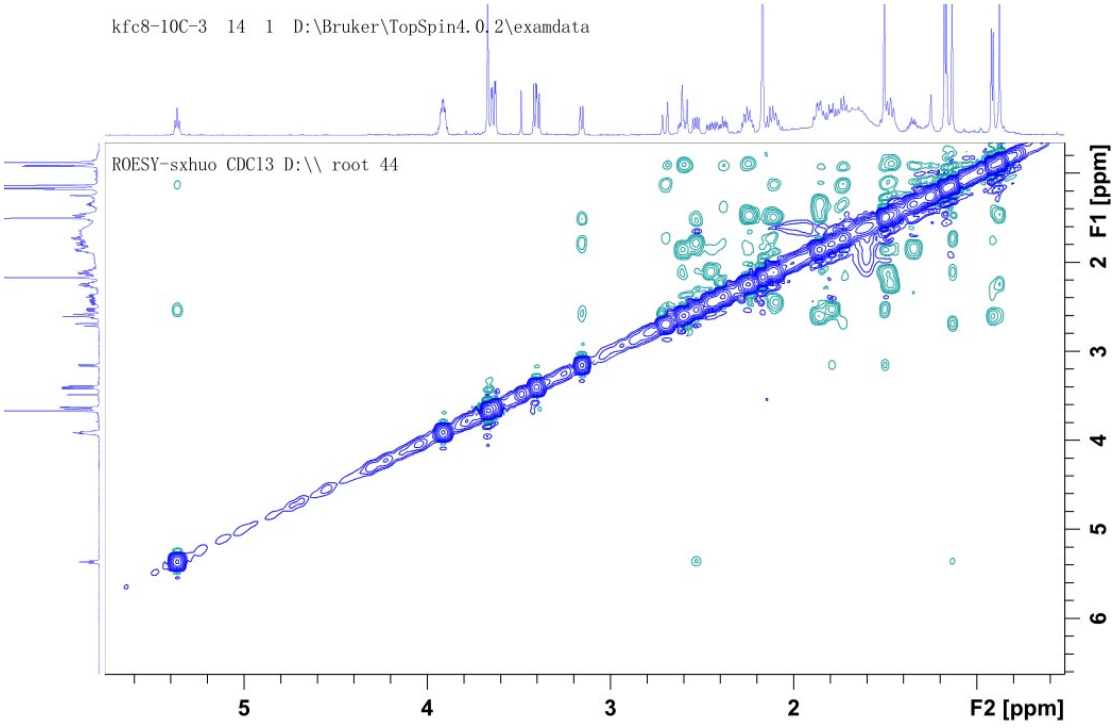

Figure S32. ^{1}H NMR spectrum (600 MH, $CDCl_3$) of compound 5.

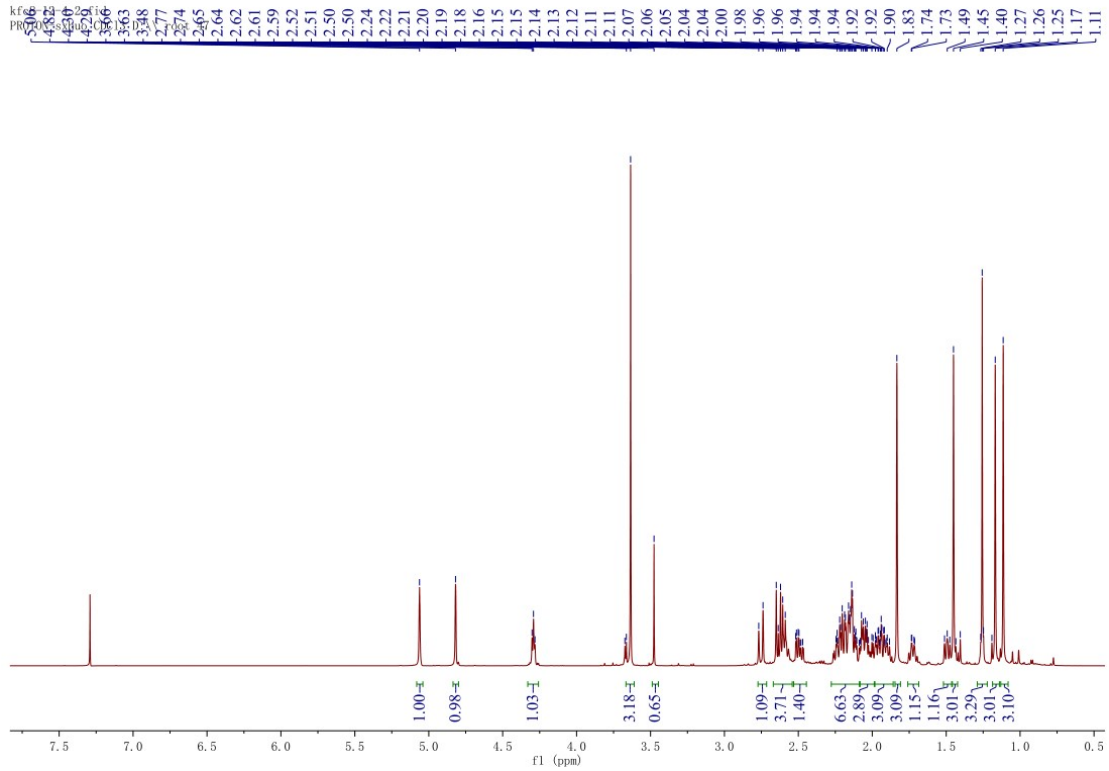

Figure S33. ^{13}C NMR spectrum (150 MH, $CDCl_3$) of compound 5.

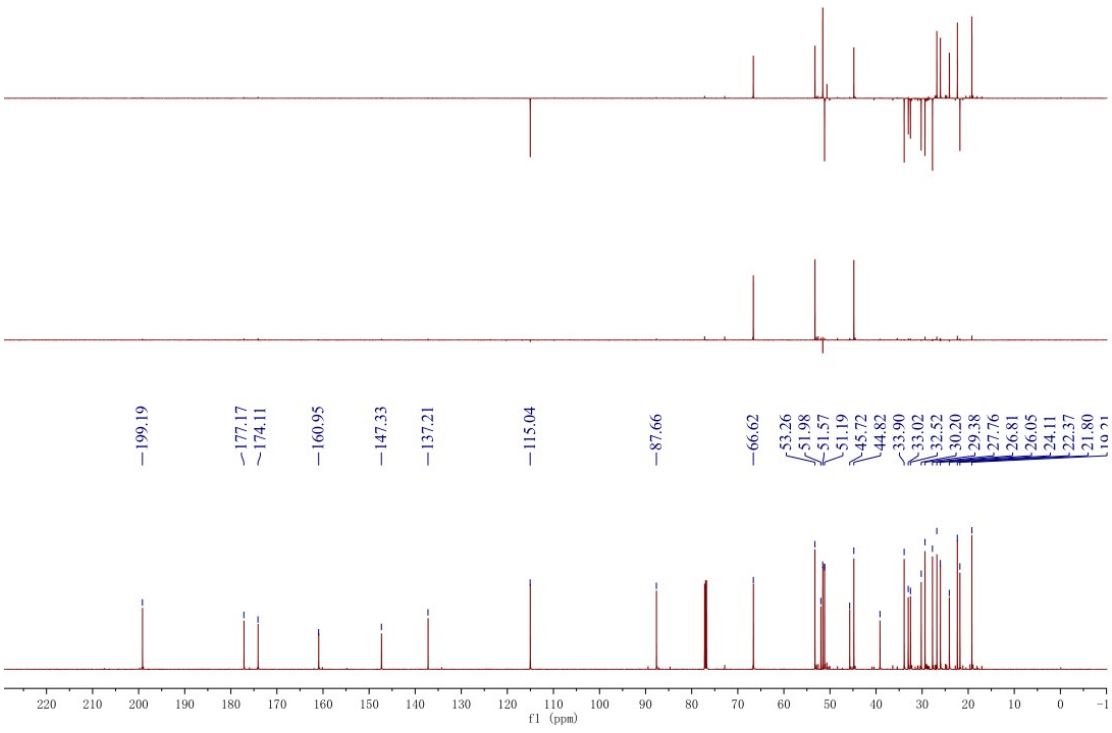

Figure S34. HSQC NMR spectrum (600/150 MH, $CDCl_3$) of compound 5.

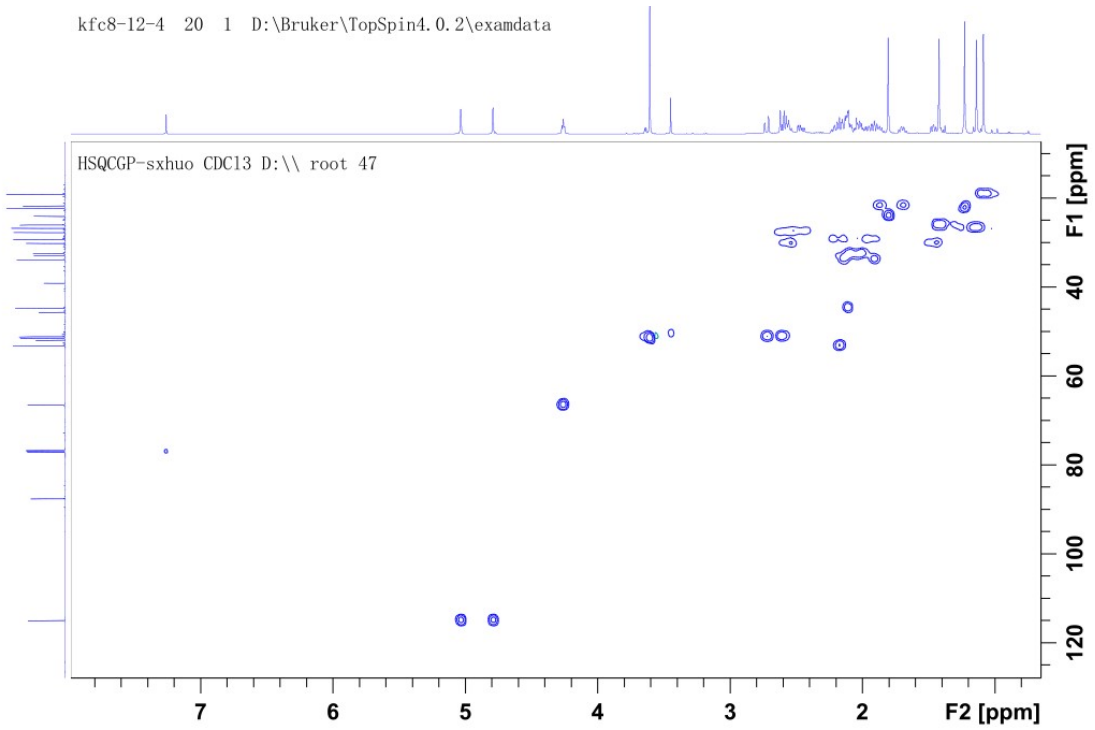

Figure S35. HMBC spectrum (600/150 MH, $CDCl_3$) of compound 5.

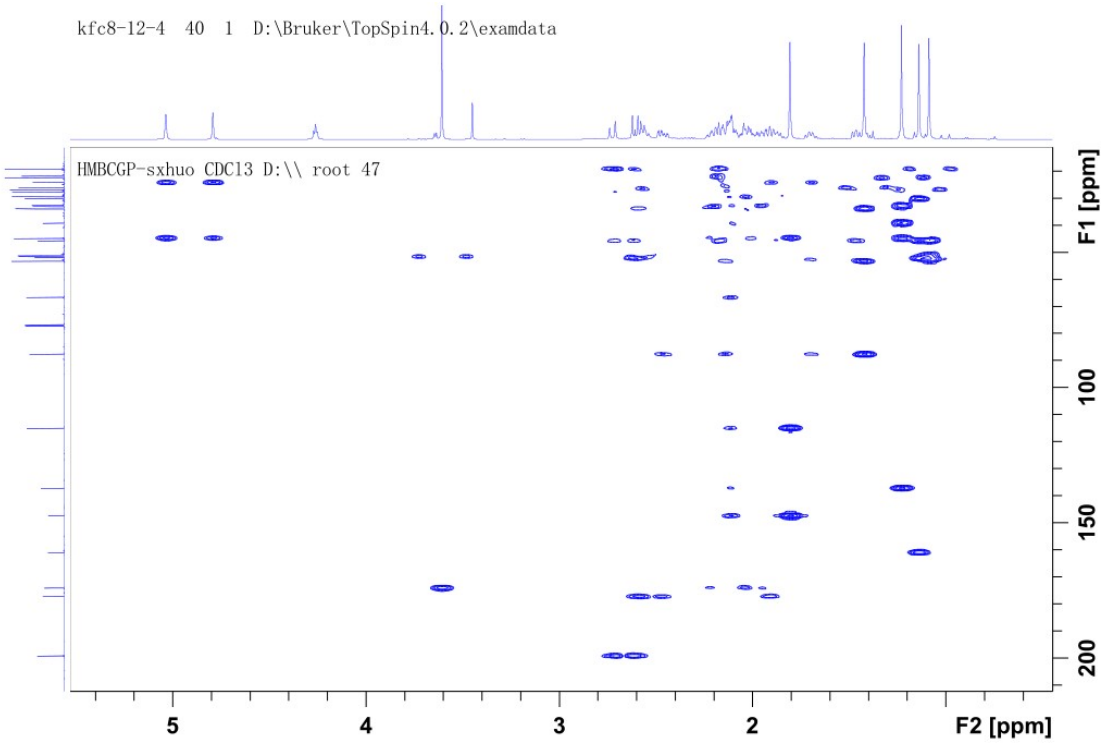

Figure S36. ^{1}H-^{1}H COSY spectrum (600 MH, $CDCl_3$) of compound 5.

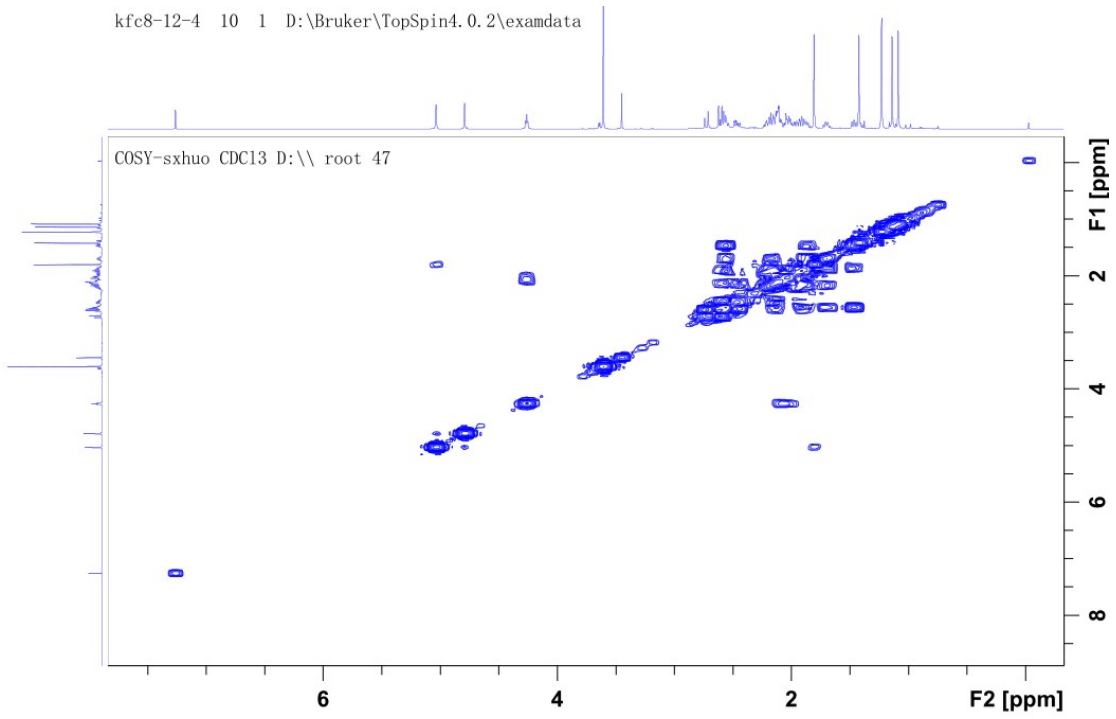

Figure S37. ROESY spectrum (600 MH, $CDCl_3$) of compound 5.

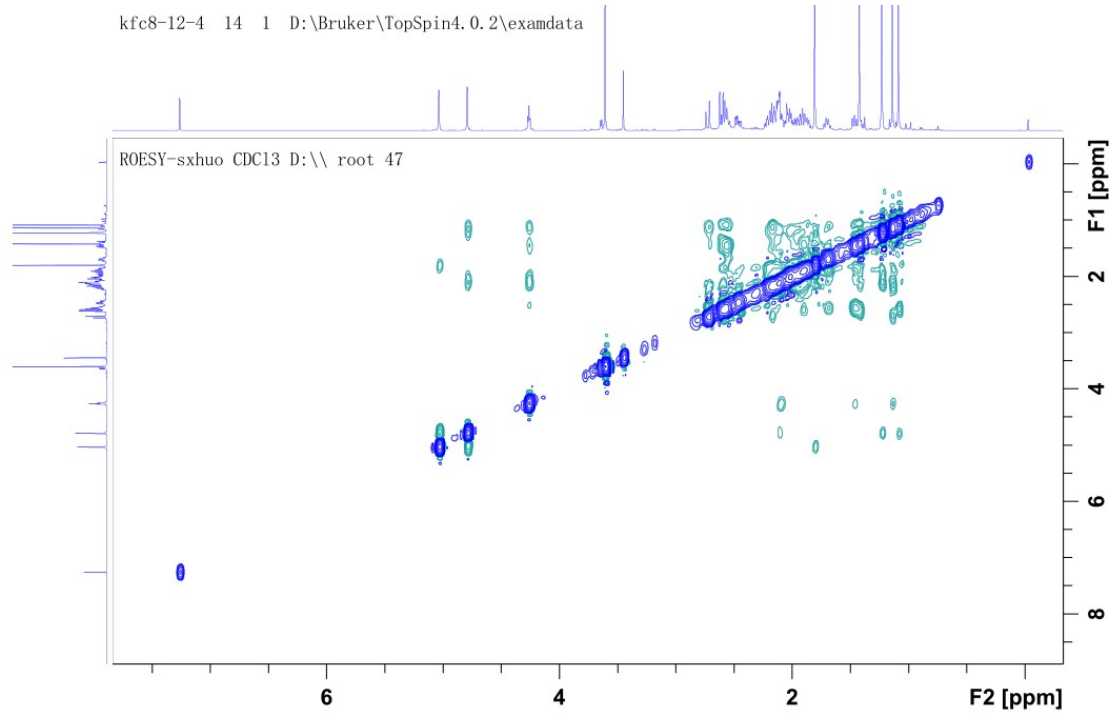

Figure S38. ^{1}H NMR spectrum (600 MH, CD_3OD) of compound 6.

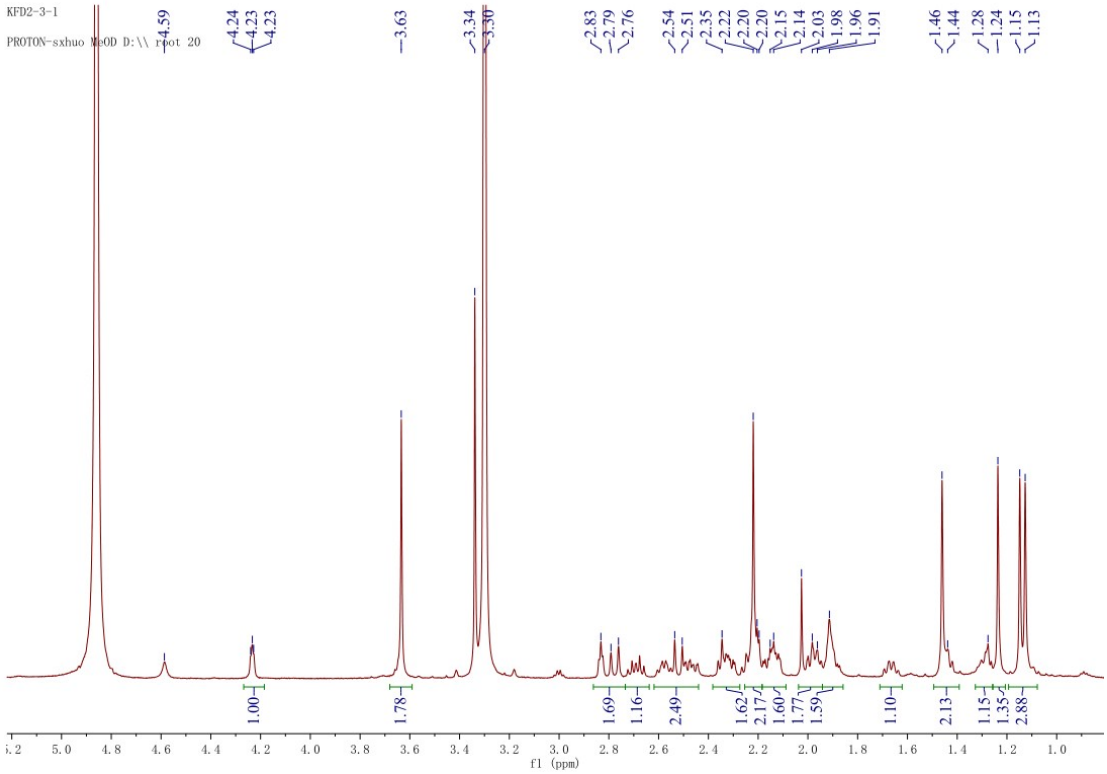

Figure S39. ^{13}C NMR spectrum (150 MH, CD_3OD) of compound 6.

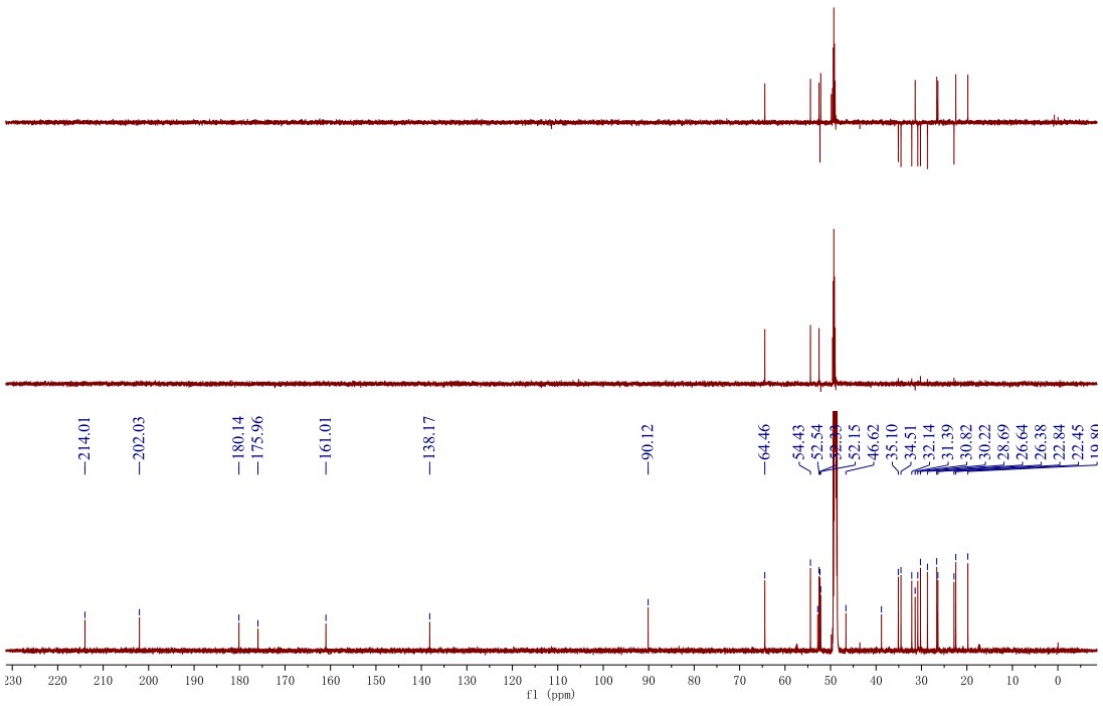

Figure S40. HSQC spectrum (600/150 MH, CD_3OD) of compound 6.

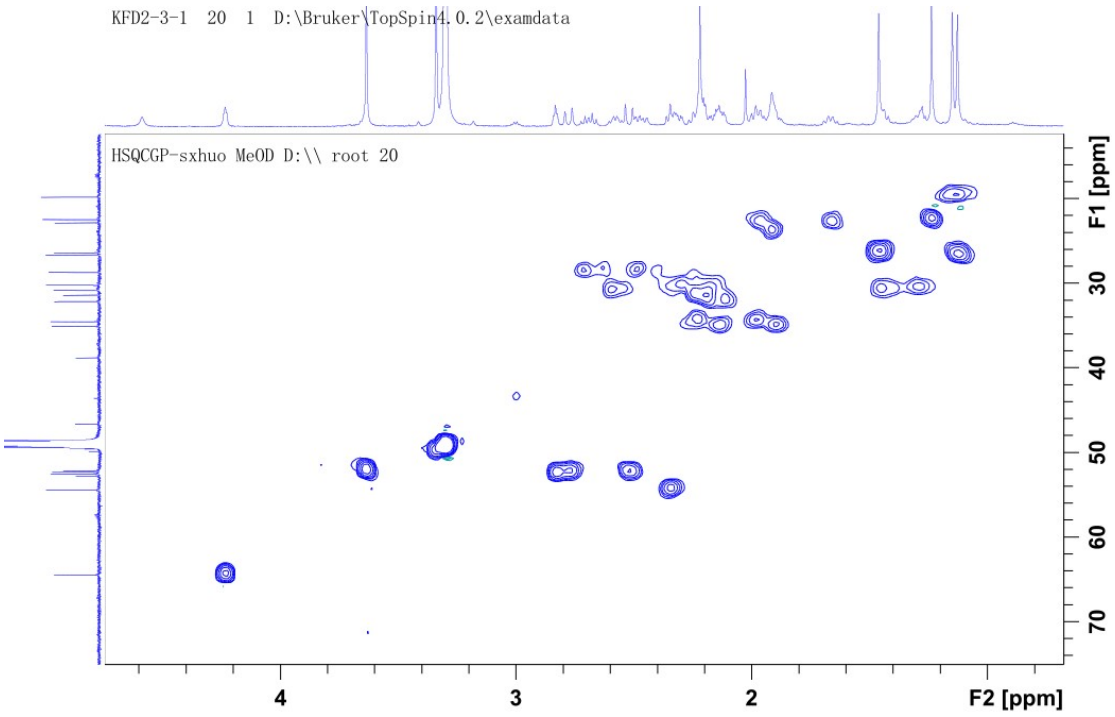

Figure S41. HMBC spectrum (600/150 MH, CD_3OD) of compound 6.

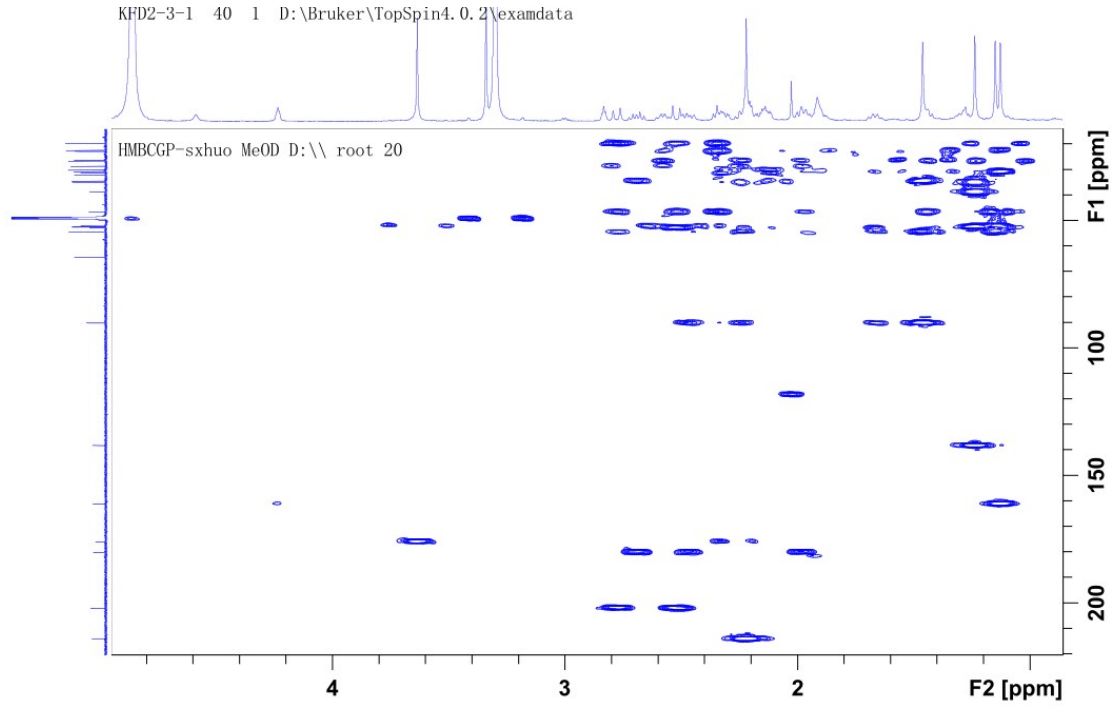

Figure S42. ^{1}H-^{1}H COSY spectrum (600 MH, CD_3OD) of compound 6.

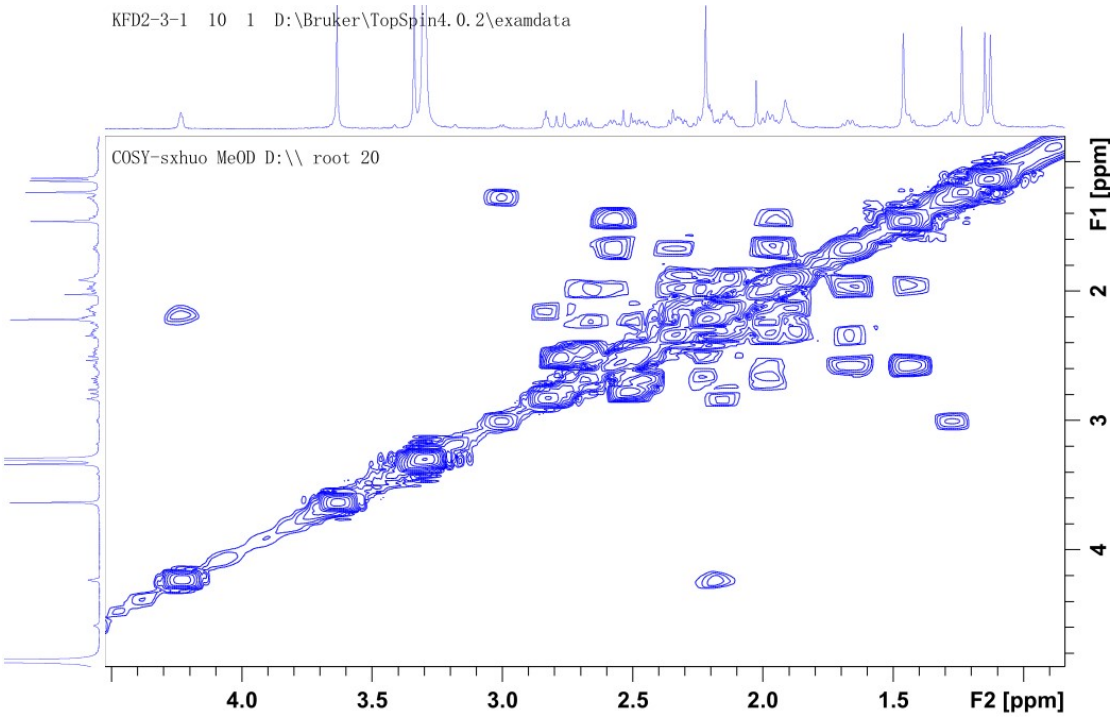

Figure S43. ^{1}H NMR spectrum (600 MH, $CDCl_3$) of compound 7.

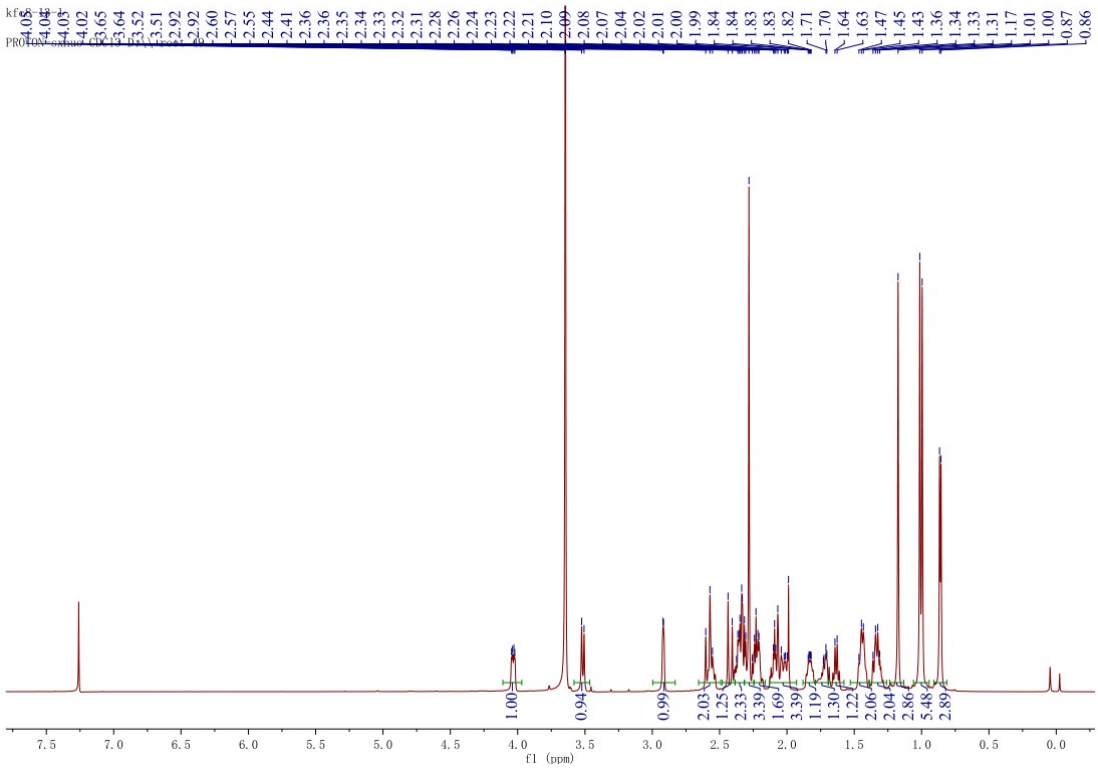

Figure S44. ^{13}C NMR spectrum (150 MH, $CDCl_3$) of compound 7.

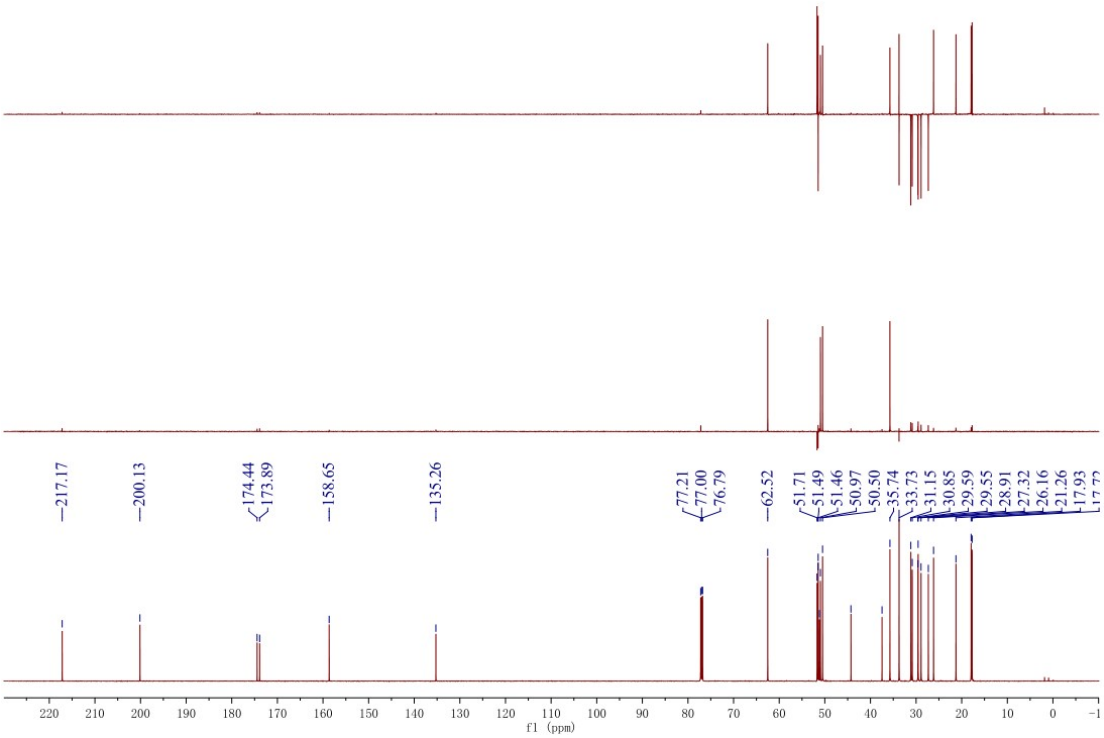

Figure S45. HSQC spectrum (600/150 MH, $CDCl_3$) of compound 7.

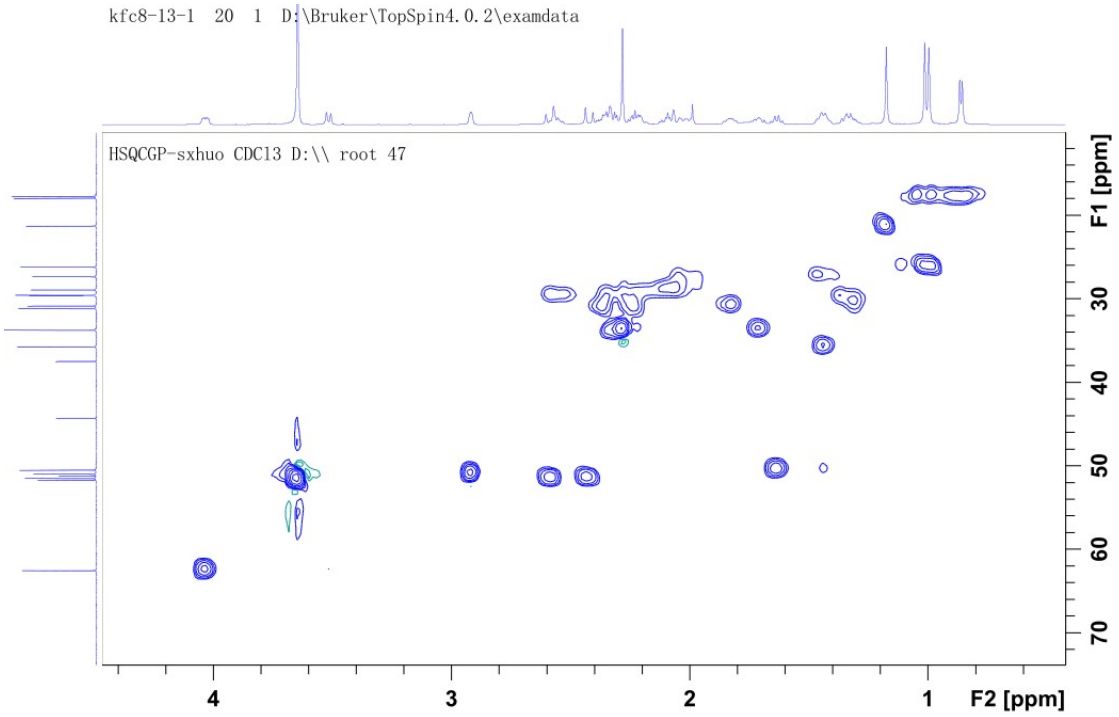

Figure S46. HMBC spectrum (600/150 MH, $CDCl_3$) of compound 7.

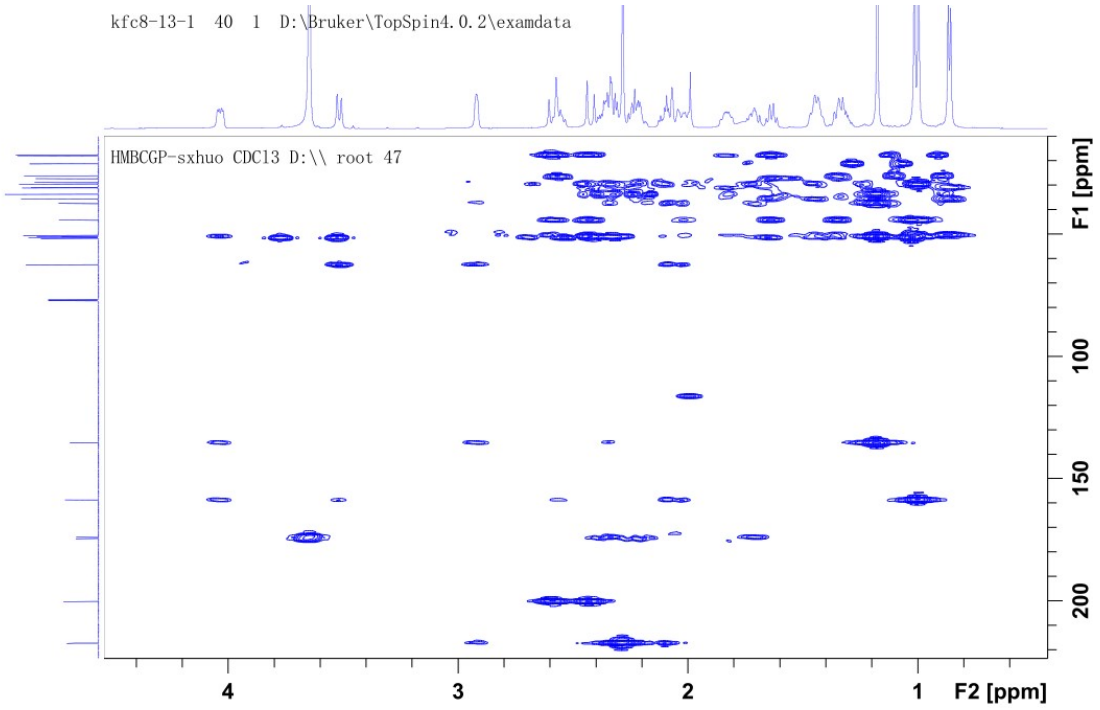

Figure S47. ^{1}H-^{1}H COSY spectrum (600 MH, $CDCl_3$) of compound 7.

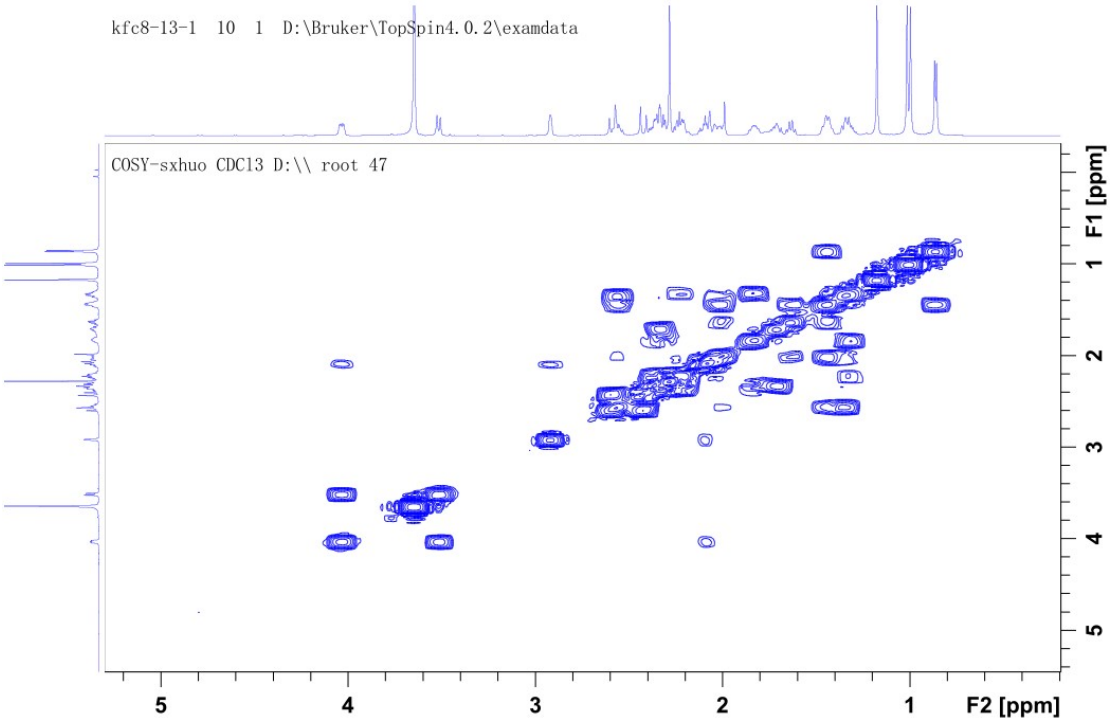

Figure S48. ROESY spectrum (600 MH, $CDCl_3$) of compound 7.

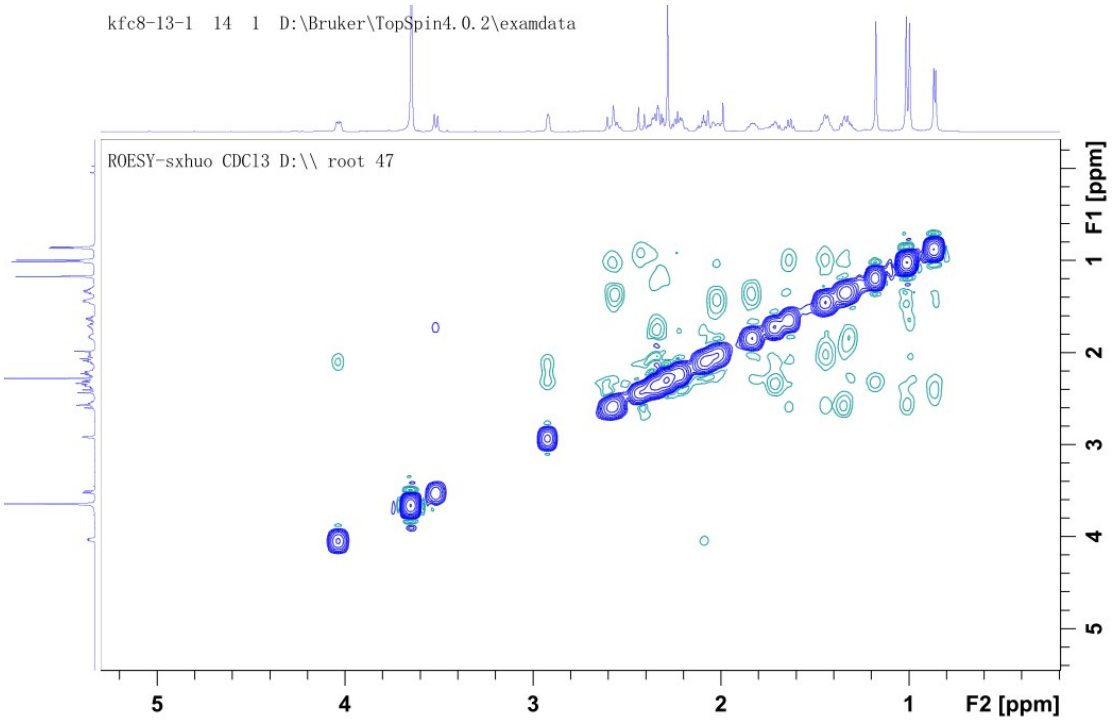

Figure S49. ^1H NMR spectrum (600 MH, $CDCl_3$) of compound 8.

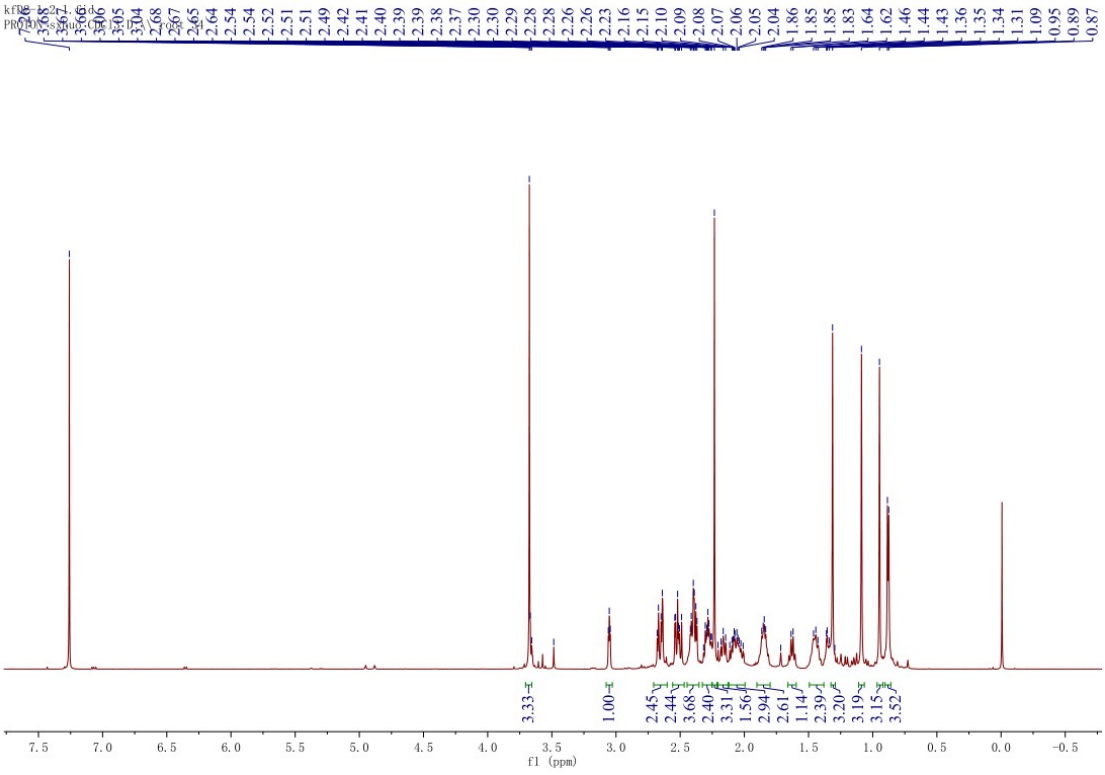

Figure S50. ^{13}C NMR spectrum (150 MH, $CDCl_3$) of compound 8.

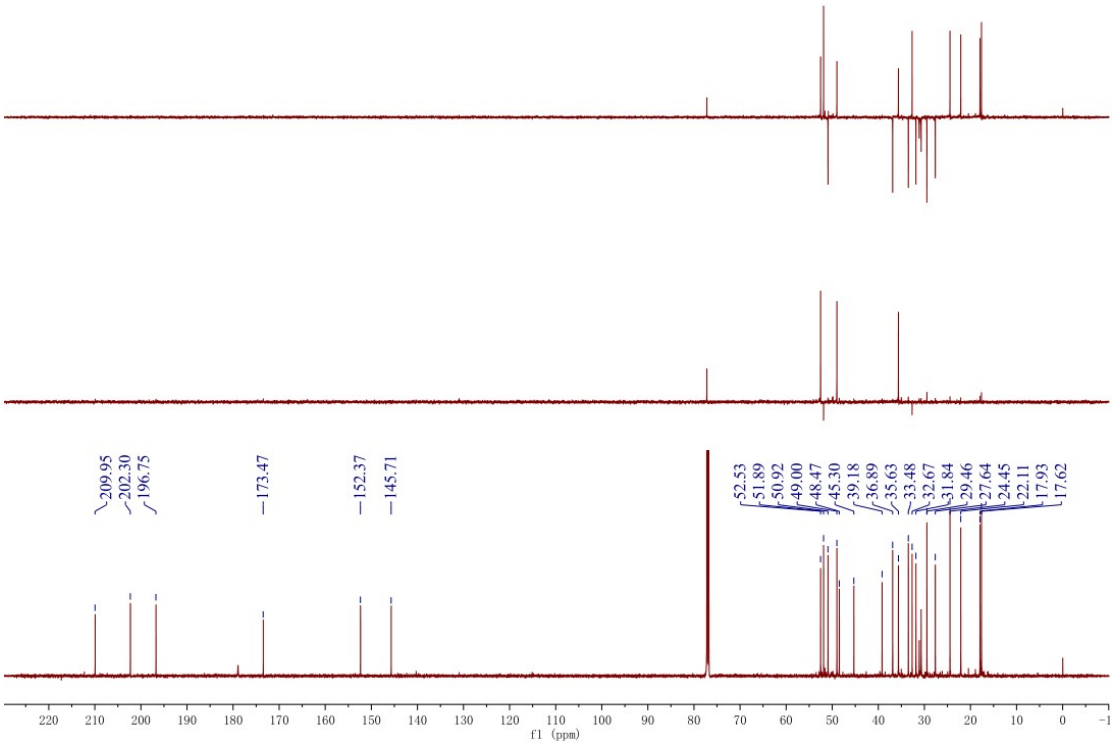

Figure S51. HSQC spectrum (600/150 MH, $CDCl_3$) of compound 8.

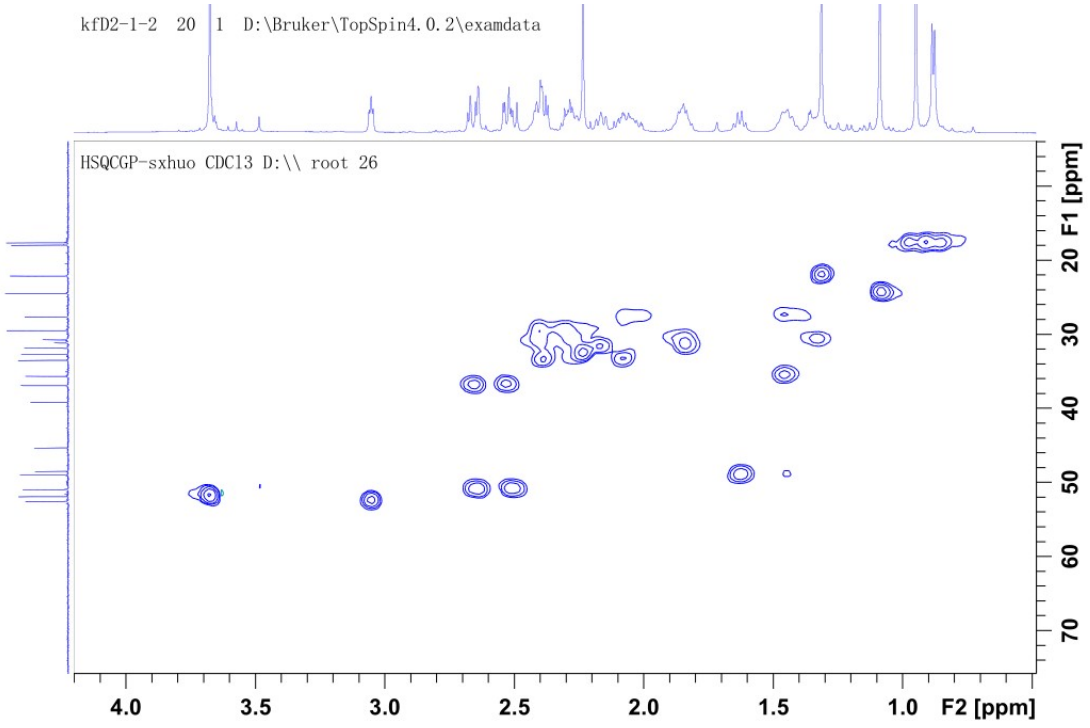

Figure S52. HMBC spectrum (600/150 MH, $CDCl_3$) of compound 8.

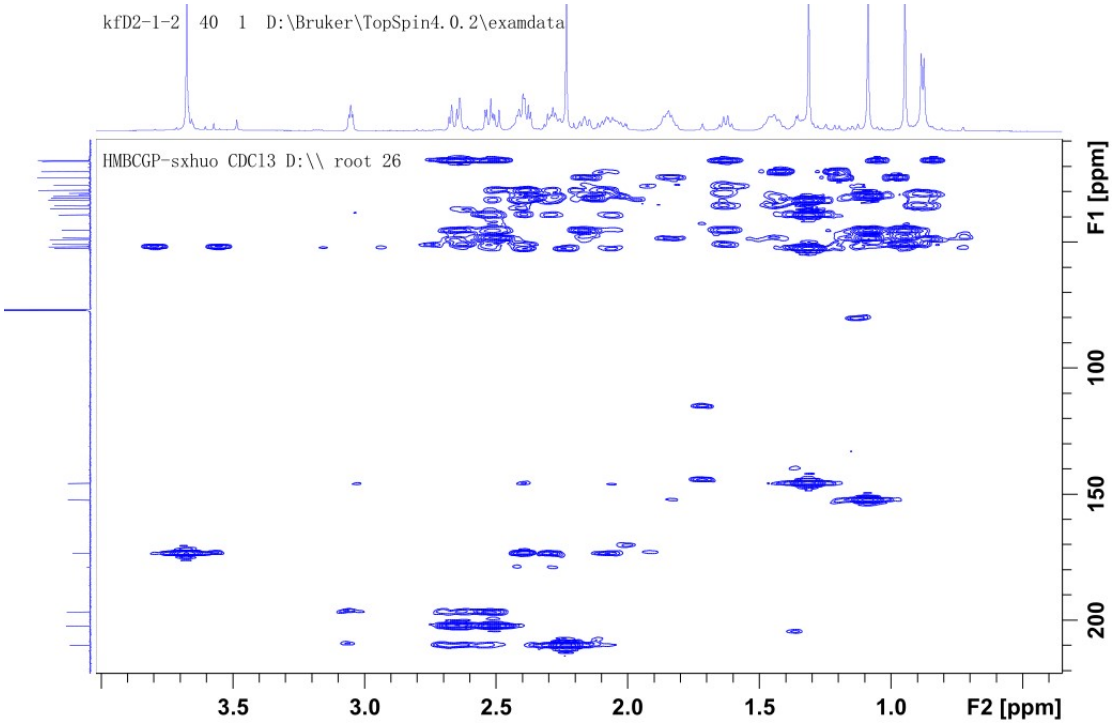

Figure S53.^{1}H-^{1}H COSY spectrum (600 MH, $CDCl_3$) of compound 8.

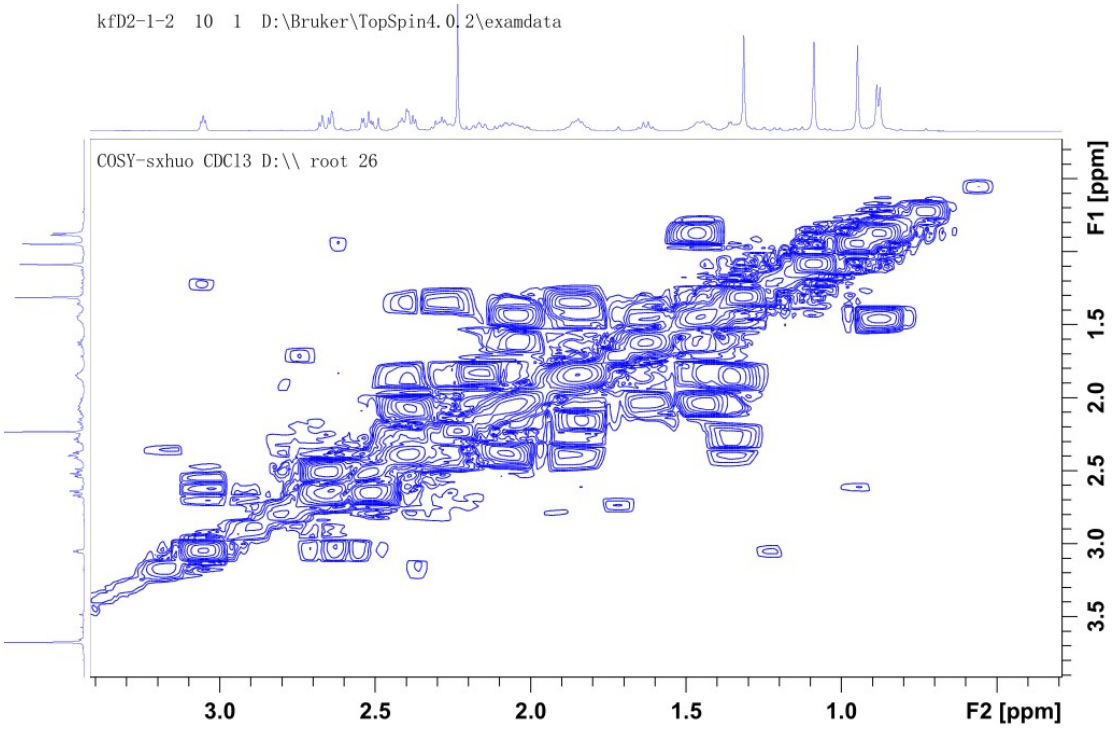

Figure S54. ROESY spectrum (600 MH, $CDCl_3$) of compound 8.

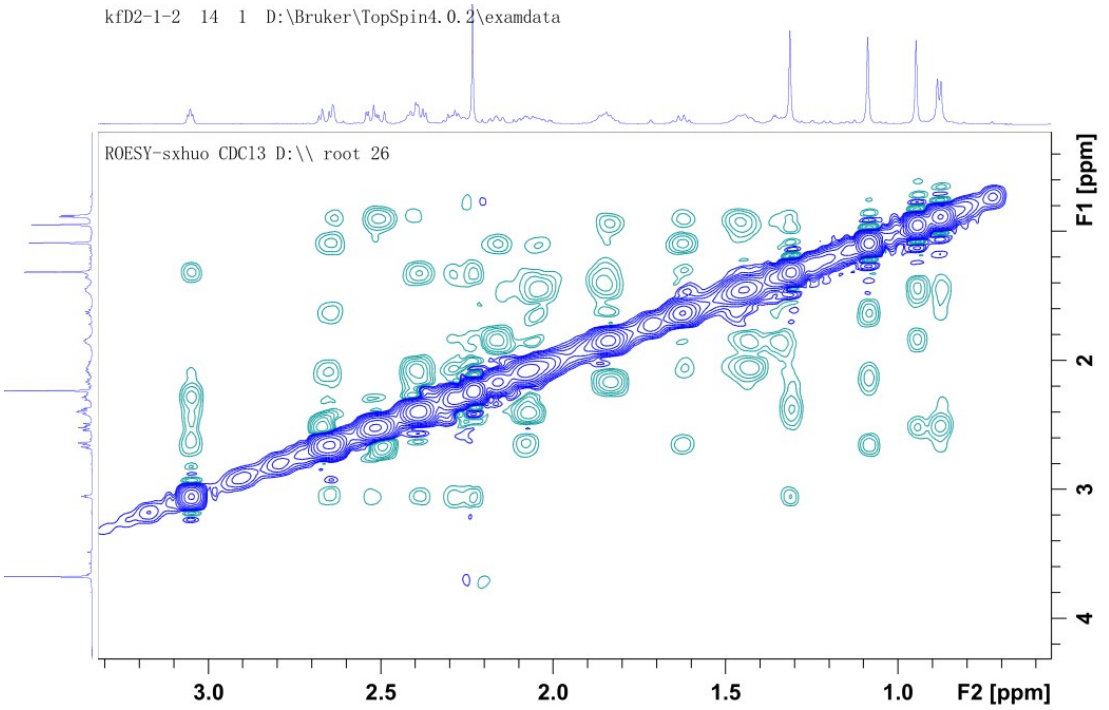

Figure S55. ^1H NMR spectrum (600 MH, $CDCl_3$) of compound 9.

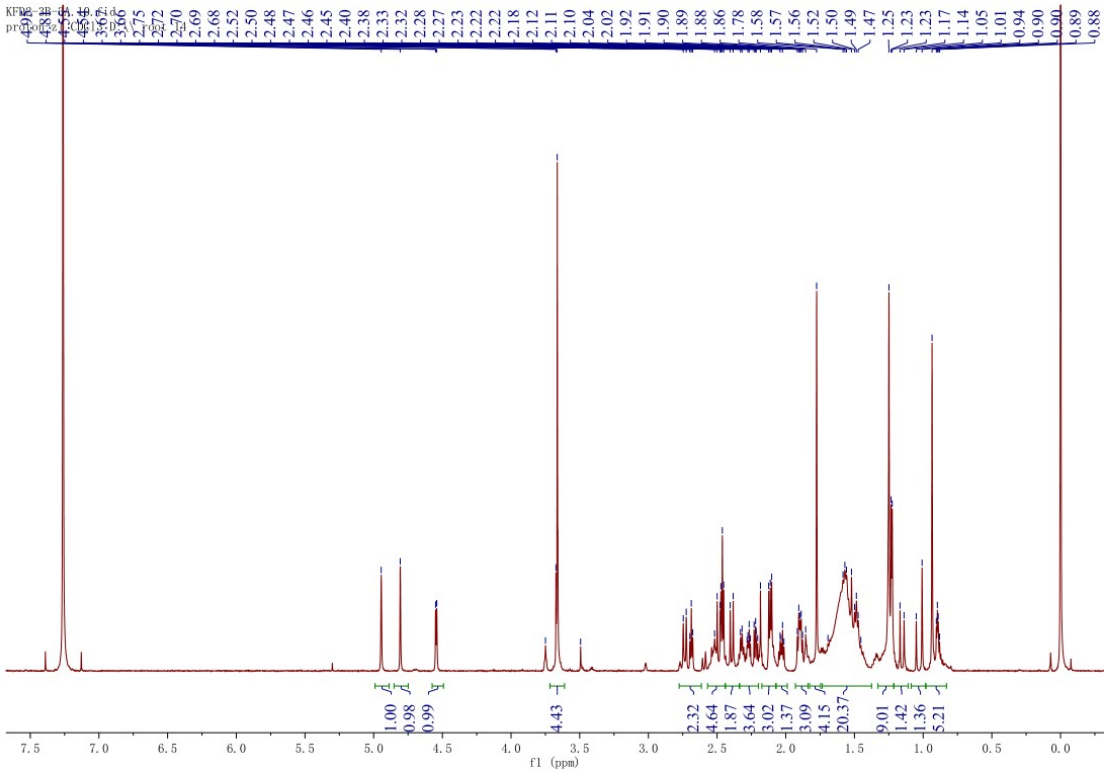

Figure S56. ^{13}C NMR spectrum (150 MH, $CDCl_3$) of compound 9.

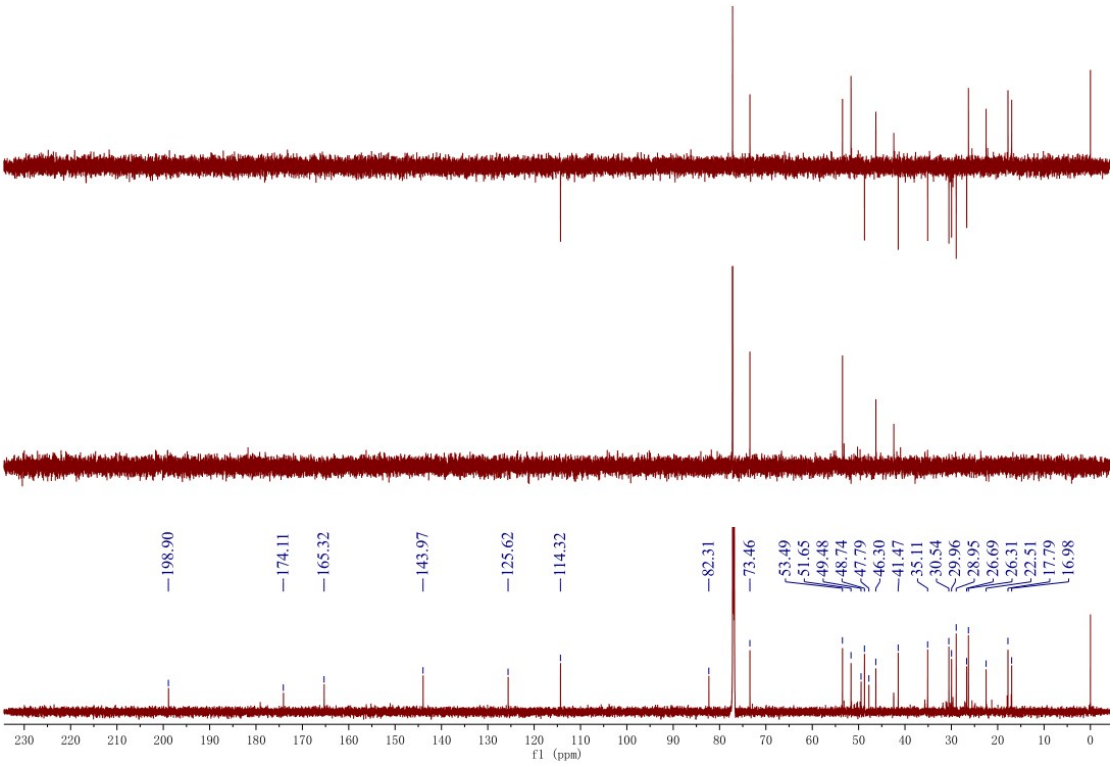

Figure S57. HSQC spectrum (600/150 MH, $CDCl_3$) of compound 9.

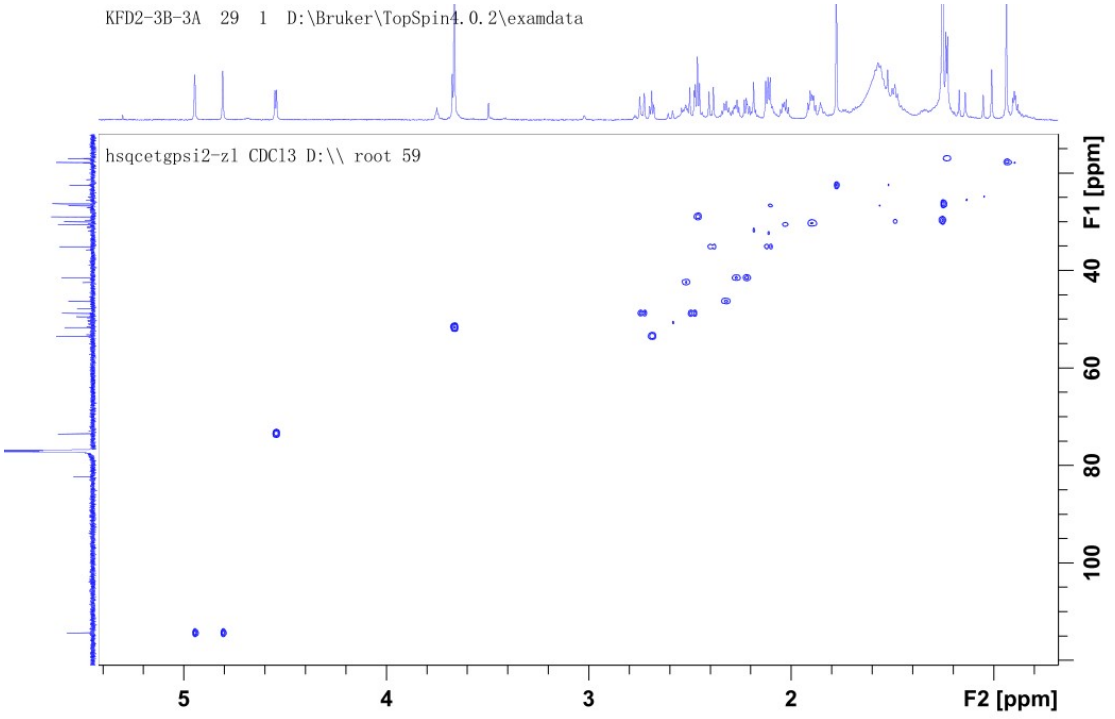

Figure S58. HMBC spectrum (600/150 MH, $CDCl_3$) of compound 9.

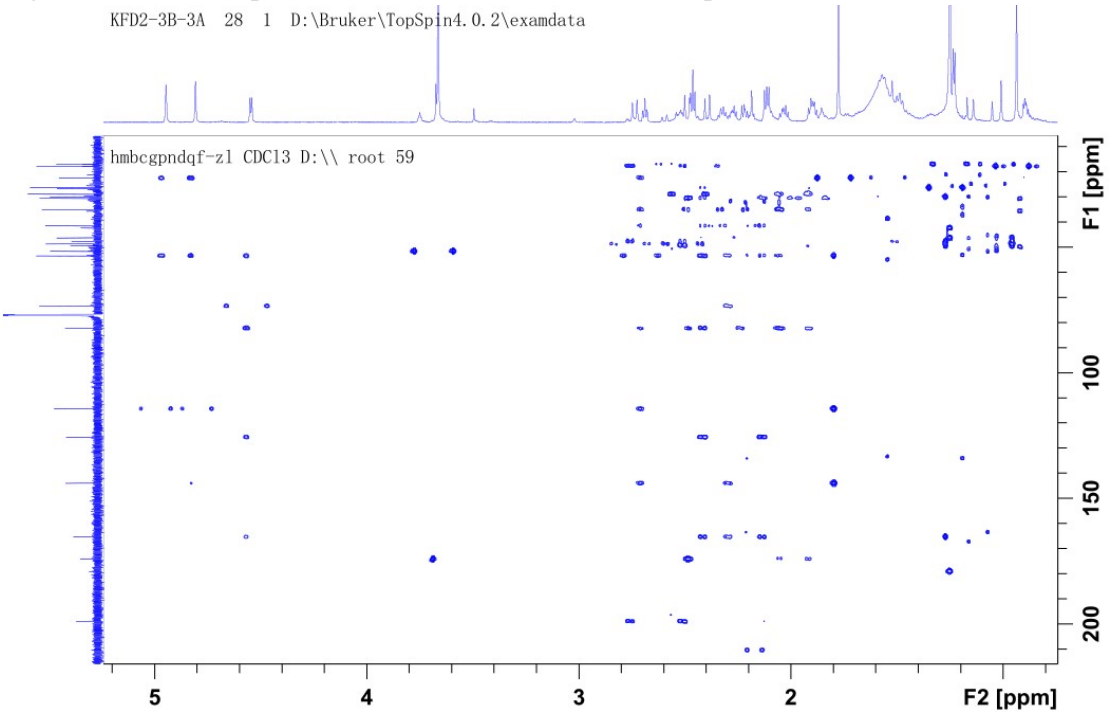

Figure S59. ^{1}H-^{1}H COSY spectrum (600 MH, $CDCl_3$) of compound 9.

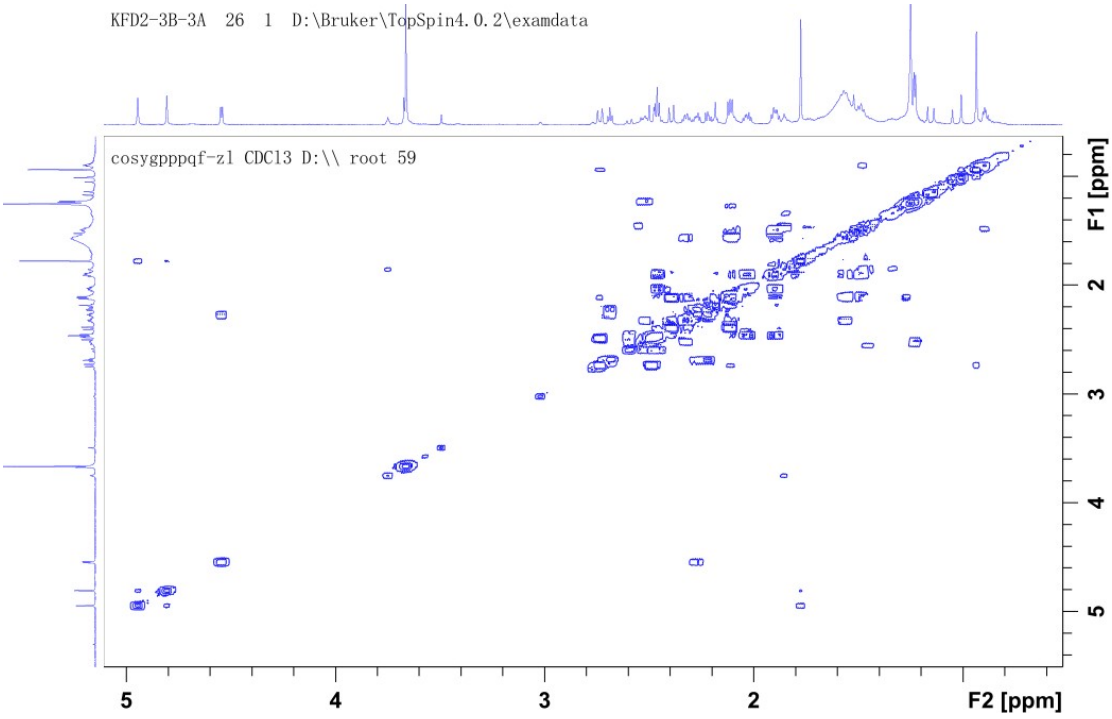

Figure S60. ROESY spectrum (600 MH, $CDCl_3$) of compound 9.

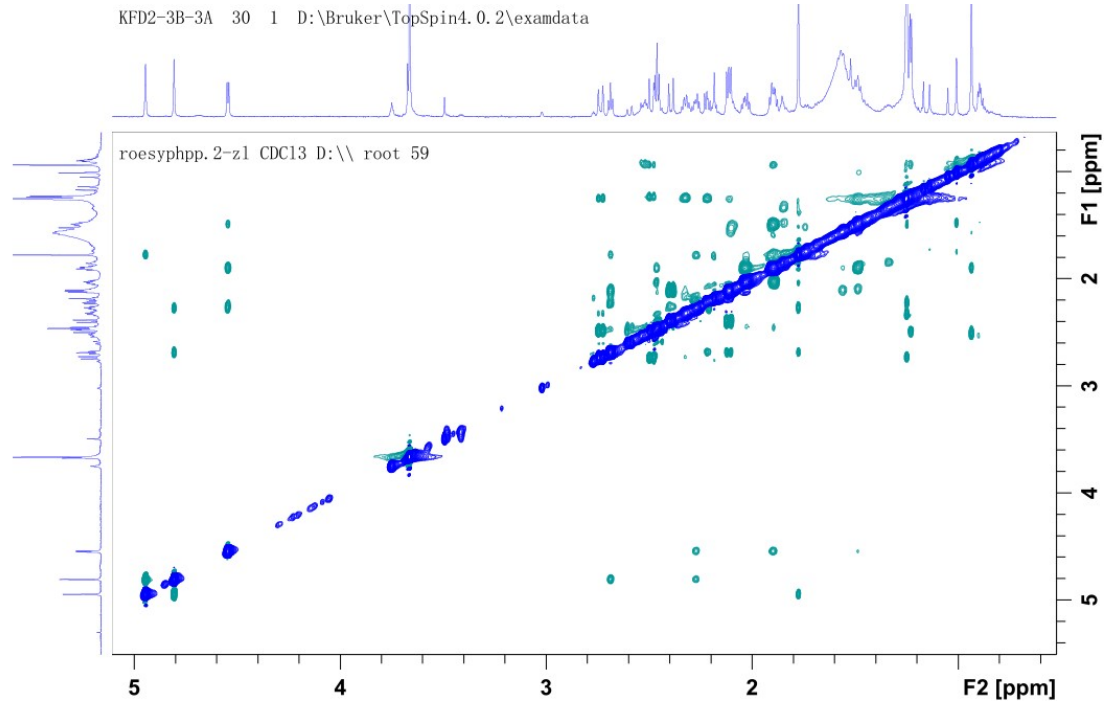

Figure S61. ^1H NMR spectrum (600 MH, $CDCl_3$) of compound 10.

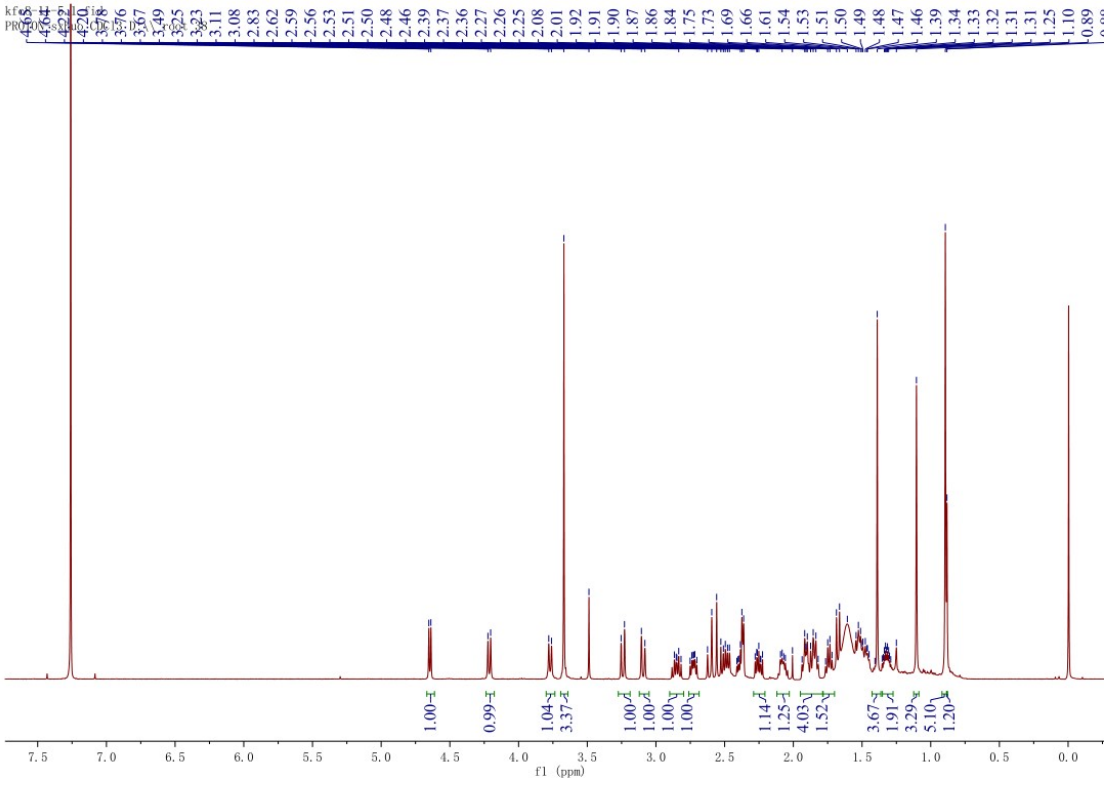

Figure S62. ^{13}C NMR spectrum (150 MH, $CDCl_3$) of compound 10.

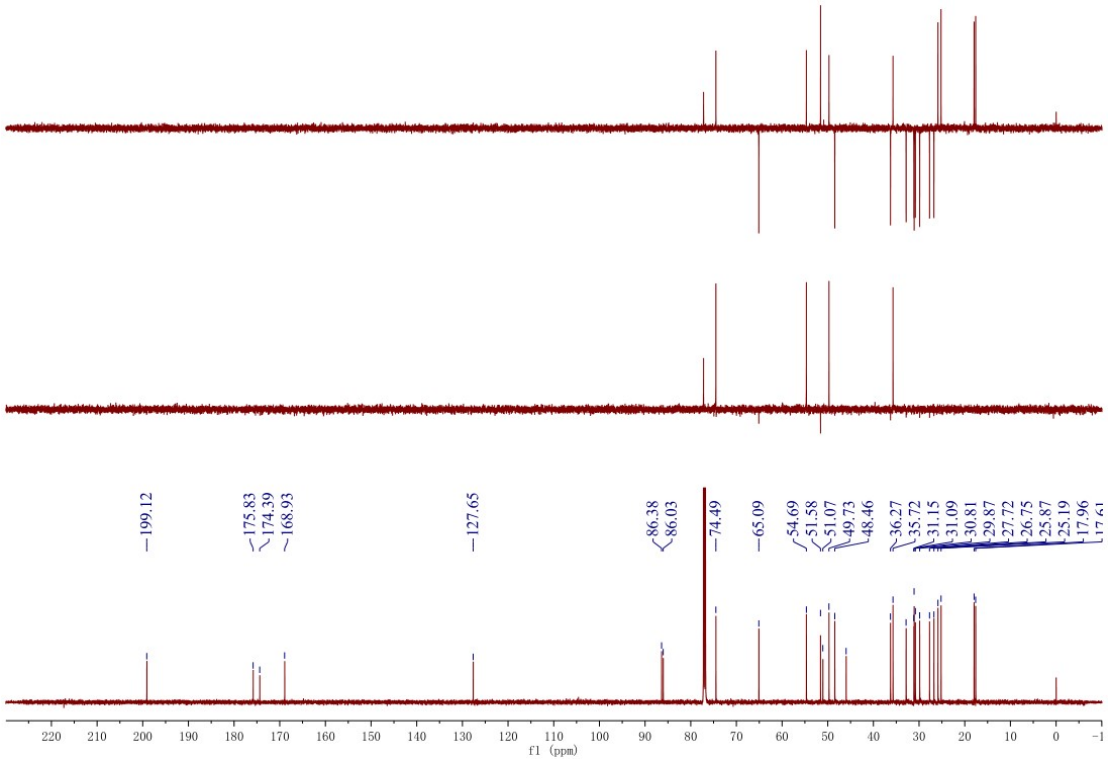

Figure S63. HSQC spectrum (600/150 MH, $CDCl_3$) of compound 10.

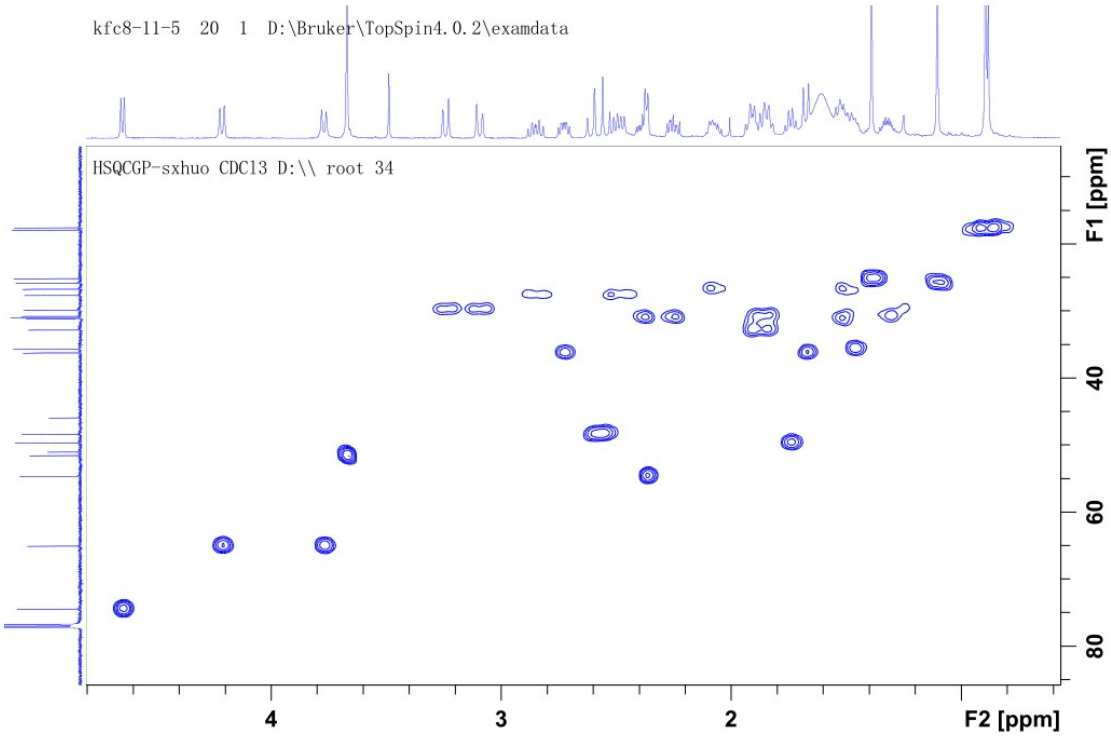

Figure S64. HMBC spectrum (600/150 MH, $CDCl_3$) of compound 10.

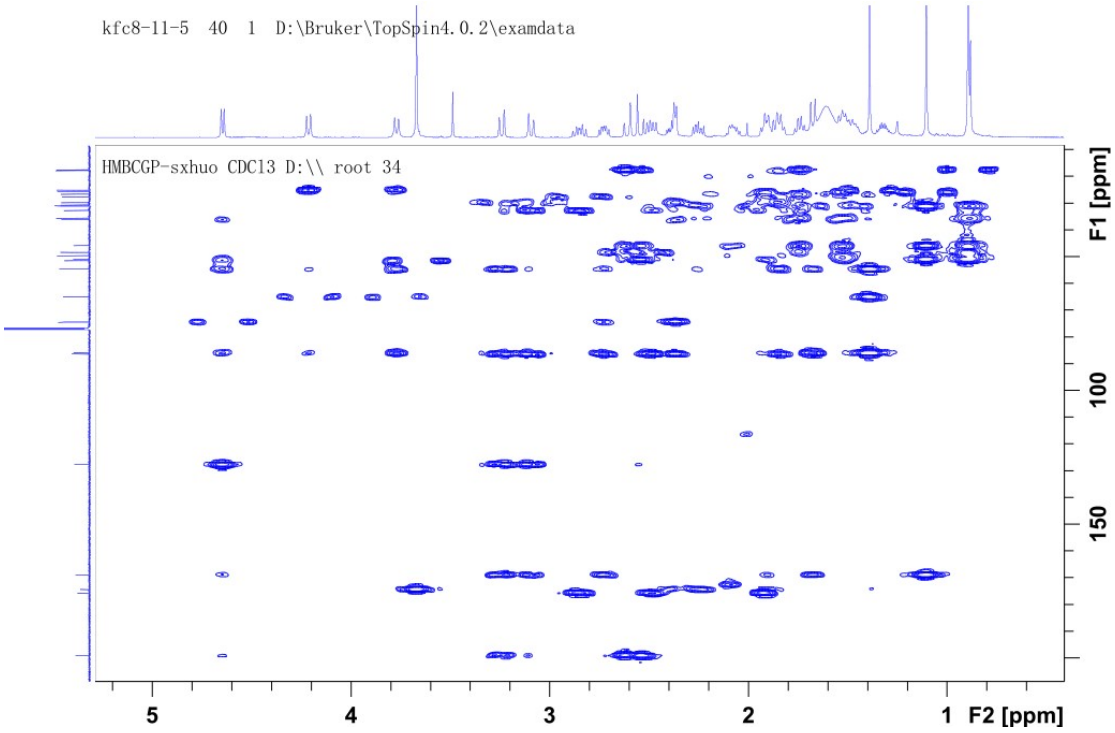

Figure S65. ^1H-^1H COSY spectrum (600 MH, $CDCl_3$) of compound 10.

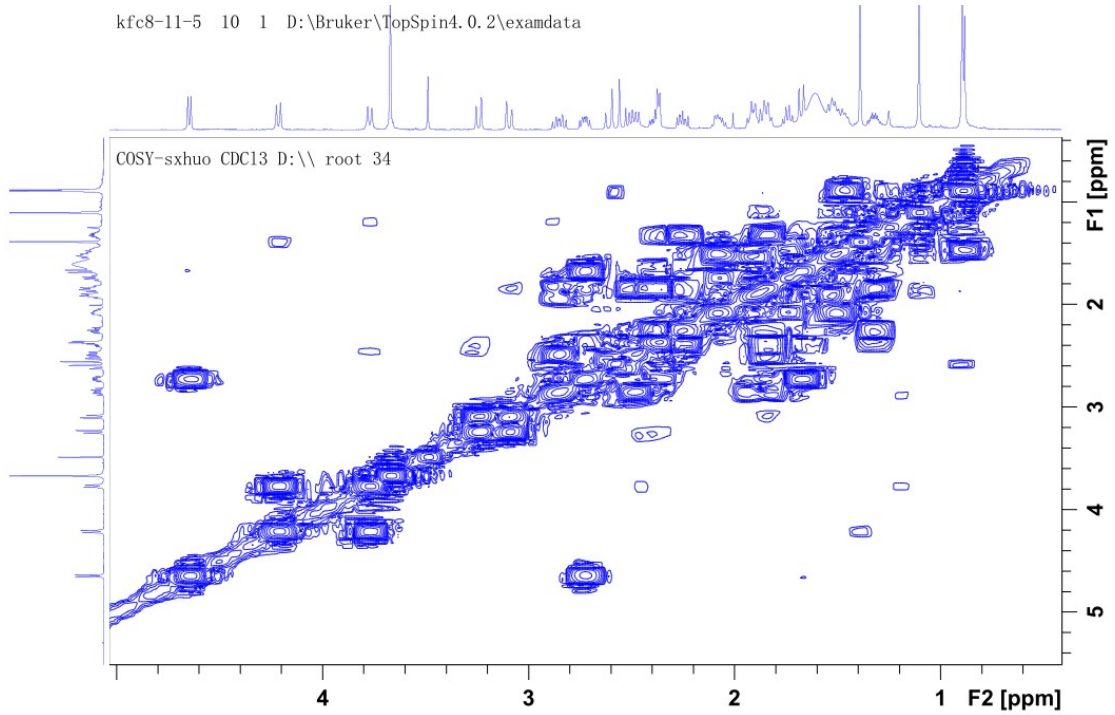

Figure S66. ROESY spectrum (600 MH, $CDCl_3$) of compound 10.

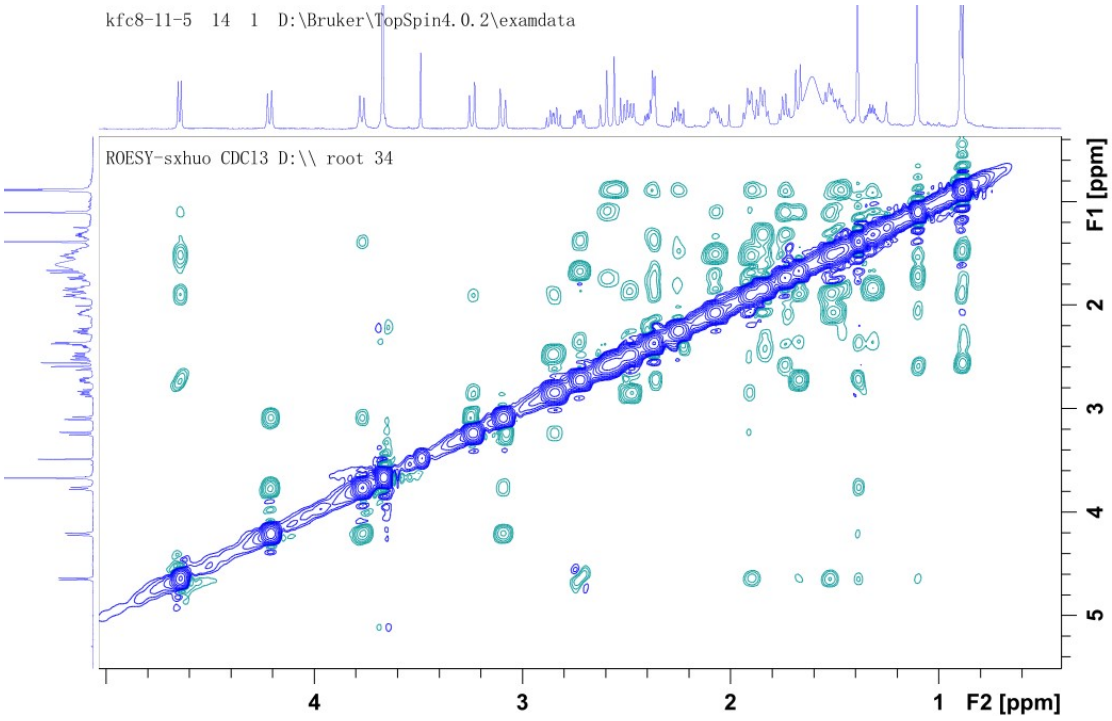

HRESIMS spectra of new compounds

Figure S67. **HRESIMS spectrum of compound 1.**

Qualitative Analysis Report

Data Filename	kfc8-12-5+.d	**Sample Name**	kfc8-12-5
Sample Type	Sample	**Position**	P1-C2
Instrument Name	Instrument 1	**User Name**	
Acq Method	s.m	**Acquired Time**	8/5/2022 7:10:04 PM
IRM Calibration Status	Success	**DA Method**	PCDL.m
Comment			

Sample Group	**Info.**
Acquisition SW Version	6200 series TOF/6500 series Q-TOF B.05.01 (B5125.2)

User Spectra

Fragmentor Voltage	Collision Energy	Ionization Mode
135	0	ESI

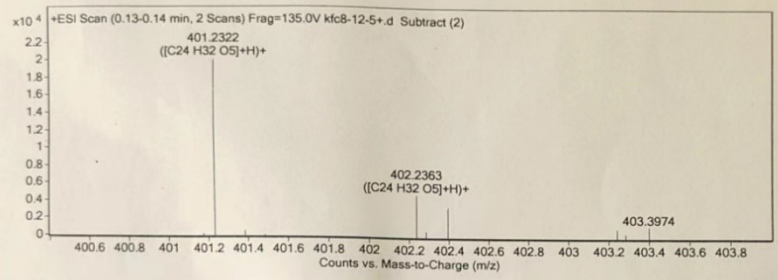

Peak List

m/z	z	Abund	Formula	Ion
274.2746	1	49620.82		
318.3008	1	46747.81		
401.2322	1	19914.69	C24 H32 O5	(M+H)+
437.1936	1	21394.35		
498.4422	1	53674.77		
499.4454	1	19708.68		
608.4251	1	47733.64		
609.4277	1	20782.95		
626.4351	1	42411.8		
627.4383	1	18953.54		

Formula Calculator Element Limits

Element	Min	Max
C	3	60
H	0	300
O	0	30
Cl	0	1

Formula Calculator Results

Formula	CalculatedMass	CalculatedMz	Mz	Diff. (mDa)	Diff. (ppm)	DBE
C24 H32 O5	400.2250	401.2323	401.2322	0.10	0.25	9.0000

--- End Of Report ---

Figure S68. HRESIMS spectrum of compound 2.

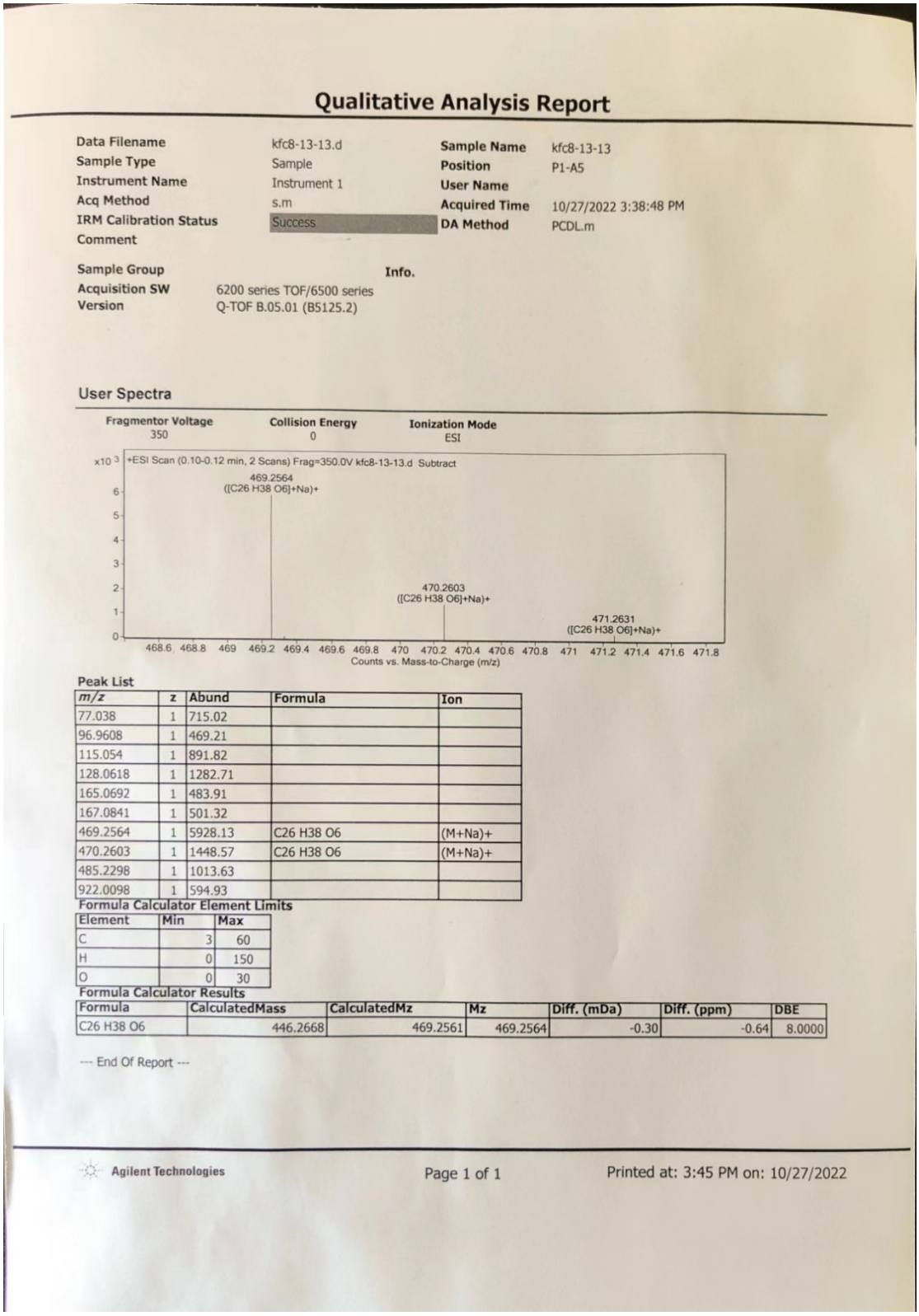

Qualitative Analysis Report

Data Filename	kfc8-13-13.d	**Sample Name**	kfc8-13-13
Sample Type	Sample	**Position**	P1-A5
Instrument Name	Instrument 1	**User Name**	
Acq Method	s.m	**Acquired Time**	10/27/2022 3:38:48 PM
IRM Calibration Status	Success	**DA Method**	PCDL.m
Comment			

Sample Group	**Info.**
Acquisition SW Version	6200 series TOF/6500 series Q-TOF B.05.01 (B5125.2)

User Spectra

Fragmentor Voltage	Collision Energy	Ionization Mode
350	0	ESI

Peak List

m/z	z	Abund	Formula	Ion
77.038	1	715.02		
96.9608	1	469.21		
115.054	1	891.82		
128.0618	1	1282.71		
165.0692	1	483.91		
167.0841	1	501.32		
469.2564	1	5928.13	C26 H38 O6	(M+Na)+
470.2603	1	1448.57	C26 H38 O6	(M+Na)+
485.2298	1	1013.63		
922.0098	1	594.93		

Formula Calculator Element Limits

Element	Min	Max
C	3	60
H	0	150
O	0	30

Formula Calculator Results

Formula	CalculatedMass	CalculatedMz	Mz	Diff. (mDa)	Diff. (ppm)	DBE
C26 H38 O6	446.2668	469.2561	469.2564	-0.30	-0.64	8.0000

--- End Of Report ---

Figure S69. HRESIMS spectrum of compound 3.

Qualitative Analysis Report

Data Filename	kfD2-1-3.d	**Sample Name**	kfD2-1-3
Sample Type	Sample	**Position**	P1-A2
Instrument Name	Instrument 1	**User Name**	
Acq Method	s-.m	**Acquired Time**	7/7/2022 3:49:00 PM
IRM Calibration Status	Success	**DA Method**	PCDL.m
Comment			

Sample Group **Info.**

Acquisition SW Version 6200 series TOF/6500 series Q-TOF B.05.01 (B5125.2)

User Spectra

Fragmentor Voltage	Collision Energy	Ionization Mode
135	0	ESI

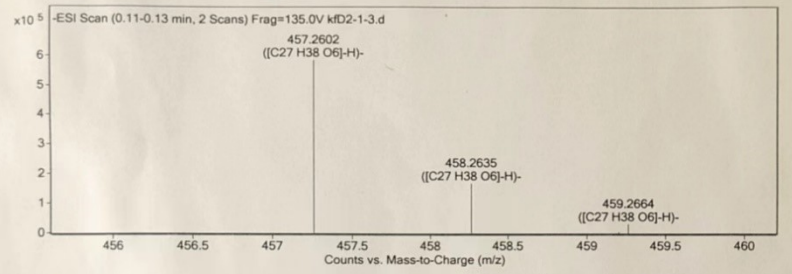

Peak List

m/z	z	Abund	Formula	Ion
112.9856		105301.97		
119.0365	1	129092.3		
457.2602	1	585371.81	C27 H38 O6	(M-H)-
458.2635	1	167561.88	C27 H38 O6	(M-H)-
503.2655	1	145443.75		
504.2686	1	45851.85		
525.2473	1	45404.75		
915.526	1	52806.61		
966.0004	1	46023.82		
1033.9881	1	97520.19		

Formula Calculator Element Limits

Element	Min	Max
C	3	120
H	0	250
O	0	30

Formula Calculator Results

Formula	CalculatedMass	CalculatedMz	Mz	Diff. (mDa)	Diff. (ppm)	DBE
C27 H38 O6	458.2668	457.2596	457.2602	-0.60	-1.31	9.0000

--- End Of Report ---

Figure S70. HRESIMS spectrum of compound 4.

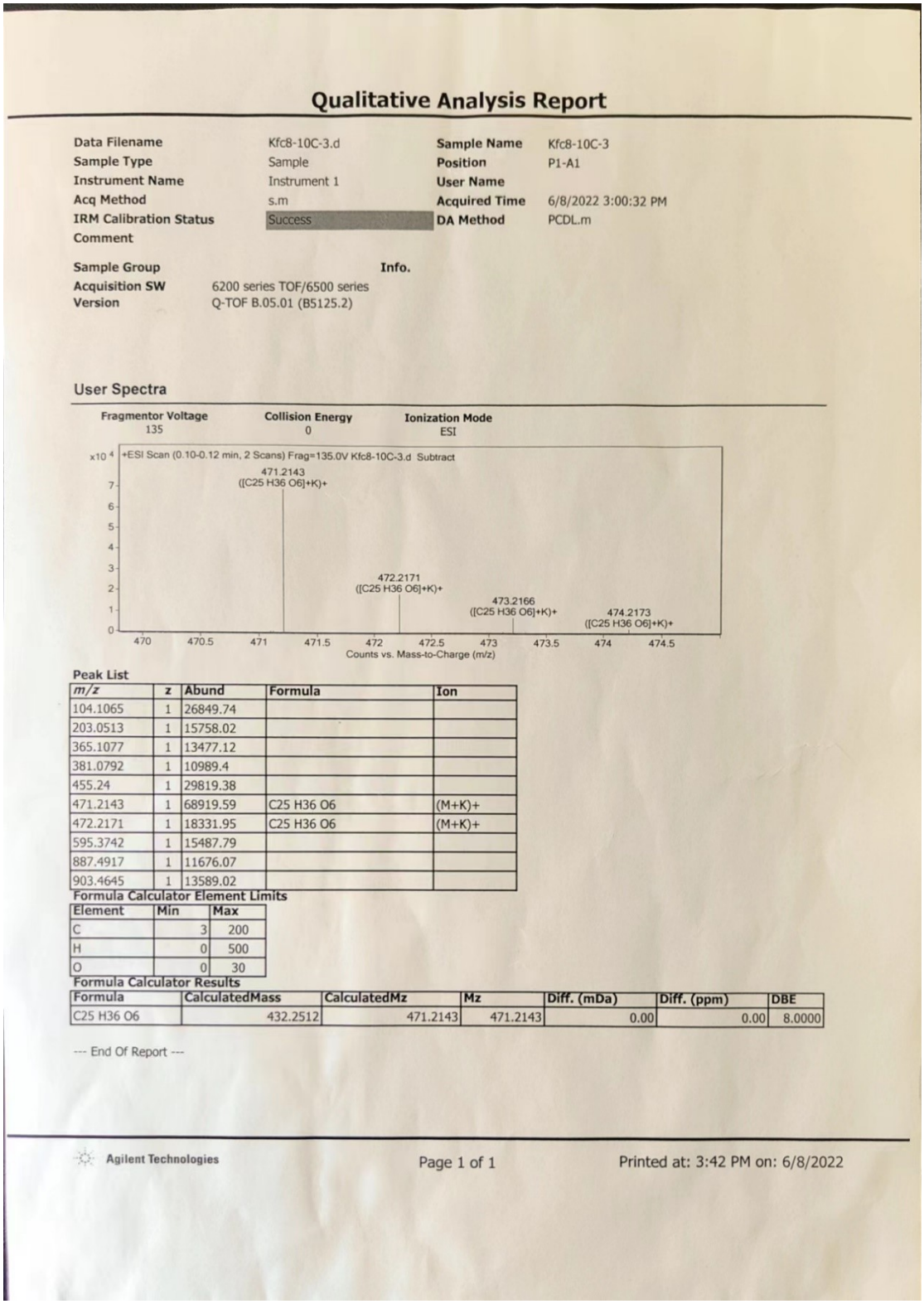

Qualitative Analysis Report

Data Filename	Kfc8-10C-3.d	**Sample Name**	Kfc8-10C-3
Sample Type	Sample	**Position**	P1-A1
Instrument Name	Instrument 1	**User Name**	
Acq Method	s.m	**Acquired Time**	6/8/2022 3:00:32 PM
IRM Calibration Status	Success	**DA Method**	PCDL.m
Comment			

Sample Group	**Info.**
Acquisition SW Version	6200 series TOF/6500 series Q-TOF B.05.01 (B5125.2)

User Spectra

Fragmentor Voltage	Collision Energy	Ionization Mode
135	0	ESI

Peak List

m/z	z	Abund	Formula	Ion
104.1065	1	26849.74		
203.0513	1	15758.02		
365.1077	1	13477.12		
381.0792	1	10989.4		
455.24	1	29819.38		
471.2143	1	68919.59	C25 H36 O6	(M+K)+
472.2171	1	18331.95	C25 H36 O6	(M+K)+
595.3742	1	15487.79		
887.4917	1	11676.07		
903.4645	1	13589.02		

Formula Calculator Element Limits

Element	Min	Max
C	3	200
H	0	500
O	0	30

Formula Calculator Results

Formula	CalculatedMass	CalculatedMz	Mz	Diff. (mDa)	Diff. (ppm)	DBE
C25 H36 O6	432.2512	471.2143	471.2143	0.00	0.00	8.0000

--- End Of Report ---

Figure S71. HRESIMS spectrum of compound 5.

Qualitative Analysis Report

Data Filename	kfc8-12-4.d	**Sample Name**	kfc8-12-4
Sample Type	Sample	**Position**	P1-A2
Instrument Name	Instrument 1	**User Name**	
Acq Method	s.m	**Acquired Time**	8/3/2022 2:25:06 PM
IRM Calibration Status	Success	**DA Method**	PCDL.m
Comment			

Sample Group **Info.**

Acquisition SW Version 6200 series TOF/6500 series Q-TOF B.05.01 (B5125.2)

User Spectra

Fragmentor Voltage	Collision Energy	Ionization Mode
135	0	ESI

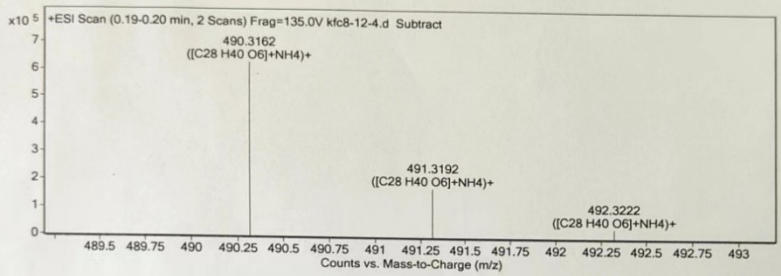

Peak List

m/z	z	Abund	Formula	Ion
473.2897	1	173277.55		
490.3162	1	626633.81	C28 H40 O6	(M+NH4)+
491.3192	1	175515	C28 H40 O6	(M+NH4)+
495.2714	1	154990.91		
518.3472	1	119163.45		
962.5977	1	99514.55		
963.601	1	62775.43		
967.5539	1	490104.38		
968.5569	1	304059.59		
969.5595	1	98724.64		

Formula Calculator Element Limits

Element	Min	Max
C	3	60
H	0	300
O	0	30

Formula Calculator Results

Formula	CalculatedMass	CalculatedMz	Mz	Diff. (mDa)	Diff. (ppm)	DBE
C28 H40 O6	472.2825	490.3163	490.3162	0.10	0.20	9.0000

--- End Of Report ---

Figure S72. HRESIMS spectrum of compound 6.

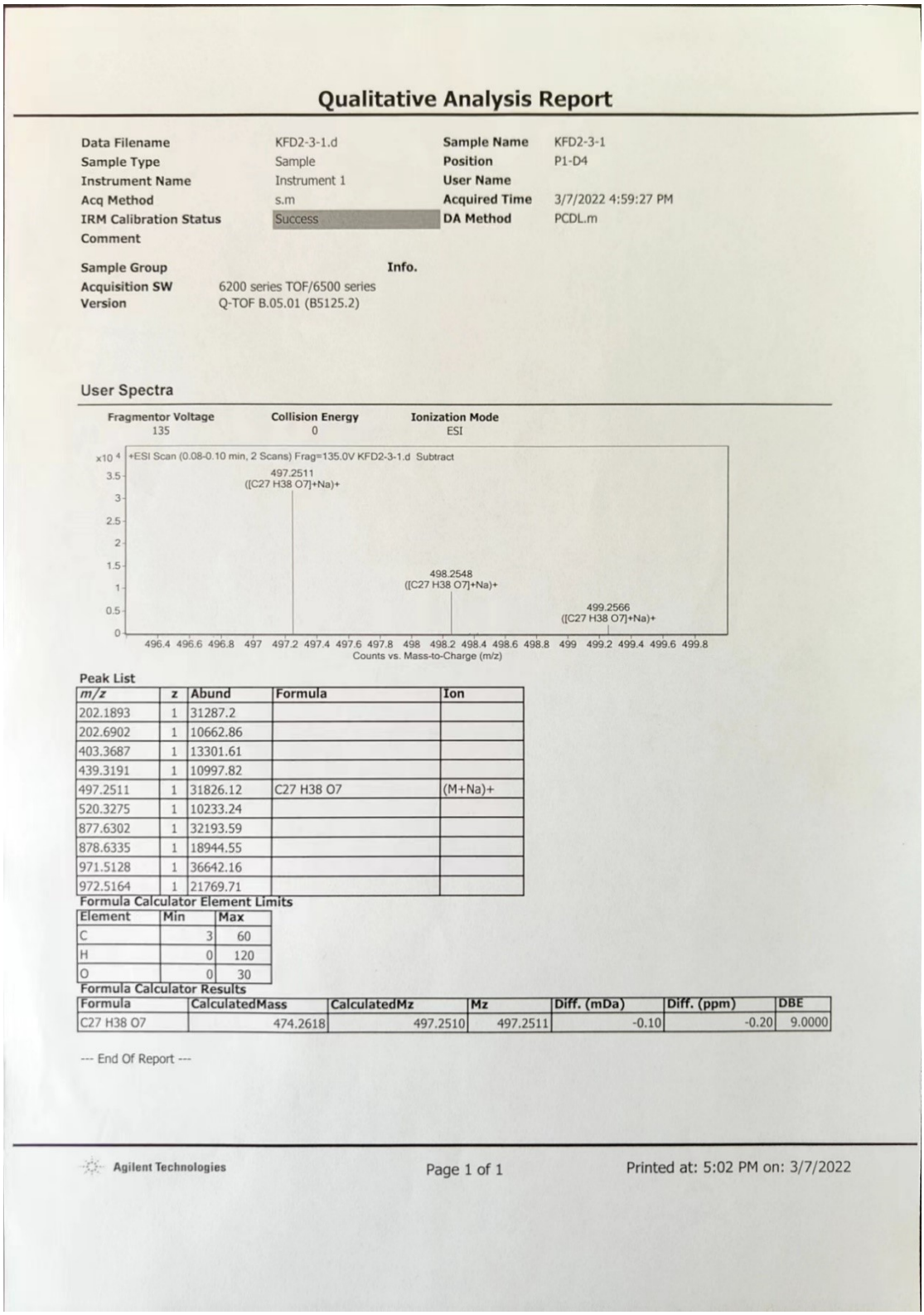

Qualitative Analysis Report

Data Filename	KFD2-3-1.d	**Sample Name**	KFD2-3-1
Sample Type	Sample	**Position**	P1-D4
Instrument Name	Instrument 1	**User Name**	
Acq Method	s.m	**Acquired Time**	3/7/2022 4:59:27 PM
IRM Calibration Status	Success	**DA Method**	PCDL.m
Comment			

Sample Group **Info.**

Acquisition SW Version 6200 series TOF/6500 series Q-TOF B.05.01 (B5125.2)

User Spectra

Fragmentor Voltage	Collision Energy	Ionization Mode
135	0	ESI

Peak List

m/z	z	Abund	Formula	Ion
202.1893	1	31287.2		
202.6902	1	10662.86		
403.3687	1	13301.61		
439.3191	1	10997.82		
497.2511	1	31826.12	C27 H38 O7	(M+Na)+
520.3275	1	10233.24		
877.6302	1	32193.59		
878.6335	1	18944.55		
971.5128	1	36642.16		
972.5164	1	21769.71		

Formula Calculator Element Limits

Element	Min	Max
C	3	60
H	0	120
O	0	30

Formula Calculator Results

Formula	CalculatedMass	CalculatedMz	Mz	Diff. (mDa)	Diff. (ppm)	DBE
C27 H38 O7	474.2618	497.2510	497.2511	-0.10	-0.20	9.0000

--- End Of Report ---

Figure S73. HRESIMS spectrum of compound 7.

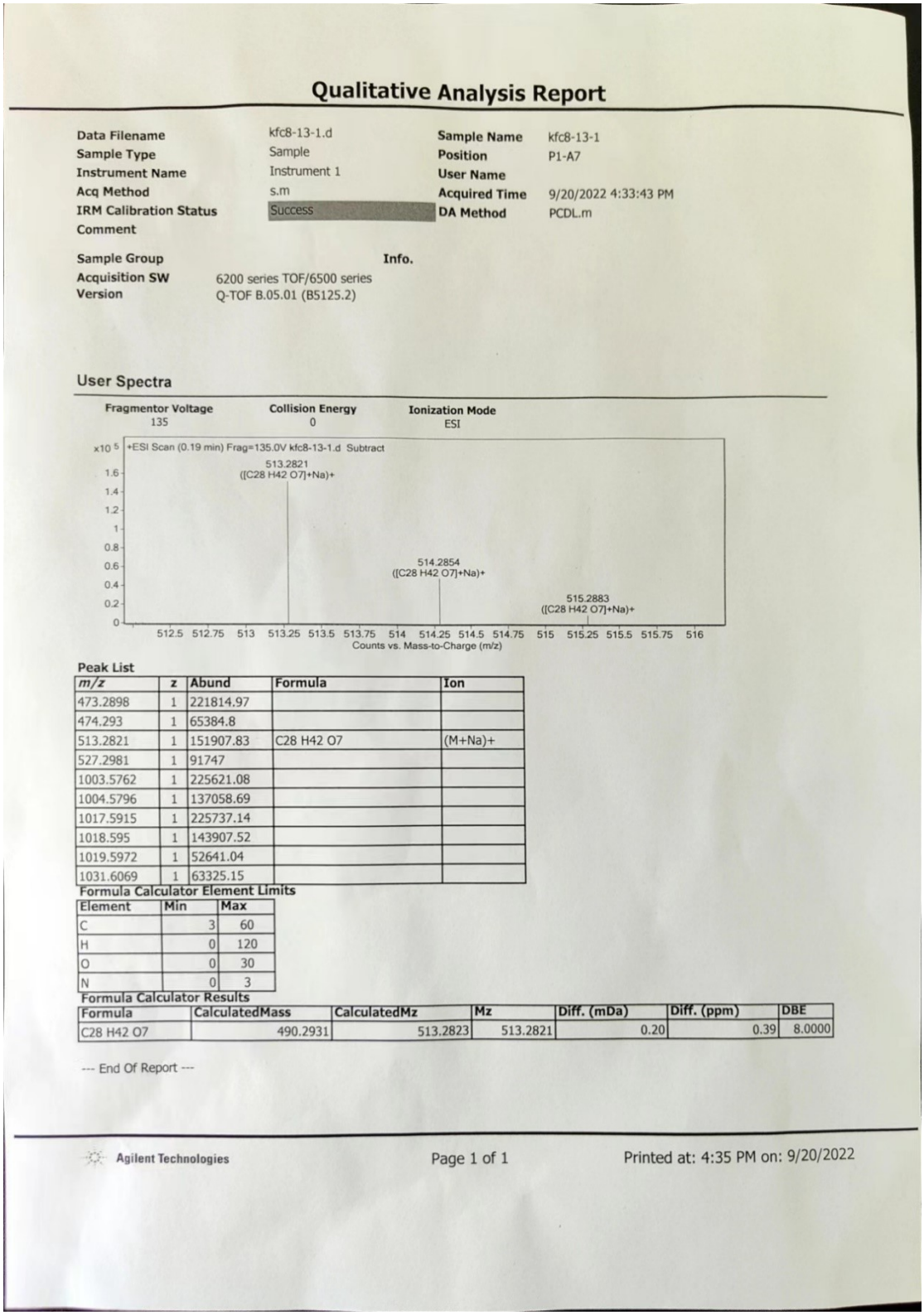

Qualitative Analysis Report

Data Filename	kfc8-13-1.d	**Sample Name**	kfc8-13-1
Sample Type	Sample	**Position**	P1-A7
Instrument Name	Instrument 1	**User Name**	
Acq Method	s.m	**Acquired Time**	9/20/2022 4:33:43 PM
IRM Calibration Status	Success	**DA Method**	PCDL.m
Comment			

Sample Group **Info.**

Acquisition SW Version 6200 series TOF/6500 series Q-TOF B.05.01 (B5125.2)

User Spectra

Fragmentor Voltage	Collision Energy	Ionization Mode
135	0	ESI

Peak List

m/z	z	Abund	Formula	Ion
473.2898	1	221814.97		
474.293	1	65384.8		
513.2821	1	151907.83	C28 H42 O7	(M+Na)+
527.2981	1	91747		
1003.5762	1	225621.08		
1004.5796	1	137058.69		
1017.5915	1	225737.14		
1018.595	1	143907.52		
1019.5972	1	52641.04		
1031.6069	1	63325.15		

Formula Calculator Element Limits

Element	Min	Max
C	3	60
H	0	120
O	0	30
N	0	3

Formula Calculator Results

Formula	CalculatedMass	CalculatedMz	Mz	Diff. (mDa)	Diff. (ppm)	DBE
C28 H42 O7	490.2931	513.2823	513.2821	0.20	0.39	8.0000

--- End Of Report ---

Figure S74. HRESIMS spectrum of compound 8.

Qualitative Analysis Report

Data Filename	kfD2-1-2.d	**Sample Name**	kfD2-1-2
Sample Type	Sample	**Position**	P1-A1
Instrument Name	Instrument 1	**User Name**	
Acq Method	s-.m	**Acquired Time**	7/7/2022 3:47:48 PM
IRM Calibration Status	Success	**DA Method**	PCDL.m
Comment			

Sample Group **Info.**

Acquisition SW Version 6200 series TOF/6500 series Q-TOF B.05.01 (B5125.2)

User Spectra

Fragmentor Voltage	Collision Energy	Ionization Mode
135	0	ESI

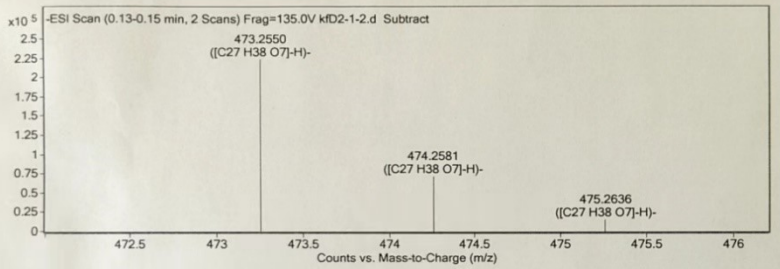

Peak List

m/z	z	Abund	Formula	Ion
112.9856		20192.06		
375.2756	1	9774.97		
473.255	1	223294.16	C27 H38 O7	(M-H)-
474.2581	1	71663.35	C27 H38 O7	(M-H)-
475.2636	1	14966.73	C27 H38 O7	(M-H)-
487.2702	1	12957.75		
519.2604	1	70048.14		
520.2635	1	21239.5		
541.2417	1	13120.13		
1033.9881	1	11821.45		

Formula Calculator Element Limits

Element	Min	Max
C	3	120
H	0	250
O	0	30

Formula Calculator Results

Formula	CalculatedMass	CalculatedMz	Mz	Diff. (mDa)	Diff. (ppm)	DBE
C27 H38 O7	474.2618	473.2545	473.2550	-0.50	-1.06	9.0000

--- End Of Report ---

Figure S75. HRESIMS spectrum of compound 9.

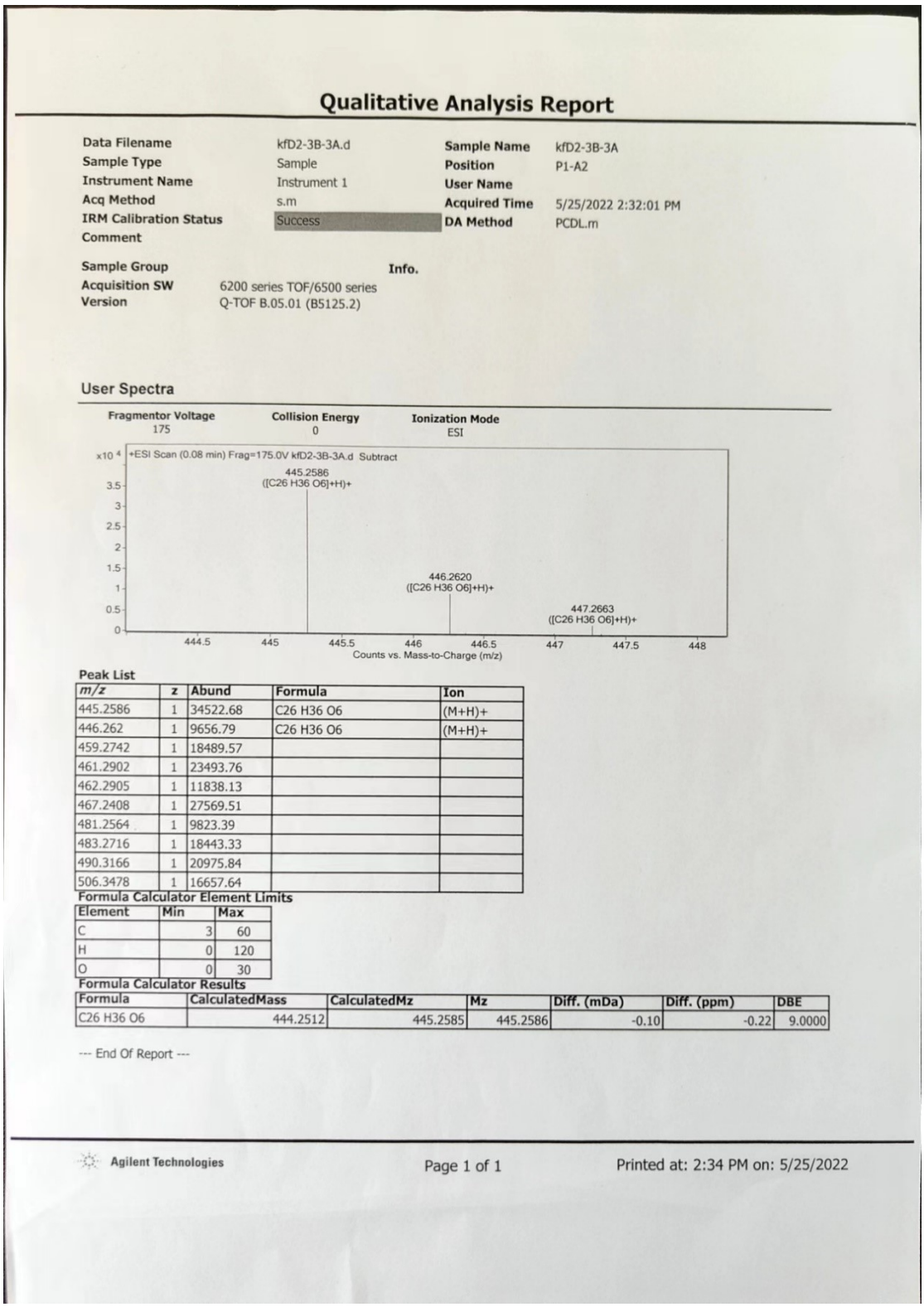

Qualitative Analysis Report

Data Filename	kfD2-3B-3A.d	**Sample Name**	kfD2-3B-3A
Sample Type	Sample	**Position**	P1-A2
Instrument Name	Instrument 1	**User Name**	
Acq Method	s.m	**Acquired Time**	5/25/2022 2:32:01 PM
IRM Calibration Status	Success	**DA Method**	PCDL.m
Comment			

Sample Group **Info.**

Acquisition SW Version 6200 series TOF/6500 series Q-TOF B.05.01 (B5125.2)

User Spectra

Fragmentor Voltage	Collision Energy	Ionization Mode
175	0	ESI

Peak List

m/z	z	Abund	Formula	Ion
445.2586	1	34522.68	C26 H36 O6	(M+H)+
446.262	1	9656.79	C26 H36 O6	(M+H)+
459.2742	1	18489.57		
461.2902	1	23493.76		
462.2905	1	11838.13		
467.2408	1	27569.51		
481.2564	1	9823.39		
483.2716	1	18443.33		
490.3166	1	20975.84		
506.3478	1	16657.64		

Formula Calculator Element Limits

Element	Min	Max
C	3	60
H	0	120
O	0	30

Formula Calculator Results

Formula	CalculatedMass	CalculatedMz	Mz	Diff. (mDa)	Diff. (ppm)	DBE
C26 H36 O6	444.2512	445.2585	445.2586	-0.10	-0.22	9.0000

--- End Of Report ---

Figure S76. HRESIMS spectrum of compound 10.

Qualitative Analysis Report

Data Filename	kfc8-11-5.d	**Sample Name**	kfc8-11-5
Sample Type	Sample	**Position**	P1-A6
Instrument Name	Instrument 1	**User Name**	
Acq Method	s.m	**Acquired Time**	7/18/2022 5:12:04 PM
IRM Calibration Status	Success	**DA Method**	PCDL.m
Comment			

Sample Group **Info.**

Acquisition SW Version 6200 series TOF/6500 series Q-TOF B.05.01 (B5125.2)

User Spectra

Fragmentor Voltage	Collision Energy	Ionization Mode
135	0	ESI

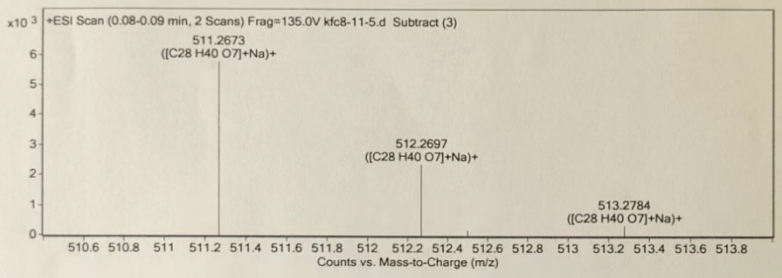

Peak List

m/z	z	Abund	Formula	Ion
274.2742	1	6710.53		
318.3016	1	4426.33		
340.2832	1	1683.01		
353.2664	1	2055.67		
437.1935	1	7427.04		
438.2055	1	1945.35		
506.3114	1	6683.55		
507.3167	1	2324.01		
511.2673	1	5780.68	C28 H40 O7	(M+Na)+
512.2697	1	2383.68	C28 H40 O7	(M+Na)+

Formula Calculator Element Limits

Element	Min	Max
C	3	120
H	0	200
O	0	30
N	0	3

Formula Calculator Results

Formula	CalculatedMass	CalculatedMz	Mz	Diff. (mDa)	Diff. (ppm)	DBE
C28 H40 O7	488.2774	511.2666	511.2673	-0.70	-1.37	9.0000

--- End Of Report ---

X-ray crystallographic data of compounds 2, 4, and 5

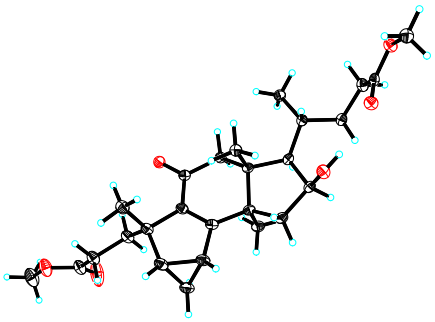

Figure S77. View of a molecule of compound **2** with the atom-labelling scheme. Displacement ellipsoids are drawn at the 30% probability level.

Table S3. Crystal data and structure refinement for compound 2.

Identification code	global	
Empirical formula	$C_{26}\ H_{38}\ O_6$	
Formula weight	446.56	
Temperature	150(2) K	
Wavelength	1.54178 Å	
Crystal system	Orthorhombic	
Space group	P21212	
Unit cell dimensions	a = 10.8614(3) Å	α= 90°.
	b = 36.7053(9) Å	β= 90°.
	c = 6.0922(2) Å	γ = 90°.
Volume	2428.78(12) Å3	
Z	4	
Density (calculated)	1.221 mg/m^3	
Absorption coefficient	0.689 mm^{-1}	
F(000)	968	
Crystal size	0.250 × 0.120 × 0.070 mm^3	
Theta range for data collection	2.41 to 68.32°.	
Index ranges	-13<=h<=12, -44<=k<=34, -7<=l<=6	
Reflections collected	15579	
Independent reflections	4402 [R(int) = 0.0887]	
Completeness to theta = 68.32°	99.80%	
Absorption correction	Semi-empirical from equivalents	
Max. and min. transmission	0.95 and 0.79	
Refinement method	Full-matrix least-squares on F2	
Data / restraints / parameters	4402 / 0 / 296	
Goodness-of-fit on F2	1.099	
Final R indices [I>2sigma(I)]	R1 = 0.0335, wR2 = 0.0856	
R indices (all data)	R1 = 0.0597, wR2 = 0.0960	
Absolute structure parameter	-0.05(6)	

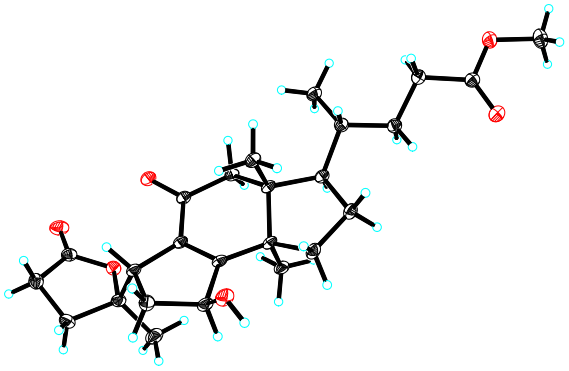

Figure S78. View of a molecule of compound **4** with the atom-labelling scheme. Displacement ellipsoids are drawn at the 30% probability level.

Table S4. Crystal data and structure refinement for compound 4.

Identification code	global	
Empirical formula	$C_{25}H_{36}O_6$	
Formula weight	432.54	
Temperature	150(2) K	
Wavelength	1.54178 Å	
Crystal system	Orthorhombic	
Space group	P212121	
Unit cell dimensions	a = 7.7089(3) Å	α = 90°.
	b = 8.1588(3) Å	β = 90°.
	c = 36.7130(13) Å	γ = 90°.
Volume	2309.08(15) Å3	
Z	4	
Density (calculated)	1.244 mg/m^3	
Absorption coefficient	0.709 mm^{-1}	
F(000)	936	
Crystal size	0.680 × 0.190 × 0.040 mm^3	
Theta range for data collection	2.41 to 69.95°.	
Index ranges	-9<=h<=9, -7<=k<=9, -44<=l<=44	
Reflections collected	16444	
Independent reflections	4355 [R(int) = 0.0890]	
Completeness to theta = 69.95°	99.90%	
Absorption correction	Semi-empirical from equivalents	
Max. and min. transmission	0.97 and 0.78	
Refinement method	Full-matrix least-squares on F2	
Data / restraints / parameters	4355 / 0 / 286	
Goodness-of-fit on F2	1.146	
Final R indices [I>2sigma(I)]	R1 = 0.0449, wR2 = 0.1142	
R indices (all data)	R1 = 0.0600, wR2 = 0.1190	
Absolute structure parameter	0.07(8)	
Largest diff. peak and hole	0.482 and -0.454 e.Å-3	

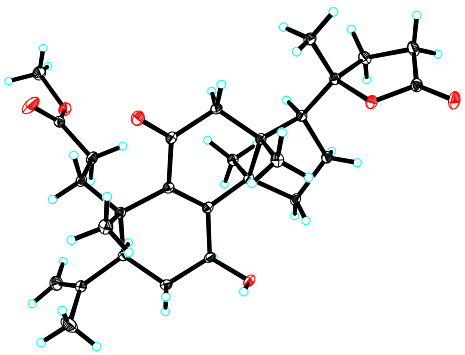

Figure S79. View of a molecule of compound **5** with the atom-labelling scheme. Displacement ellipsoids are drawn at the 30% probability level.

Table S5. Crystal data and structure refinement for compound 5.

Identification code	global	
Empirical formula	C_{28} $H_{40}O_6$	
Formula weight	472.6	
Temperature	150(2) K	
Wavelength	1.54178 Å	
Crystal system	Monoclinic	
Space group	P 1 21 1	
Unit cell dimensions	a = 8.1802(3) Å	α = 90°.
	b = 13.5202(4) Å	β = 90°.
	c = 11.2870(4) Å	γ = 90°.
Volume	1246.94(7) Å3	
Z	2	
Density (calculated)	1.259 mg/m^3	
Absorption coefficient	0.701 mm^{-1}	
F(000)	512	
Crystal size	0.540 × 0.450 × 0.280 mm^3	
Theta range for data collection	3.92 to 72.31°.	
Index ranges	-8<=h<=10, -16<=k<=16, -13<=l<=13	
Reflections collected	22359	
Independent reflections	4854 [R(int) = 0.0348]	
Completeness to theta = 69.95°	99.00%	
Absorption correction	Semi-empirical from equivalents	
Max. and min. transmission	0.83 and 0.69	
Refinement method	Full-matrix least-squares on F2	
Data / restraints / parameters	4854 / 1 / 314	
Goodness-of-fit on F2	0.978	
Final R indices [I>2sigma(I)]	R1 = 0.0311, wR2 = 0.1015	
R indices (all data)	R1 = 0.0312, wR2 = 0.1017	
Absolute structure parameter	-0.09(3)	
Largest diff. peak and hole	0.213 and -0.214 e.Å-3	

Calculated ECD data of compound 3

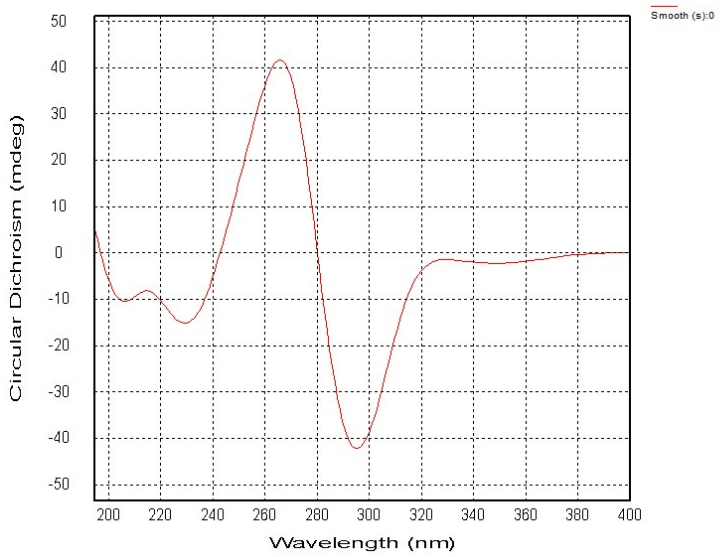

File: compound 2-1mm (195-400) 22090803.dsx
ProBinaryX
Attributes :
- Time Stamp: Thu Sep 08 13:38:16 2022
- File ID : F361B51F-DFB3-4086-8AA1-5D9E05E7A180
- Is CFR Compliant: false
- Original data has not been modified.
Remarks:
- User: CD
- Date: 2022/09/08
- Instrument: 0547
- DetectorType: LAAPD
- DichOS Calibration Correction Curve: 0547/2
- HV (CDDC channel): 0 v
- Time per point: 1 s
- Description: Sample 1
- Concentration: 0.4600 mg/mL MeOH
- Pathlength: 1 mm
- Temperature: 20℃
Settings:
- Time-per-point: 1s (25us x 40000)
- SE
- Wavelength: 195nm - 400nm
- Step Size: 1nm
- Bandwidth: 1nm

Figure S80. The CD spectrum of compound 3.

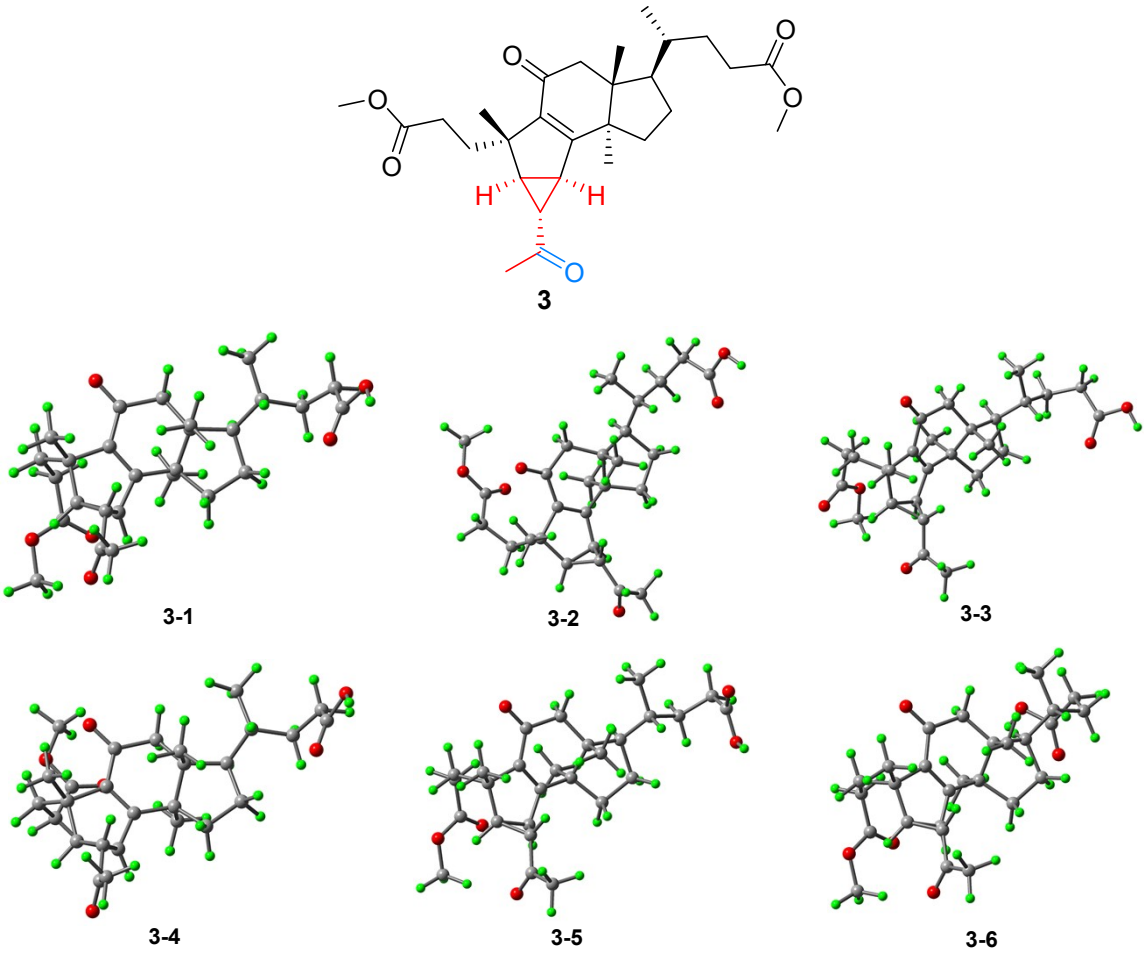

Figure S81. Six optimized conformers of 3.

Table S6. Conformational analysis of the six optimized conformers of 3 in the gas phase (T = 298.15 K)

Conformer	E (Hartree)	C (Hartree)	G (kcal/mol)	ΔG (kcal/mol)	Population
3-1	-1502.963528	0.537406	-942787.415691	0	50.38%
3-2	-1502.961835	0.536663	-942786.819782	0.595908597	18.42%
3-3	-1502.961967	0.537037	-942786.667542	0.748148798	14.24%
3-4	-1502.961837	0.537663	-942786.193728	1.221962773	6.40%
3-5	-1502.962021	0.537875	-942786.175875	1.239815433	6.21%
3-6	-1502.963046	0.539234	-942785.965986	1.449704978	4.35%

Electronic energy obtained at M062X/6-311+G(2d,p) EmpiricalDispersion=GD3 of theory; Thermal correction to Gibbs free energy obtained at B3LYP/6-31G(d) Scale=0.9813 SCRF=(IEFPCM,Solvent=Methanol) EmpiricalDispersion=GD3BJ of theory; Gibbs free energy (E + C); The relative Gibbs free energy; The Boltzmann distribution of each conformer.

Table S7. Atomic coordinates (Å) of 3-1 obtained at the Cam-B3LYP/6-311+G(d,p) level of theory in the MeOH.

C	-3.23512	0.526145	-0.56739	H	0.119621	-2.313954	0.32708
C	-2.122056	2.896378	-0.333574	H	0.932854	1.843407	2.580452
C	-1.13449	0.773697	0.569663	H	1.159912	2.32409	0.903301
C	-1.824834	-0.010336	-0.300388	H	3.317207	1.374559	1.078659
C	0.19691	0.375992	1.122447	H	2.906236	0.525473	2.556464
C	1.018129	-0.352274	-0.001508	H	2.240756	-1.418372	1.42333
C	0.207584	-1.568463	-0.473631	H	1.875098	1.435588	-0.975986
C	-1.219404	-1.201115	-0.89923	H	1.752793	0.019954	-2.016593
C	1.178004	1.466868	1.582592	H	0.308422	0.950923	-1.62946
C	2.5539	0.744099	1.544493	H	-0.729933	-1.391108	2.084626
C	2.37444	-0.581764	0.725174	H	0.786959	-0.862865	2.855399
C	1.24866	0.574155	-1.219442	H	-0.695622	0.065459	3.074908
C	-0.12209	-0.524864	2.351256	H	3.808412	-0.068877	-0.792381
O	-1.811074	-1.911788	-1.716835	H	3.074056	-3.015872	-0.36453
C	-1.894902	1.997591	0.899677	H	4.370407	-2.489437	-1.446797
C	3.615907	-0.918382	-0.125625	H	2.708263	-2.027755	-1.78732
C	3.428958	-2.179904	-0.980128	H	4.840201	-0.320261	1.575478
C	4.850734	-1.078924	0.789155	H	4.800665	-2.054169	1.290153
C	6.187484	-0.969472	0.053952	H	7.015565	-1.257482	0.715448
C	6.485584	0.434647	-0.422474	H	6.250334	-1.643829	-0.806332
O	7.5108	0.453524	-1.303706	H	7.666171	1.387841	-1.542075
O	5.917714	1.449686	-0.0675	H	-4.587147	1.070781	-2.180456
C	-3.585291	0.643382	-2.058433	H	-3.554387	-0.332164	-2.546478
C	-4.320083	-0.278333	0.203834	H	-2.872753	1.295602	-2.573463
C	-3.173286	1.904277	0.119222	H	-4.073245	-0.255477	1.270618
C	-2.38695	4.33414	-0.060752	H	-5.263685	0.2677	0.081917
C	-1.86563	5.315466	-1.085307	H	-2.123343	6.336742	-0.798902
O	-2.990992	4.69569	0.942761	H	-0.776564	5.21837	-1.174124
C	-4.562293	-1.732381	-0.210113	H	-2.285984	5.088097	-2.072495
C	-3.570128	-2.718017	0.366447	H	-5.550165	-2.046474	0.15403
O	-3.611285	-3.887548	-0.295365	H	-4.58428	-1.858993	-1.294175
O	-2.850457	-2.523466	1.329283	H	-1.651088	-4.534083	-0.035085
C	-2.671157	-4.884598	0.141134	H	-2.804144	-5.10518	1.202588
H	-4.086743	2.334432	0.517025	H	-2.878612	-5.767613	-0.462583
H	-1.809333	2.499346	1.857341				
H	-1.539323	2.667968	-1.220473				
H	0.663282	-2.079206	-1.324518				

Table S8. Atomic coordinates (Å) of 3-2 obtained at the Cam-B3LYP/6-311+G(d,p) level of theory in the MeOH.

C	2.79563	-0.680457	1.390819	H	-0.971786	-2.854745	0.019287
C	2.253769	1.860815	0.967764	H	-0.512386	1.333837	-2.353118
C	0.992294	-0.055739	-0.061568	H	-0.853291	1.911142	-0.726491
C	1.375258	-0.941184	0.894516	H	-3.119431	1.416268	-1.174525
C	-0.299256	-0.200235	-0.799252	H	-2.70924	0.467029	-2.589887
C	-1.396287	-0.716837	0.201496	H	-2.598587	-1.545554	-1.387277
C	-0.933739	-2.064621	0.779735	H	-2.328413	-0.135438	2.0802
C	0.501252	-2.030152	1.332218	H	-0.66748	0.431175	1.933556
C	-0.961535	1.0526	-1.395634	H	-1.961149	1.24348	1.047634
C	-2.450815	0.631029	-1.540007	H	0.237855	-2.187098	-1.617189
C	-2.657523	-0.683452	-0.709736	H	-0.860791	-1.257846	-2.654587
C	-1.593906	0.268625	1.377489	H	0.851171	-0.819779	-2.537107
C	-0.011174	-1.183595	-1.970829	H	-4.152325	0.141132	0.596154
O	0.880276	-2.912542	2.106212	H	-3.984226	-2.902256	0.252736
C	2.02811	0.980112	-0.272846	H	-5.279195	-2.099291	1.151181
C	-4.046809	-0.74386	-0.043294	H	-3.619491	-1.979677	1.719159
C	-4.239964	-1.998527	0.819845	H	-4.87735	0.052342	-1.894535
C	-5.15073	-0.67031	-1.121889	H	-5.233152	-1.6464	-1.616907
C	-6.524701	-0.274218	-0.579214	H	-7.295821	-0.403862	-1.3504
C	-6.591822	1.171867	-0.14129	H	-6.84135	-0.901106	0.260874
O	-7.711346	1.422968	0.573971	H	-7.702476	2.374237	0.795008
O	-5.777991	2.038676	-0.396402	H	2.250285	0.219608	3.305303
C	2.896829	-0.575603	2.921481	H	3.927143	-0.350532	3.219686
C	3.765093	-1.793494	0.908793	H	2.594346	-1.517018	3.386211
C	3.128508	0.65176	0.697344	H	4.78745	-1.502312	1.174859
C	2.874484	3.188217	0.708724	H	3.529027	-2.701568	1.471526
C	2.429324	4.322631	1.601415	H	1.346039	4.467469	1.507354
O	3.69805	3.346568	-0.186403	H	2.626073	4.073882	2.651334
C	3.710207	-2.156426	-0.586911	H	2.949992	5.244066	1.334669
C	4.115498	-1.061826	-1.549684	H	4.392114	-2.999647	-0.754726
O	5.314822	-0.535429	-1.22911	H	2.709619	-2.483114	-0.87513
O	3.46957	-0.699432	-2.515736	H	5.104361	1.451901	-1.812029
C	5.742739	0.589136	-2.022653	H	6.767096	0.791887	-1.711836
H	4.160319	0.87564	0.45736	H	5.702501	0.347191	-3.086178
H	2.199825	1.43578	-1.240555				
H	1.51023	1.812324	1.756957				
H	-1.568952	-2.407157	1.600183				

Table S9. Atomic coordinates (Å) of 3-3 obtained at the Cam-B3LYP/6-311+G(d,p) level of theory in the MeOH.

C	-2.830567	-0.689934	-1.430543	H	0.892765	-2.84227	0.038079
C	-2.302268	1.857478	-1.056942	H	0.475589	1.427938	2.257021
C	-1.026725	-0.032334	0.008477	H	0.837853	1.941083	0.613658
C	-1.409647	-0.939055	-0.9275	H	3.094428	1.438762	1.105227
C	0.259729	-0.160121	0.75781	H	2.658246	0.54156	2.546426
C	1.359086	-0.721254	-0.214889	H	2.541277	-1.508739	1.410107
C	0.885565	-2.081511	-0.75289	H	1.959183	1.201644	-1.121502
C	-0.537057	-2.041249	-1.335537	H	2.30721	-0.215726	-2.107291
C	0.930152	1.106682	1.314781	H	0.655339	0.383143	-1.986073
C	2.413026	0.673549	1.488895	H	0.801507	-1.168878	2.647426
C	2.613471	-0.670252	0.704768	H	-0.894316	-0.685517	2.523304
C	1.576829	0.222927	-1.421219	H	-0.326404	-2.103802	1.647033
C	-0.047804	-1.095721	1.963396	H	4.126295	0.096507	-0.615448
O	-0.908871	-2.930915	-2.104524	H	3.924386	-2.932033	-0.174169
C	-2.063206	1.004648	0.199524	H	5.236512	-2.172262	-1.085105
C	4.007236	-0.765801	0.051932	H	3.58383	-2.054028	-1.673538
C	4.195208	-2.050011	-0.767817	H	4.829794	0.081772	1.884029
C	5.103201	-0.66705	1.136663	H	5.17363	-1.627662	1.662826
C	6.484558	-0.299443	0.592714	H	7.248947	-0.412112	1.373189
C	6.56757	1.131867	0.111187	H	6.801732	-0.954421	-0.225498
O	7.696778	1.352557	-0.598797	H	7.697539	2.296544	-0.849313
O	5.757537	2.012038	0.330116	H	-2.275607	0.182588	-3.356375
C	-2.925414	-0.605223	-2.963213	H	-3.954124	-0.382581	-3.268373
C	-3.789251	-1.809396	-0.942614	H	-2.622826	-1.55372	-3.413265
C	-3.171356	0.651513	-0.754291	H	-4.810628	-1.556317	-1.250216
C	-2.921677	3.189853	-0.819688	H	-3.508477	-2.729734	-1.462069
C	-2.517259	4.295465	-1.766348	H	-3.039765	5.220695	-1.516836
O	-3.713059	3.371713	0.09921	H	-1.433296	4.454845	-1.710918
C	-3.783964	-2.096906	0.568704	H	-2.742998	4.006658	-2.800061
C	-4.448425	-1.006365	1.377907	H	-4.359488	-3.013382	0.746868
O	-3.676955	-0.585561	2.398672	H	-2.771429	-2.2675	0.937886
O	-5.553022	-0.549193	1.146986	H	-5.166096	0.246913	3.60922
C	-4.205163	0.514614	3.164959	H	-3.464761	0.711762	3.939163
H	-4.201736	0.87365	-0.504086	H	-4.330334	1.389366	2.521302
H	-2.221685	1.492172	1.153875				
H	-1.567647	1.79206	-1.853187				
H	1.531188	-2.465897	-1.545966				

Table S10. Atomic coordinates (Å) of 3-4 obtained at the Cam-B3LYP/6-311+G(d,p) level of theory in the MeOH.

C	-3.153679	0.39634	-0.869514	H	0.165579	-2.356128	0.316631
C	-2.25723	2.804436	-0.325539	H	0.830543	1.911184	2.428515
C	-1.158136	0.670856	0.445269	H	1.080915	2.31793	0.734748
C	-1.761872	-0.109811	-0.48915	H	3.265316	1.451443	1.011653
C	0.179718	0.347103	1.029811	H	2.840126	0.650505	2.511939
C	1.049861	-0.390264	-0.051639	H	2.271354	-1.360721	1.441925
C	0.288462	-1.64443	-0.509325	H	1.811142	-0.068956	-2.065501
C	-1.118181	-1.312966	-1.019991	H	0.354146	0.862516	-1.730203
C	1.110818	1.495965	1.455701	H	1.905356	1.377159	-1.06596
C	2.509419	0.816122	1.482791	H	-0.679563	-1.409939	2.073545
C	2.394537	-0.548252	0.714271	H	0.801346	-0.770312	2.830548
C	1.289163	0.504273	-1.29344	H	-0.723667	0.097268	2.983656
C	-0.115457	-0.504606	2.298342	H	3.8517	-0.045797	-0.785604
O	-1.68584	-2.065692	-1.816335	H	2.843399	-2.075192	-1.732524
C	-2.023106	1.81157	0.823414	H	3.201572	-2.997333	-0.263967
C	3.668281	-0.875044	-0.091571	H	4.509399	-2.468324	-1.331091
C	3.545924	-2.173363	-0.901354	H	4.826084	-0.170164	1.61498
C	4.881967	-0.959133	0.860964	H	4.8481	-1.914488	1.400225
C	6.234886	-0.836928	0.158195	H	7.052452	-1.071784	0.852909
C	6.503581	0.555165	-0.36826	H	6.342683	-1.54323	-0.671542
O	7.560356	0.572171	-1.211447	H	7.69287	1.500197	-1.485466
O	5.889047	1.564056	-0.079616	H	-2.551874	1.402438	-2.7229
C	-3.288561	0.670662	-2.379223	H	-4.287406	1.061137	-2.605877
C	-4.291388	-0.578107	-0.46373	H	-3.139199	-0.25503	-2.940208
C	-3.248552	1.690496	-0.035022	H	-5.227998	-0.008896	-0.472972
C	-2.660002	4.18243	0.065526	H	-4.385492	-1.350624	-1.229766
C	-2.175078	5.300231	-0.828482	H	-1.078728	5.300353	-0.864459
O	-3.345229	4.390386	1.060187	H	-2.526118	5.139874	-1.85516
C	-4.133573	-1.265266	0.908692	H	-2.532815	6.263637	-0.460703
C	-3.354691	-2.56227	0.841358	H	-3.645224	-0.615372	1.637995
O	-3.914723	-3.421221	-0.028025	H	-5.128533	-1.513837	1.296576
O	-2.359121	-2.834459	1.488555	H	-2.223254	-4.406064	-0.71987
C	-3.186715	-4.64079	-0.262524	H	-3.035051	-5.184615	0.672293
H	-4.214811	2.010564	0.341484	H	-3.804209	-5.221139	-0.947476
H	-2.032011	2.219882	1.82853				
H	-1.612736	2.715253	-1.193926				
H	0.796317	-2.181827	-1.312937				

Table S11. Atomic coordinates (Å) of 3-5 obtained at the Cam-B3LYP/6-311+G(d,p) level of theory in the MeOH.

C	-2.741717	-0.666045	-1.438733	H	1.083615	-2.745604	-0.062543
C	-2.310669	1.87572	-0.90264	H	0.395446	1.312848	2.470357
C	-0.999385	-0.030994	0.081966	H	0.737608	1.979672	0.878608
C	-1.324888	-0.89213	-0.916478	H	3.006452	1.569902	1.327184
C	0.279491	-0.155577	0.845111	H	2.636284	0.557557	2.710401
C	1.41992	-0.585294	-0.149408	H	2.612853	-1.422983	1.440584
C	1.025244	-1.926744	-0.790438	H	1.91184	1.431506	-0.904371
C	-0.399133	-1.929626	-1.371615	H	2.377547	0.112321	-1.974998
C	0.873213	1.096836	1.509957	H	0.687019	0.591959	-1.859498
C	2.377934	0.738412	1.663529	H	-0.19585	-2.195056	1.567657
C	2.656637	-0.536561	0.794611	H	0.840718	-1.267746	2.668805
C	1.60352	0.453107	-1.28106	H	-0.883948	-0.892243	2.527304
C	0.004806	-1.198242	1.967806	H	4.159559	0.394443	-0.429606
O	-0.725929	-2.7986	-2.183496	H	5.365385	-1.69536	-1.130387
C	-2.079717	0.955225	0.307519	H	3.675929	-1.738039	-1.603678
C	4.068473	-0.52065	0.172456	H	4.212697	-2.665695	-0.195065
C	4.343733	-1.722454	-0.739982	H	4.888145	0.404642	1.956324
C	5.116664	-0.44118	1.302619	H	5.051538	-1.346039	1.920661
C	6.575923	-0.292119	0.825455	H	7.217864	-0.115102	1.695808
C	6.737985	0.861437	-0.133408	H	6.933734	-1.191238	0.321529
O	6.443674	2.047028	0.449834	H	6.540002	2.735044	-0.236373
O	7.063249	0.775866	-1.301526	H	-3.839492	-0.30849	-3.282996
C	-2.808691	-0.504198	-2.966383	H	-2.456885	-1.41385	-3.458944
C	-3.678603	-1.833706	-1.026834	H	-2.185505	0.330404	-3.302092
C	-3.143063	0.623687	-0.702258	H	-4.705085	-1.569566	-1.304961
C	-2.991121	3.166097	-0.608185	H	-3.395517	-2.707482	-1.621169
C	-2.577908	4.350426	-1.449973	H	-2.744731	4.132727	-2.511908
O	-3.837808	3.256555	0.274664	H	-3.142208	5.238674	-1.160352
C	-3.643038	-2.257679	0.453223	H	-1.503682	4.537042	-1.329234
C	-4.109555	-1.220394	1.450908	H	-4.296604	-3.13141	0.569828
O	-5.320633	-0.725182	1.12529	H	-2.637562	-2.559784	0.751013
O	-3.498354	-0.875867	2.445665	H	-6.831169	0.527228	1.628665
C	-5.807599	0.347491	1.955771	H	-5.783328	0.060354	3.008489
H	-4.188245	0.79773	-0.479434	H	-5.196455	1.24079	1.798604
H	-2.292345	1.364392	1.287827				
H	-1.547505	1.887842	-1.674279				
H	1.687545	-2.208879	-1.612406				

Table S12. Atomic coordinates (Å) of 3-6 obtained at the Cam-B3LYP/6-311+G(d,p) level of theory in the MeOH.

C	2.632342	0.016763	1.567426	H	-1.761599	-1.181504	1.800101
C	2.698618	1.835883	-0.334578	H	-0.71321	0.401955	-2.644578
C	0.806003	0.219608	0.026269	H	-0.549544	1.893254	-1.725449
C	1.124582	-0.005684	1.327335	H	-2.894586	2.031481	-1.740309
C	-0.596642	0.101818	-0.475209	H	-3.073982	0.382005	-2.311087
C	-1.572921	0.654939	0.62704	H	-3.183504	-0.521043	-0.139376
C	-1.372519	-0.161866	1.914092	H	-0.260255	2.286415	1.305477
C	0.101333	-0.278745	2.337009	H	-1.431554	2.790969	0.084368
C	-1.014466	0.903143	-1.719614	H	-1.955947	2.485149	1.738368
C	-2.559618	1.001834	-1.574575	H	-0.785573	-2.031133	0.09727
C	-2.929411	0.543835	-0.124816	H	-1.75713	-1.578605	-1.317405
C	-1.282621	2.139077	0.948554	H	-0.000112	-1.748233	-1.450244
C	-0.809911	-1.406451	-0.799109	H	-3.935299	2.365038	0.403628
O	0.382492	-0.60771	3.491964	H	-4.505179	-0.164055	2.038412
C	2.013701	0.530053	-0.771187	H	-5.45518	1.323647	2.185781
C	-4.156318	1.289563	0.435815	H	-3.73716	1.328079	2.584778
C	-4.478244	0.921686	1.892078	H	-6.16959	1.809769	-0.119322
C	-5.405761	1.100053	-0.457809	H	-5.174905	1.361496	-1.49529
C	-6.054249	-0.298982	-0.437171	H	-6.25544	-0.632422	0.58258
C	-5.258063	-1.352915	-1.169386	H	-7.018797	-0.236619	-0.955518
O	-4.99811	-2.435169	-0.400371	H	-4.495177	-3.064962	-0.953017
O	-4.88875	-1.276093	-2.326124	H	4.144859	0.962676	2.812782
C	3.053854	0.956603	2.70902	H	2.613184	0.627326	3.653049
C	3.166174	-1.407249	1.880625	H	2.724968	1.982328	2.515982
C	3.158131	0.494013	0.202944	H	4.26072	-1.367633	1.915157
C	3.583628	2.46848	-1.349988	H	2.818941	-1.675514	2.882828
C	3.643132	3.97784	-1.34129	H	3.974697	4.334405	-0.358455
O	4.224699	1.794395	-2.14951	H	4.324074	4.336772	-2.115132
C	2.72485	-2.534305	0.928602	H	2.640815	4.391348	-1.507168
C	3.197285	-2.415902	-0.503909	H	3.120035	-3.480435	1.319551
O	4.529886	-2.223934	-0.575717	H	1.637299	-2.620913	0.901155
O	2.486571	-2.504569	-1.488215	H	4.722579	-1.017811	-2.261367
C	5.063223	-1.990228	-1.894334	H	6.146142	-1.991055	-1.774798
H	4.1451	0.184396	-0.116784	H	4.74969	-2.778242	-2.581287
H	2.105256	0.248467	-1.813297				
H	2.137062	2.502906	0.311882				
H	-1.902682	0.267764	2.767534				

Uncropped images of western blot

Figure S82. Uncropped images of western blot in figure 5 of paper.

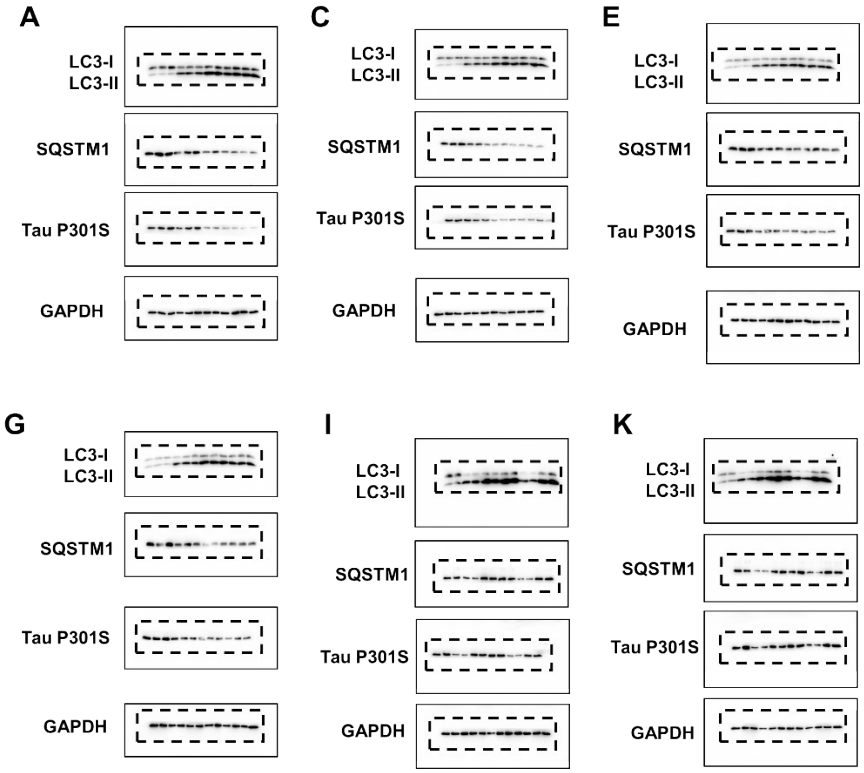

Figure S83. Uncropped images of western blot in figure S6 of Supplementary information.

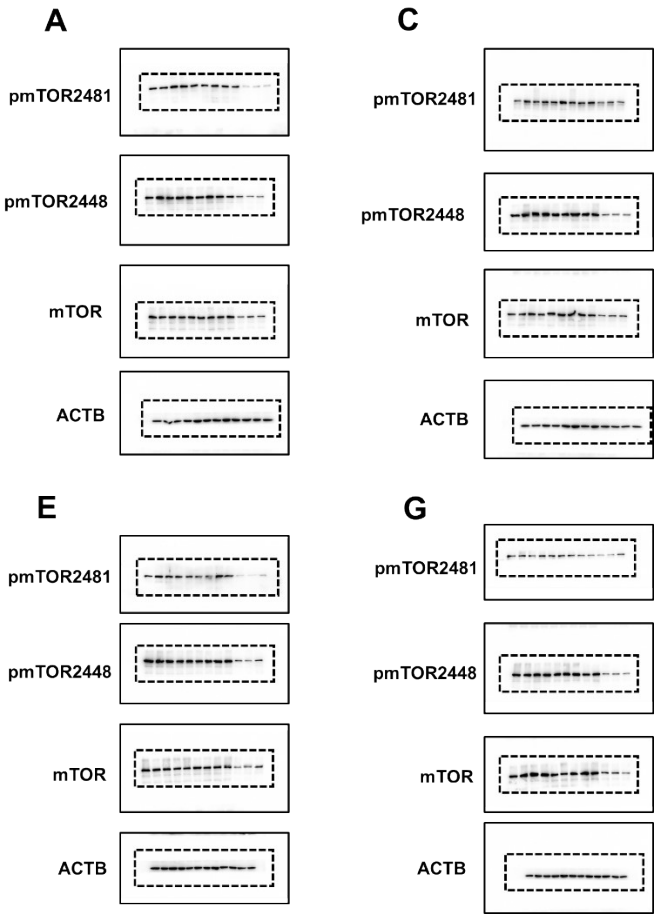

Figure S84. Uncropped images of western blot in figure 6 of paper.

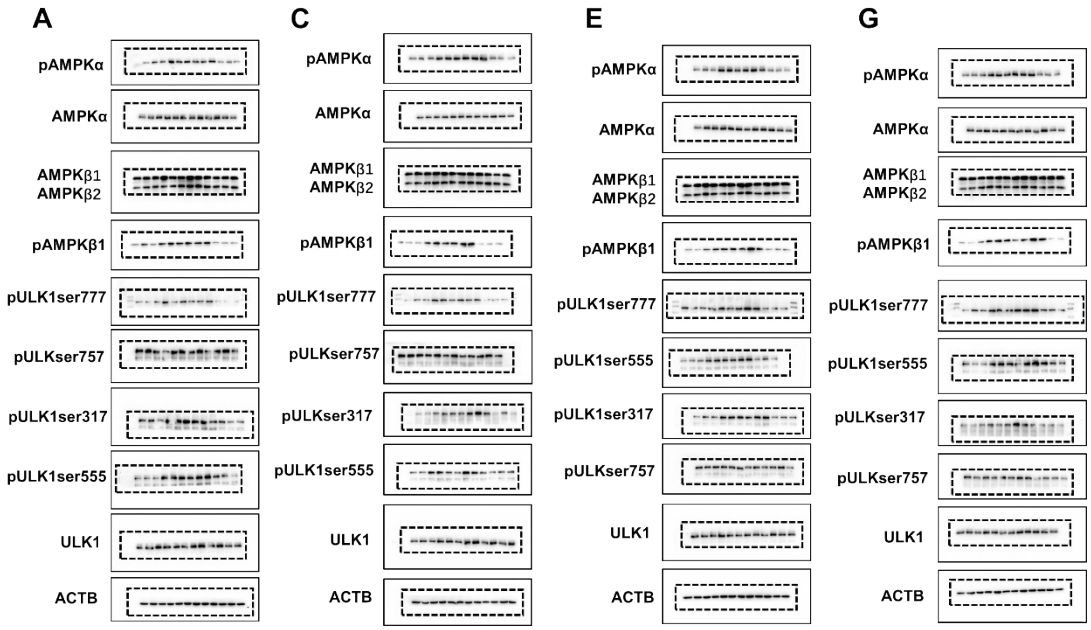

References:

[1] X. Peng, R. Luo, X. Ran, Y. Guo, Y. G. Yao, M. Qiu, *Bioorg. Chem.* **2023**, *132*, 106375.

[2] L. Feng, Y. Ma, J. Sun, Q. Shen, L. Liu, H. Lu, F. Wang, Y. Yue, J. Li, S. Zhang, X. Lin, J. Chu, W. Han, X. Wang, H. Jin, *Autophagy* **2014**, *10*, 1442-1453.

[3] B. Ravikumar, C. Vacher, Z. Berger, J. E. Davies, S. Luo, L. G. Oroz, F. Scaravilli, D. F. Easton, R. Duden, C. J. O'Kane, D. C. Rubinsztein, *Nat. Genet.* **2004**, *36*, 585-595.